Methodologies for the Analysis of Vortex Flows in Aerodynamics and Aeroacoustics

Paolo Gradassi

Tutor

Prof. Luigi Morino

Coordinator

Prof. Edoardo Bemporad

Università degli Studi "Roma Tre"
Scuola Dottorale di Ingegneria
Sezione di Ingegneria Meccanica ed Industriale

April 2013

"I have always thirsted for knowledge, I have always been full of questions."

Hermann Hesse, *Siddhartha*.

"All real fluid motions are rotational."

Truesdell, *The Kinematics of Vorticity*,
Indiana University Press, 1954.

Contents

Chapter 1

Introduction

Vorticity and vortex flows have been extensively studied because of the important role they play in so many different fields. The theoretical foundations of the vorticity kinematics/dynamics are well understood (see for instance the works by Truesdell, Ref. [51], Serrin, Ref. [49], and more recently Saffman, Ref. [46]).[1] Other relevant issues are the relationship of vorticity with turbulence (see for instance the monograph by Chorin, Ref. [4]) and that with sound generation (see for instance Howe, Ref. [11]). It is apparent that the field is extremely wide and therefore some form of selection is required, as discussed below.[2]

Here, the common thread is the analysis of the aerodynamics and aeroacoustics of jets. As we will see, the vortical region behind a jet may be subdivided into four stages. In the first, we have the generation of two boundary layers, inside and outside the nacelle; here, the role of viscosity is essential (first stage). Next, we have a thin vortical layer, similar to that of the wake behind a wing or a rotor blade (second stage). Because of the Kelvin–Helmholtz instability, this layer rolls up to form a vortex ring, where the vorticity evolution is dominated by convection (third stage). After that, the vortex rings break down and form so–called mushroom structure, for which the viscosity becomes again relevant (fourth stage).

Here, we limit ourselves to incompressible flows and address rarely used formulations that we believe to be particularly well suited for the specific flow of each stage. In particular, we address specific methodologies for three types of flows, which in order of increasing complexity may be classified as follows:

1. Incompressible thin vortex–layer flows (second stage),
2. Incompressible Euler vortex–ring flows (third stage),
3. Incompressible Navier–Stokes flows (first and fourth stages).

The vortex flows of the first group are the so–called *almost potential flows*; these comprise all the flows which are irrotational everywhere but in some thin layers.[3] These occur when we have attached high–Reynolds flows, such as the flow around a civilian–aircraft wing at a small angle of attack. Another important example is the flow generated by helicopter blades, again at small angles of attack. These flows are closely related to quasi–potential flows, which are defined as "flows in which vorticity is concentrated in some zero–thickness layers of fluid".[4] Therefore, for

[1] It may be of interest to note that the term vortex dynamics is often used, although the evolution of vorticity does not involve forces; thus, Truesdell, Ref. [51], refers to it as vorticity kinematics. Here, we consistently use the term "vorticity kinematics/dynamics".

[2] Because of the extent and the complexity of the field of vortex flows, the review of the state of the art is also limited to methodologies related to those used here for the study of these specific vortex flows.

[3] Following Chorin and Marsden, Ref. [3], p. 60, an *almost potential flow* is defined as "a flow in which vorticity is concentrated in some thin layers of fluid".

[4] The relationship between almost potential flows and quasi–potential flows, is addressed in Appendix A, where it is shown that the viscous–flow formulation of Chapter 4 yields, in the limit as the thickness and the viscosity

the first type of flows, we consider a modified quasi–potential formulation, that takes into account the effect of the viscosity. The approach used is addressed in greater depth in Section 1.1, along with a review of the state of the art. The mathematical details of the formulation are presented in Chapter 2, along with the numerical results obtained.

For the second type of flows (inviscid vortex rings), we used an approach based upon a result obtained by Cauchy in 1815. Again, the approach used is addressed in greater depth in Section 1.2, along with a review of the state of the art; the mathematical details of the formulation are presented in Chapter 3, along with the numerical results obtained.

For the third type of flows (viscous flows), we used a novel formulation named the natural velocity decomposition. Again, the approach used is addressed in greater depth in Section 1.3, along with a review of the state of the art; the mathematical details of the formulation are presented in Chapter 4, along with the numerical results obtained.

In Chapter 5, we present concluding remarks. In particular, we show how an alternate formulation of the natural velocity decomposition, discussed in details in Appendix B, may provide a unified approach to study all four stages with the same methodology, with the appropriate simplifications afforded by the specific peculiarities of the flow. This novel natural velocity decomposition has been obtained only very recently, and hence only very preliminary results are presented.

1.1 Incompressible thin vortex–layer flows

The first group of flows analyzed are incompressible quasi–potential flows, namely flows that are potential everywhere except for those points that come into contact with the body surface. The *potential wake* is a surface of discontinuity for the potential, and is defined as the locus of all such points. In the past, this methodology has been applied to a non–permeable aerodynamic bodies, such as wings and rotors. Here, it is extended to analyze jets, which are modelled as nacelle–like three–dimensional bodies with prescribed flow through at the nacelle inlet and outlet. The main assumption behind such an approach is that the Kelvin–Helmholtz instability is primarily governed by convection, whereas the effect of viscosity is not that important. Such azimuthal instability of the jet column dominates in the first few diameters downstream of the nozzle and leads to the creation of large coherent structures. Thus, as long as the assumption holds, the study of jet aerodynamics and aeroacoustics is facilitated by the use of the Euler equations which, in turn, yields quasi–potential flows, provided that the flow is initially irrotational.

A common tool for the analysis of quasi–potential flows are the *boundary element methods* (also known as *panel methods*), which model the body surface using distributions of aerodynamic sources and doublets, while the wake surface is modelled as a doublet layer.[5]

Boundary element methods are a numerical version of boundary integral equation method (see for instance the 1929 monograph by Kellog, Ref. [12]). This approach was largely neglected as numerical method, until computer became available; indeed the first numerical works on this subject, albeit initially limited to potential flows, appeared around 1960 (see, for instance, the works of Smith and Pierce, Ref. [50], in 1958, and of Hess and Smith, Ref. [10], in 1964). Thus, these methods have been extensively used for over fifty years. The formulation used here for quasi–potential flows is based on that of Ref. [23], which is valid for unsteady three–dimensional flows around bodies having arbitrary shapes and motions. This method has been widely used for the analysis of quasi–potential flows around wings (as well as rotors, see Ref. [39]; for details and reviews of the developments of the methodology and of its applications, see Refs. [36], [27] and [28]).

Here, the formulation has been extended to jets and applied to a specific jet for which

tend to zero, the formulation for quasi–potential flows.

[5] Using the equivalence between doublet and vortex layers (Batchelor, Ref. [1]), this is equivalent to modelling the wake as a vortex layer.

experimental results are available.

Of course, quasi–potential flows are closely related to almost potential flows. Here, the relationship between the two (quasi–potential and almost potential flows) has been obtained and is presented in Appendix A; the analysis is based upon the natural velocity decomposition, presented in Chapter 4.

1.2 Euler vortex–ring flows

The second group of vortex flows examined in this work pertains incompressible inviscid flows, namely incompressible Euler flows. For these types of flows, we chose a formulation based upon a result obtained by Cauchy in 1815 (see Ref. [49], Eq. 17.5, p. 152; see also Eq. 3.18 here). This result was reinterpreted in terms of material contravariant components in Ref. [24], which includes the extension of the result to viscous flows, an extension made possible by the material–contravariant component–approach used. No numerical applications are included in Ref. [24]; on the other hand, the inviscid formulation was used by Casciola and Piva, Ref. [2], for a numerical study of the vorticity intensification in swirling rings.

In order to take advantage of the Cauchy result mentioned above (namely that material contravariant components of the vorticity remain constant in time, so that vortex lines are material lines), the point of view used is of Lagrangian (not Eulerian) nature, which means that we follow the material points. By taking advantage of such peculiarity of the material contravariant components of the vorticity, we are able to study a flow with spatially bounded vorticity by simply following the deformation of the vortical region. Indeed, once the vorticity has been initially set, the only unknowns left will be the time evolution of the material points inside the vortical domain. For inviscid flows, the vorticity is confined within the core of the vortex tube. For, the outer surface of the vortex ring is a stream surface; indeed, in the absence of viscosity, the vorticity never propagates outside the material region where vorticity was originally confined. Moreover, as we have seen before, taking advantage of the invariant nature of the material contravariant components of the vorticity, the unknowns that remains are the material covariant base vector at the grid points. Choosing one curvilinear coordinates along the original vortex lines, we have that the vorticity will exist only along such a direction. Thus, only one covariant base vector has to be evaluated (step–by–step), in order to solve the problem. The velocity is then obtained through Biot–Savart law.

The review of such a methodology is limited to the three works mentioned above, as we are not aware of additional works based upon this methodology. Thus, the remainder of this section is devoted to a review of the state of the art on vortex ring kinematics/dynamics. Vortex rings have been extensively studied for a long time, for several reasons (see, for instance, the 1858 work by Helmholtz, Ref. [9]). A very comprehensive reviews of vortex ring analysis can be found in both Refs. [47] and [20]. In the aeronautical community, vortex rings have been studied initially for aerodynamic reasons, in order to successfully capture the vorticity kinematics/dynamics of stable/unstable, viscous/inviscid vortex rings (see Refs. [2], [21], [48], [52], [53] and [54]). Of course, they are of interest also for aeroacoustic reasons, since unstable vortex rings represent a noise source (Ref. [13]) and can be also used to study jet noise (Refs. [14], [15] and [44]).

In the present analysis, the study of a vortex ring is primarily carried out in order to investigate the evolution of the aeronautical jet. As stated above, the coherent structures created by the Kelvin–Helmholtz instability are known to evolve into vortex rings. Indeed, these coherent structures are subject to the same azimuthal and core instabilities of a vortex ring; such instabilities subsequently lead to their breakdown (puffs) into smaller structures through mushroom like structures. Thus, the dynamic of these structures could be better understood by studying the instabilities of a vortex ring. Although in this final stage of the vortex ring evolution the viscous effects are no longer negligible, here only vortex rings in incompressible inviscid flows are investigated.

A vortex ring model has been selected in order to study vortex rings' instabilities. Such vortex ring model belongs to the well known family of steady vortex rings in an ideal fluid (see Refs. [8] and [40]). This family of vortex rings are described by a parameter α (non-dimensional mean core radius). In order to satisfy the vorticity equation, the vorticity inside the core is set to be linearly varying with the distance from the ring axis. Finally this model has been subjected to both azimuthal and core instabilities.

1.3 Navier–Stokes flows

In the first and fourth stages, the viscosity is not negligible. Thus, contrary to the two first cases, this time the governing equations will be the Navier-Stokes equations. No other simplifying assumption is available, except for the fact that, for the cases of interest in the aeronautical community, the vorticity is present in a small fraction of the whole fluid region, the so–called vortical region (here understood as the region where the vorticity is not negligible, namely boundary layer and wake). Therefore, the last methodology proposed takes advantage of such a fact.

Specifically, it would be desirable to limit our computational domain to the vortical region. To this end, one could use a vorticity based formulation. The classical approach of this type is based upon the Helmholtz decomposition of the velocity field into a potential non–solenoidal portion and a rotational but solenoidal portion (see Serrin, Ref. [49], p. 165). For incompressible flows, this is particularly convenient because in the infinite space the potential contribution vanishes. However, the vorticity based decompositions have some drawbacks, for instance (see Refs. [25] and [26] for a detailed analysis):

1. Imposing that the vorticity remains solenoidal,
2. Transforming the velocity boundary condition, $\mathbf{v} = \mathbf{v}_{\text{B}}$, into a vorticity boundary condition.

Attempts to remove this drawbacks have led to different decompositions (see Ref. [26]), which however did not fully resolve the problems (see Ref. [33] for a detailed analysis of the state of the art). Alternatively, a boundary integral formulation in primitive variables has been proposed in Refs. [42] and [43], and further refined in Refs. [35], [29] and [30]. These works led to a comprehensive reformulation of the approach, presented in Ref. [31], where the situation is fully reversed. The starting point is still a boundary integral formulation in primitive variables; however, the end result is a decomposition of the velocity field (there called the natural velocity decomposition), into a potential portion, $\mathbf{v}_{\text{P}} = \nabla\varphi$, and a rotational portion, $\mathbf{w}$ (akin to the Helmholtz decomposition). In other words, the starting point is a primitive–variable formulation, the end result is a non–primitive variable formulation. This formulation is adopted here. Among the advantages of such a decomposition, we have

1. It provides a differential equation directly for $\mathbf{w}$ (no need to evaluate the vorticity),
2. The rotational portion, $\mathbf{w}$ vanishes outside the vortical region (computational grid is limited to the vortical region),
3. The potential φ is governed by the Poisson equation and may be evaluated through the use of a standard boundary element method,
4. The velocity field may be obtained independently of the pressure p,
5. The pressure may be obtained through a generalized Bernoulli theorem, which is valid even in the rotational region.

A very preliminary validation of the methodology has been presented in Ref. [17]. A more exhaustive formulation is presented here. The test case is the incompressible flow behind an infinite cylinder (two-dimensional problem). Although very limited in its breadth, the validation has been successful.

Chapter 2

Quasi–potential flows

The objective of this chapter is to introduce a simple model based upon the assumption that the vorticity is concentrated within a thin layer whose thickness is negligible. Such thin vortex layer can be used to model a wake. In this case, one may use a formulation based upon the assumption of quasi–potential flows, namely flows that are potential everywhere in the fluid field, except for the wake points (which are defined below). We first illustrate the formulation for potential flows and then extend it to quasi–potential flows. The present formulation is an extension to jets of the formulation of Refs. [23] and [39] for wings and rotors (for details and reviews of the method, see Refs. [36], [27] and [28]).

In this chapter, we first review the formulation of purely potential flows (Section 2.1), and then that for quasi–potential flows around a wing (Section 2.2). Next, we discuss how the formulation for quasi–potential flows is modified when we deal with jets (Section 2.3). Finally, numerical results are presented in Section 2.4.

2.1 Potential incompressible flows

Consider an irrotational flow, *i.e.*, a flow with zero vorticity in the whole flow field. Irrotational flows are *potential*, namely there exists a function $\phi(\mathbf{x})$, called the velocity potential, such that

$$\mathbf{v}(\mathbf{x}) = \nabla \phi(\mathbf{x}) \qquad \text{(for all } \mathbf{x} \in \mathcal{V}\text{)}, \tag{2.1}$$

where $\mathbf{v}(\mathbf{x})$ denotes velocity and $\mathcal{V}$ the fluid region.

Combining Eq. 2.1 with the continuity equation for incompressible flows,

$$\nabla \cdot \mathbf{v} = 0 \qquad \text{(for all } \mathbf{x} \in \mathcal{V}\text{)}, \tag{2.2}$$

one obtains

$$\nabla^2 \phi = 0 \qquad \text{(for all } \mathbf{x} \in \mathcal{V}\text{)}. \tag{2.3}$$

In order to complete the problem, one needs boundary conditions. For the time being, we assume the boundary surface, $\mathcal{S}_{\text{B}}$, to be impermeable. This implies

$$\mathbf{v} \cdot \mathbf{n} = \mathbf{v}_{\text{B}} \cdot \mathbf{n}. \tag{2.4}$$

Combining with Eq. 2.1 yields the following Neumann boundary condition

$$\frac{\partial \phi}{\partial n} = \chi(\mathbf{x}) \qquad \text{(for all } \mathbf{x} \in \mathcal{S}_{\text{B}}\text{)}, \tag{2.5}$$

where

$$\chi(\mathbf{x}) := \mathbf{v}_{\text{B}} \cdot \mathbf{n}. \tag{2.6}$$

The boundary condition at infinity, in the *air frame* (namely in a frame of reference rigidly connected to the undisturbed air) is given by $\mathbf{v}_\infty = o(r^{-1})$, or, using Eq. 2.1,

$$\phi = o(1). \tag{2.7}$$

The problem defined by Eqs. 2.3–2.7 is known as the exterior Neumann problem for the Laplace equation, which has a unique solution (Kress, Ref. [16], pp. 62–67).

Once the above problem has been solved, the pressure, p, is obtained from Bernoulli's theorem (a first integral of the Euler equations), which in the air frame is given by

$$\frac{\partial \phi}{\partial t} + \frac{1}{2} v^2 + \frac{p}{\rho} = \frac{p_\infty}{\rho}. \tag{2.8}$$

It should be noted that the original problem is formulated in terms of four non–linear differential equations (continuity and Euler equations), for four unknowns (velocity and pressure), with four independent variables (space and time). For potential flows, the formulation is considerably simpler (one linear differential equation for one unknown); the time dependence and the non–linearities appear only in the evaluation of the pressure via Bernoulli's theorem, where they appear respectively as a time derivative and as an algebraic non–linearity. Note also that, for potential flows, one solves for the velocity independently of the pressure – the pressure appears to be "driven" by the velocity. Moreover, potential flows have no memory.

2.1.1 Boundary integral formulation for Poisson equation

Next, consider a boundary integral formulation for potential flows. For future reference, we present the boundary integral formulation for the Poisson equation

$$\nabla^2 \phi = \sigma \qquad \text{(for all } \mathbf{x} \in \mathcal{V}\text{)}. \tag{2.9}$$

Boundary integral methods are based on the use of the so–called fundamental solution G, which, for the Laplace equation, is defined by

$$\nabla^2 G = \delta(\mathbf{x} - \mathbf{y}), \tag{2.10}$$

where $\delta(\mathbf{x} - \mathbf{y})$ denotes the three–dimensional Dirac delta function, placed at $\mathbf{x} = \mathbf{y}$. The fundamental solution G is subject only to the boundary condition $G = o(1)$ at infinity (compare to Eq. 2.7). This gives

$$G(\mathbf{x}, \mathbf{y}) = \frac{-1}{4\pi r}, \tag{2.11}$$

with $r = \|\mathbf{x} - \mathbf{y}\|$.

Multiplying Eq. 2.3 by $G(\mathbf{x}, \mathbf{y})$ and Eq. 2.10 by $\phi(\mathbf{x})$, subtracting, using

$$\nabla \cdot (v \, \nabla u - u \, \nabla v) = v \, \nabla^2 u - u \, \nabla^2 v, \tag{2.12}$$

integrating over the fluid volume, using Gauss' divergence theorem, as well as Eqs. 2.5 and 2.7, and interchanging the variables $\mathbf{x}$ and $\mathbf{y}$, one obtains the following *boundary integral representation* for $\phi(\mathbf{x})$:

$$E(\mathbf{x})\phi(\mathbf{x}) = \oint_{\mathcal{S}_{\text{B}}} \left(\frac{\partial \phi}{\partial n} \, G - \phi \, \frac{\partial G}{\partial n} \right) \mathrm{d}\mathcal{S}(\mathbf{y}) + \int_{\mathcal{V}} \sigma \, G \mathrm{d}\mathcal{V}(\mathbf{y}) \qquad (\mathbf{x} \in \mathcal{V}), \tag{2.13}$$

where $\partial/\partial n = \mathbf{n}\cdot\nabla$ ($\mathbf{n}$ being the outward normal), whereas

$$\begin{aligned} E(\mathbf{x}) &= 1 && \text{for } \mathbf{x}\in\mathcal{V} \\ &= 0 && \text{for } \mathbf{x}\in\mathbb{R}^3\backslash\mathcal{V}. \end{aligned} \tag{2.14}$$

In Eq. 2.13, $\phi(\mathbf{x})$ on $\mathcal{S}_{\text{B}}$ is not known. However, if $\mathbf{x}$ is a smooth point of $\mathcal{S}_{\text{B}}$, one obtains, using Eq. 2.5,[1]

$$\frac{1}{2}\,\phi(\mathbf{x}) = \oint\!\!\!\!\!\!\int_{\mathcal{S}_{\text{B}}} \left(\chi\, G - \phi\,\frac{\partial G}{\partial n}\right)\mathrm{d}\mathcal{S}(\mathbf{y}) + \int_{\mathcal{V}} \sigma\, G\mathrm{d}\mathcal{V}(\mathbf{y}), \qquad (\mathbf{x}\in\mathcal{S}_{\text{B}}). \tag{2.15}$$

Contrary to Eq. 2.13, Eq. 2.15 is a *boundary integral equation*, which relates $\phi(\mathbf{x})$ on $\mathcal{S}_{\text{B}}$ to $\chi(\mathbf{x}) = \partial\phi/\partial n$, also on $\mathcal{S}_{\text{B}}$. Note that this equation is a constraint on the Cauchy data of the problem, $\phi(\mathbf{x})$ and $\chi(\mathbf{x})$, a constraint that must be satisfied by any solution of the Poisson equation.

It may be worth noting that Eqs. 2.13 and 2.15 may be combined by defining

$$\begin{aligned} E(\mathbf{x}) &= 1 && \text{for } \mathbf{x}\in\mathcal{V} \\ &= \frac{1}{2} && \text{for } \mathbf{x}\in\mathcal{S}_{\text{B}} \\ &= 0 && \text{for } \mathbf{x}\in\mathbb{R}^3\backslash\mathcal{V}. \end{aligned} \tag{2.16}$$

The solution procedure consists of solving first the boundary integral equation, Eq. 2.15, so as to obtain $\phi(\mathbf{x})$ on $\mathcal{S}_{\text{B}}$; then, one may use the boundary integral representation, Eq. 2.13, to obtain $\phi(\mathbf{x})$ in the field, and hence, via Bernoulli's theorem, the pressure in the field.

It is apparent that the presence of σ makes the approach much less convenient. Thus, the fact that for potential flows $\sigma = 0$ makes the use of boundary integral methods particularly advantageous. In general, the smaller is the region where $\sigma \neq 0$, the more advantageous is the use of boundary integral methods.

It may be noted that in aerodynamics, we are typically interested in the pressure on the body, whereas the pressure in the field is of interest in aeroacoustics. Moreover, the evaluation of the pressure on the body does not require the use of Eq. 2.13. For, one may obtain the velocity also on $\mathcal{S}_{\text{B}}$ (the tangential components from $\phi(\mathbf{x})$ on $\mathcal{S}_{\text{B}}$, the normal one from Eq. 2.5), and hence, via Bernoulli's theorem, the pressure still on $\mathcal{S}_{\text{B}}$. Thus, if we were to ask a mathematician what is the difference between the evaluation of the pressure on the surface (aerodynamic problem) and that in the field (aeroacoustic problem), the reply would be: "The same difference that there is between a boundary integral equation and a boundary integral representation."

2.1.2 Boundary element formulation

Consider the boundary element formulation for the above problem, namely the discretization of the boundary integral formulation. Let $\mathcal{S}_{\text{B}}$ be divided into N_{B} triangular and/or quadrilateral elements, $\mathcal{S}_j$, and let $\phi(\mathbf{x})$ and $\chi(\mathbf{x})$ to be treated as constant within each element. This yields

$$\phi(\mathbf{x}) = \sum_{j=1}^{N_{\text{B}}} B_j(\mathbf{x})\,\chi_j + \sum_{j=1}^{N_{\text{B}}} C_j(\mathbf{x})\,\phi_j, \tag{2.17}$$

[1] Throughout the paper we assume that the surface $\mathcal{S}_{\text{B}}$ is smooth. This is justified by the fact that in the zeroth–order formulation used for the discretization, the collocation points are at the centers of the elements, where the surface is indeed smooth. This would not be acceptable in the higher order formulations, where the collocation points are placed at the corner of the elements, which include in particular the trailing edge points; for an analysis of this point see Ref. [32].

where

$$B_j(\mathbf{x}) = \int_{\mathcal{S}_j} G \, \mathrm{d}\mathcal{S}(\mathbf{y}),$$
$$C_j(\mathbf{x}) = -\int_{\mathcal{S}_j} \frac{\partial G}{\partial n} \, \mathrm{d}\mathcal{S}(\mathbf{y}). \tag{2.18}$$

Next, consider the so–called collocation method, which consists of satisfying Eq. 2.17 at N_{B} prescribed collocation points, which are assumed to coincide with the element centers $\mathbf{x}_k$ ($k = 1, ..., N_{\mathrm{B}}$). This yields

$$\frac{1}{2}\,\phi_k = \sum_{j=1}^{N_{\mathrm{B}}} B_{kj}\,\chi_j + \sum_{j=1}^{N_{\mathrm{B}}} C_{kj}\,\phi_j, \tag{2.19}$$

where $B_{kj} = B_j(\mathbf{x}_k)$ and $C_{kj} = C_j(\mathbf{x}_k)$. The above is a system of linear algebraic equations relating the unknowns ϕ_j to the values of χ_j, known from the boundary condition, Eq. 2.5. Once the values of ϕ_j have been obtained, Eq. 2.17 gives $\phi(\mathbf{x})$ in the field, as an infinitely differentiable function of $\mathbf{x}$. This implies in particular that one may use derivatives – instead of finite differences – in order to evaluate $\mathbf{v}$ in the field.

2.2 Quasi–potential incompressible flows

Things are not quite as simple in aircraft aerodynamics. Indeed, let us recall the d'Alembert paradox: "Steady incompressible potential flows around $\mathcal{S}_{\mathrm{B}}$ produce no force on $\mathcal{S}_{\mathrm{B}}$". Therefore, one needs a generalization that is capable of predicting lift and drag. This is addressed in this section. As we will see, this generalization includes zero–thickness vortex layers (surfaces of discontinuity for the potential).

To this end, let us introduce the material circulation

$$\Gamma_{\mathrm{M}}(t) = \oint_{\mathcal{C}_{\mathrm{M}}(t)} \mathbf{v} \cdot \mathrm{d}\mathbf{x} = \int_{\mathcal{S}_{\mathrm{M}}(t)} \mathbf{n} \cdot \boldsymbol{\zeta} \, \mathrm{d}\mathcal{S},$$

where $\mathcal{C}_{\mathrm{M}}(t) = \partial\mathcal{S}_{\mathrm{M}}(t)$ is a material contour (*i.e.*, a contour composed of material points), and recall Kelvin's theorem for incompressible inviscid flows, which states that $\mathrm{d}\Gamma_{\mathrm{M}}/\mathrm{d}t = 0$. Next, consider for simplicity an attached flow around an isolated wing (*i.e.*, a flow that leaves the wing surface at a sharp trailing edge) and assume the vorticity, $\boldsymbol{\zeta} = \nabla \times \mathbf{v}$, to be initially vanishing in the whole fluid region $\mathcal{V}$ (*e.g.*, start from rest), so that $\Gamma_{\mathrm{M}}(0) = 0$ for all the $\mathcal{C}_{\mathrm{M}}$ in $\mathcal{V}$. Then, Kelvin's theorem implies $\Gamma_{\mathrm{M}}(t) = 0$ for all the $\mathcal{C}_{\mathrm{M}}$ that remain in $\mathcal{V}$ between 0 and t. This in turn implies that the vorticity vanishes everywhere in the field, except for the locus of the points that came in contact with the trailing edge, for which the above assumption (that $\mathcal{C}_{\mathrm{M}}$ remains in $\mathcal{V}$ between time 0 and time t) does not apply. These points form a surface, which is called the *wake* and is denoted by $\mathcal{S}_{\mathrm{W}}$. Hence, the velocity is still given by Eq. 2.1, which however does not hold on $\mathcal{S}_{\mathrm{W}}$:

$$\mathbf{v}(\mathbf{x}) = \nabla\,\phi(\mathbf{x}) \qquad\qquad (\text{for all } \mathbf{x} \in \mathcal{V}\backslash\mathcal{S}_{\mathrm{W}}). \tag{2.20}$$

It should be noted that the fact that $\Delta\phi$ is not constant over $\mathcal{S}_{\mathrm{W}}$ implies a tangential discontinuity in the velocity, and hence the presence of vorticity (*i.e.*, the wake corresponds to a zero–thickness vortex layer). Therefore, these flows are called *quasi–potential*.

The equation that governs quasi–potential incompressible flows is again the Laplace equation, which however does not hold on $\mathcal{S}_{\mathrm{W}}$:

$$\nabla^2\phi = 0 \qquad\qquad (\text{for all } \mathbf{x} \in \mathcal{V}\backslash\mathcal{S}_{\mathrm{W}}). \tag{2.21}$$

The boundary conditions on the wing and at infinity are the same as those for potential flows (Eqs. 2.5 and 2.7). In addition, we now need boundary conditions on the wake. For a surface of discontinuity, the principles of conservation of mass and momentum (see Serrin, Ref. [49], p. 219, Eq. 54.1) imply, for incompressible flows,[2]

$$\mathbf{v} \cdot \mathbf{n} = \mathbf{v}_{\mathrm{W}} \cdot \mathbf{n}, \tag{2.22}$$

$$\Delta p = 0. \tag{2.23}$$

In turn, these imply

$$\Delta \left(\frac{\partial \phi}{\partial n} \right) = 0, \tag{2.24}$$

and[3]

$$\frac{D_{\mathrm{W}} \Delta \phi}{Dt} := \left(\frac{\partial}{\partial t} + \mathbf{v}_{\mathrm{W}} \cdot \nabla \right) \Delta \phi = 0, \tag{2.25}$$

where $\mathbf{v}_{\mathrm{W}} = \frac{1}{2}(\mathbf{v}_1 + \mathbf{v}_2)$. If we introduce the concept of a wake point, $\mathbf{x}_{\mathrm{W}}$, as a point having velocity $\mathbf{v}_{\mathrm{W}}$, Eq. 2.25 implies

$$\Delta \phi = \text{constant, following } \mathbf{x}_{\mathrm{W}}, \tag{2.26}$$

or

$$\Delta \phi(\mathbf{x}_{\mathrm{W}}, t) = \Delta \phi(\mathbf{x}_{\mathrm{TE}}, t - \theta_{\mathrm{C}}), \tag{2.27}$$

where $\mathbf{x}_{\mathrm{TE}}$ is the trailing–edge point from which $\mathbf{x}_{\mathrm{W}}$ originates, whereas $\theta_{\mathrm{C}} = \theta_{\mathrm{C}}(\mathbf{x}_{\mathrm{W}}, t)$ is the convection time from $\mathbf{x}_{\mathrm{TE}}$ to $\mathbf{x}_{\mathrm{W}}$.

Finally, we need a boundary condition at the trailing edge. The Joukowski hypothesis of smooth flow at the trailing edge implies that

$$\lim_{\mathbf{x}_{\mathrm{W}} \to \mathbf{x}_{\mathrm{TE}}} \Delta \phi(\mathbf{x}_{\mathrm{W}}) = \lim_{\mathbf{x}_2 \to \mathbf{x}_{\mathrm{TE}}} \phi(\mathbf{x}_2) - \lim_{\mathbf{x}_1 \to \mathbf{x}_{\mathrm{TE}}} \phi(\mathbf{x}_1), \tag{2.28}$$

where 2 and 1 here denote the sides of the wing surface corresponding to the sides 2 and 1 of the wake, respectively.

2.2.1 Boundary integral formulation for quasi–potential flows

Next, consider the boundary integral formulation for quasi–potential incompressible flows. Operating as in Section 2.1.1, one obtains that the boundary integral representation for quasi–potential incompressible flows is obtained by writing Eq. 2.13 for a volume outside a surface $\mathcal{S}_{\mathrm{BW}}$ that surrounds the (closed) surface of the body, $\mathcal{S}_{\mathrm{B}}$, and the (open) surface of the wake, $\mathcal{S}_{\mathrm{W}}$. Then, we take the limit as $\mathcal{S}_{\mathrm{BW}}$ tends to

$$\mathcal{S} = \mathcal{S}_{\mathrm{B}} \cup \mathcal{S}_{\mathrm{W}_1} \cup \mathcal{S}_{\mathrm{W}_2}, \tag{2.29}$$

and use Eqs. 2.24 and 2.27 to obtain

$$E(\mathbf{x})\, \phi(\mathbf{x}, t) = \oint_{\mathcal{S}_{\mathrm{B}}} \left(\chi\, G - \phi\, \frac{\partial G}{\partial n} \right) \mathrm{d}\mathcal{S}(\mathbf{y}) - \int_{\mathcal{S}_{\mathrm{W}}} \Delta \phi(\mathbf{y}_{\mathrm{TE}}, t - \theta_{\mathrm{C}})\, \frac{\partial G}{\partial n}\, \mathrm{d}\mathcal{S}(\mathbf{y}), \tag{2.30}$$

[2] For any function f, $\Delta f := f_2 - f_1$ denotes the discontinuity of f across $\mathcal{S}_{\mathrm{W}}$, with the subscripts 1 and 2 denoting the two sides of the wake at a given point.

[3] Equation 2.24 is obtained by combining $\Delta p = 0$ with the Bernoulli theorem, Eq. 2.8, to yield

$$\frac{\partial \phi_2}{\partial t} - \frac{\partial \phi_1}{\partial t} + \frac{1}{2}(\mathbf{v}_1 + \mathbf{v}_2) \cdot (\mathbf{v}_2 - \mathbf{v}_1) = 0.$$

where $\chi(\mathbf{x}) := \mathbf{v}_{\text{B}} \cdot \mathbf{n}$ and $\Delta\phi$ is the potential discontinuity over the wake, whereas $E(\mathbf{x})$ is given again by Eq. 2.16; finally, $\mathbf{n}$ on $\mathcal{S}_{\text{W}}$ points from side 1 to side 2.

We have that $\chi(\mathbf{x})$ is known from the boundary conditions, Eq. 2.5, whereas $\Delta\phi$ is known from the time history at the trailing edge of the body, Eq. 2.28; hence, as before, if $\mathbf{x} \in \mathcal{S}_{\text{B}}$ is a smooth point, we have $E(\mathbf{x}) = 1/2$, and Eq. 2.30 is a boundary integral equation which allows one to solve for $\phi(\mathbf{x})$, and hence for $\mathbf{v}(\mathbf{x})$ and $p(\mathbf{x})$, on $\mathcal{S}_{\text{B}}$ (aerodynamic problem). Then, for $\mathbf{x} \in \mathcal{V}$, Eq. 2.30 is a boundary integral representation which allows one to obtain $\phi(\mathbf{x})$, and hence $p(\mathbf{x})$, in $\mathcal{V}$ (aeroacoustic problem).

Note that the wake surface $\mathcal{S}_{\text{W}}$ must be determined as an integral part of the solution by integrating the equation

$$\frac{\mathrm{d}\mathbf{x}_{\text{W}}}{\mathrm{d}t} = \mathbf{v}_{\text{W}}(\mathbf{x}_{\text{W}}), \tag{2.31}$$

where $\mathbf{v}_{\text{W}}(\mathbf{x}_{\text{W}})$ is obtained by taking the gradient of the above boundary integral representation, Eq. 2.30 (*free–wake analysis*). In practical applications, the geometry of the wing wake has minor effects on the solution, and hence it is often prescribed *a priori*, typically in the direction of the undisturbed flow. However, this is not true for rotors in hover, especially in BVI (Blade Vortex Interaction) conditions, for which a free–wake analysis is essential (see Ref. [39]). The same holds true for a jet wake, the problem at stake here, which is addressed in Section 2.3.

2.2.2 Boundary element formulation

Consider the boundary element formulation for the *quasi–potential incompressible flows*. Proceeding as in Subsection 2.1.2, let $\mathcal{S}_{\text{B}}$ and $\mathcal{S}_{\text{W}}$ be divided, respectively, into N_{B} and N_{W} triangular and/or quadrilateral elements, $\mathcal{S}_j$, and let $\phi(\mathbf{x})$ and $\chi(\mathbf{x})$ to be treated as constant within each element. Then, Eq. 2.30, with $\mathbf{x}_k \in \mathcal{S}_{\text{B}}$, is approximated by

$$\frac{1}{2}\phi_k(t) = \sum_{j=1}^{N_{\text{B}}} B_{kj}\,\chi_j(t) + \sum_{j=1}^{N_{\text{B}}} C_{kj}\,\phi_j(t) + \sum_{n=1}^{N_{\text{W}}} F_{kn}\,\Delta\phi_n(t-\theta_n), \tag{2.32}$$

where θ_n is the time required for a wake point to be convected from the trailing edge point $\mathbf{x}_n^{\text{TE}}$ to the wake point $\mathbf{x}_n^{\text{W}}$. Also,

$$\Delta\phi_n(t) = \sum_{j=1}^{N_{\text{B}}} S_{nj}\,\phi_j(t), \tag{2.33}$$

where S_{nj} is introduced to implement the trailing–edge condition, Eq. 2.28. If a free–wake analysis is being considered, then the vertices of the wake elements are displaced by an amount $\mathbf{v}_n \Delta t$, namely (explicit Euler scheme, see Subsection C.1)

$$\mathbf{x}_n^{\text{W}}(t_{q+1}) = \mathbf{x}_n^{\text{W}}(t_q) + \Delta t\,\mathbf{v}_n^{\text{W}}\big[\mathbf{x}_1^{\text{W}}(t_q), \ldots, \mathbf{x}_{N_{\text{W}}}^{\text{W}}(t_q)\big], \tag{2.34}$$

where $\mathbf{v}_n^{\text{W}}$ is evaluated by taking the gradient of the discretized boundary integral representation, akin to Eq. 2.17.

2.3 Quasi–potential flows for jets

Here, we present the extension to jets of the above quasi–potential formulation of Refs. [23] and [32] for wings and rotors. Let us exclude from the fluid volume the portion inside the nacelle, by introducing two surfaces across the inlet and outlet of the nacelle denoted, respectively, by $\mathcal{S}_{\text{Inlet}}$

and $\mathcal{S}_{\text{Outlet}}$. In other words, the volume $\mathcal{V}$ is now defined as the volume outside the surface $\mathcal{S}$ that surrounds the nacelle and the wake. In the limit, we have, instead of Eq. 2.29,

$$\mathcal{S} = \mathcal{S}_{\text{B}} \cup \mathcal{S}_{\text{W}_1} \cup \mathcal{S}_{\text{W}_2} \cup \mathcal{S}_{\text{Inlet}} \cup \mathcal{S}_{\text{Outlet}}. \tag{2.35}$$

Consider an attached initially–irrotational inviscid incompressible flow field due to a jet. Assume that the velocity of the jet is uniform across the nozzle, so that no vorticity is introduced in the flow field by the jet itself. Thus, the only vorticity in the field is due to the fact that the velocity of the jet is higher than that of the surrounding environment. As a consequence, the flow field is potential everywhere, except for the surface that emanates from the trailing edge of the nacelle. Here, this is referred to as the *wake* and is denoted by $\mathcal{S}_{\text{W}}$. In physical terms, this surface corresponds to the limit of the shear layer as the viscosity tends to zero.

The governing equation are the same as those in the preceding section, with the exception of the boundary condition in Eq. 2.5; this equation is still valid on $\mathcal{S}_{\text{B}}$, the (outer) surface of the nacelle. However, the surfaces $\mathcal{S}_{\text{Inlet}}$ and $\mathcal{S}_{\text{Outlet}}$ are not impermeable and the boundary condition is still given by Eq. 2.5; however χ now is given by

$$\begin{aligned} \chi &= \mathbf{v}_{\text{B}} \cdot \mathbf{n} + \mathbf{v}_{\text{Inlet}} \cdot \mathbf{n} \qquad (\text{for all } \mathbf{x} \in \mathcal{S}_{\text{Inlet}}), \\ \chi &= \mathbf{v}_{\text{B}} \cdot \mathbf{n} + \mathbf{v}_{\text{Outlet}} \cdot \mathbf{n} \qquad (\text{for all } \mathbf{x} \in \mathcal{S}_{\text{Outlet}}), \end{aligned} \tag{2.36}$$

where $\mathbf{v}_{\text{Inlet}}$ and $\mathbf{v}_{\text{Outlet}}$ are, respectively the inlet and outlet velocities, relative to a body frame.

In addition, contrary to wing wakes, jet wakes are such that as the time tends to infinity (and the wake becomes infinitely long), the value of $\Delta\phi$ at the trailing edge tends to infinity, as t tends to infinity. Hence, steady–state flows cannot be addressed with the present formulation; only a time–domain formulation makes sense for jets. This is the main difference between the formulation for wing and that for jets.

2.4 Numerical results

The method has been amply validated for wings and rotors (for reviews, see Refs. [36], [27] and [28]). Therefore, the numerical results presented here are limited to jets.[4]

As previously mentioned, the present formulation has been used to model an incompressible axisymmetric jet as depicted in Figure 2.1, p. 13. As described by Crow and Champagne, Ref. [6], observing the flow downstream of the nozzle, we first notice some ripples on the jet column surface, soon after those ripples grow into waves and eventually into organized axisymmetric structures (Kelvin–Helmholtz instability). Finally these structures become unstable and break down into a series of puffs.

Assuming that in the region close to the nozzle the viscosity effects are negligible, the initial instability of the jet column must then be governed mainly by convective effects; hence it is possible to study it using a quasi–potential flow formulation.

According to Eq. 2.30, the body surface is modelled by patches of uniform sources and a vortex lattice; on the other hand the wake is modelled by a vortex lattice (uniform doublets).[5] A vortex core has then been introduced, its dimensions and its evolution is meant to reproduce some behavior of the shear layer. Although viscosity has been neglected, the evolution of the vortex core could be interpreted as a diffusion due to the viscosity.[6] That been said, an important by–product of such evolution was to eliminate numerical instabilities from the algorithm.

[4] These results supersedes those presented in [34] (see in particular, Footnote 5, p. 11).

[5] As already pointed out in Footnote 5, p. 2, doublet layers equivalent to vortex layers. In particular, a constant doublet element is fully equivalent to a series of vortex filaments along the sides of the element (Batchelor, Ref. [1]). When compared to the results of Ref. [34], the present result differ because the distance between the vortices is smaller than their diameters, so as to form an uninterrupted distribution of vorticity.

[6] The law used is that of the diffusion of a vorticity Gaussian distribution across the wake (see also Footnote 5 above).

Taking into consideration that the usage of the quasi–potential formulation can only justified for the study of the first few diameters from the nozzle but that by only modelling that first region would alter the results, a longer portion of the wake has been modelled. However, a distinction has been made between the first portion of the wake (the one up to 2 diameters away from the nozzle) and the second part. While the first part has been treated as a free–wake, the second has been convected downstream. Indeed, the second portion of the wake, because of its distance, has little influence over the body and affects primarily the first portion of the wake.

The evolution of the jet column is shown in Figures 2.2–2.7 (pp. 14–19). The sequence of images captures the arising and development of the Kelvin–Helmholtz instability[7]. In Figure 2.2, p. 14, the jet column is shown at rest in its initial geometry. In Figure 2.3, p. 15, we can observe some ripples appearing along the jet column. The Kelvin–Helmholtz instability has been triggered. From Figures 2.4–2.7, pp. 16–19, we notice the evolution of the instability. The ripples grow and roll-up into large coherent structures similar to vortex rings.

The numerical results obtained have been qualitatively compared to the results obtained by Romano, Ref. [45] and the comparison has been reported in Figure 2.8, p. 20. While observing Figure 2.8, it is important to recall the initial assumption for the use of this methodology, that is: the vorticity must be concentrated within a zero–thickness layer. Thus, as it can be seen in the comparison, this methodology can only be used to model the first few diameters downstream of the nozzle; the convected portion of the wake has been removed in order to enable a better comparison between the numerical and the experimental results. The further away we move from the nozzle, the more the vorticity is diffused by the viscosity.

A couple of last results have been obtained by evaluating the Strouhal number of the Kelvin–Helmholtz instability with respect to the outlet speed and the nozzle diameter: $\mathrm{St}_{\mathrm{D}} = fD/v_{\mathrm{Outlet}}$. For such evaluation, velocity and pressure have been measured at a point whose coordinates are $(1.5, 1.0, 0.5)$. In Figure 2.9, p. 20, we can observe the velocity Strouhal number where a fundamental frequency can be found around Strouhal number $\mathrm{St}_{\mathrm{D}} = 2.5Hz$. Such peak is related to the passage of the large coherent structures previously discussed. While in Figure 2.10, p. 21, one can observe the pressure Strouhal number. These values are in the right ballpark of the experimental data, for the problem under consideration.

[7] In a first step, the jet column position has been maintained fixed so that the starting vortex could leave the wake without altering its geometry. Finally in a second step, the wake has been enabled to evolve freely. The time indicated in the captions does not take into account the first step.

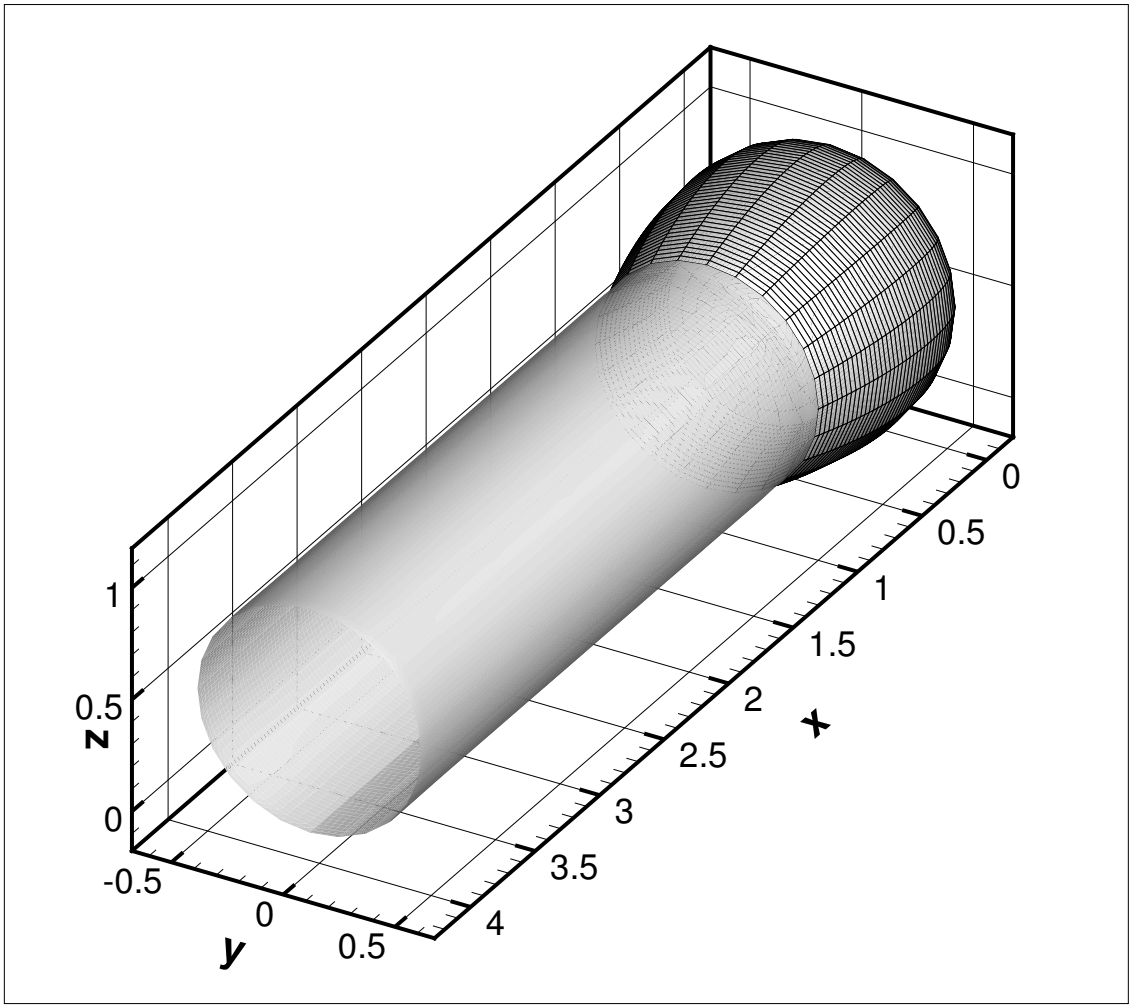

Figure 2.1: Nacelle geometry

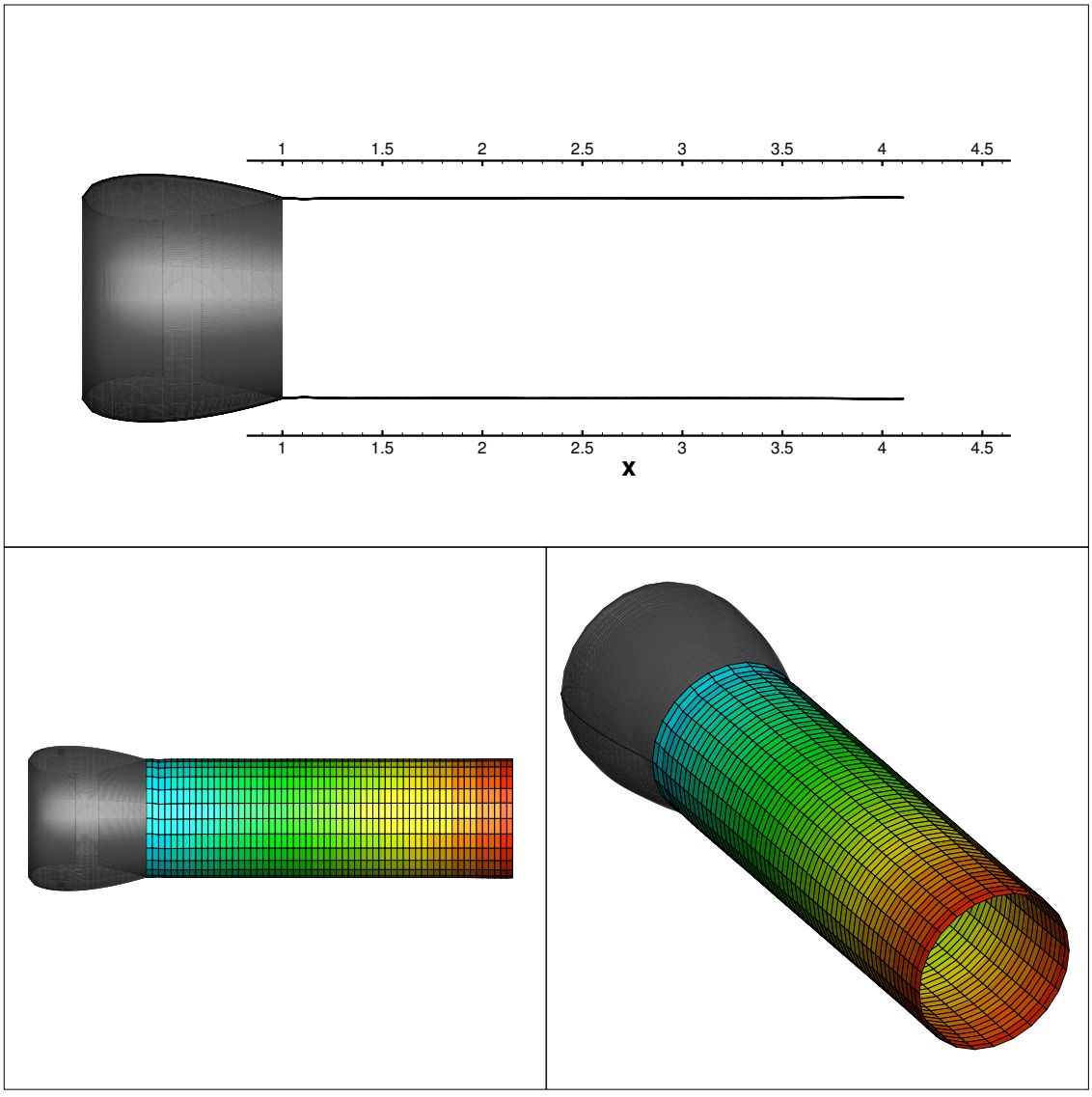

Figure 2.2: Jet column at $t = 0.0$

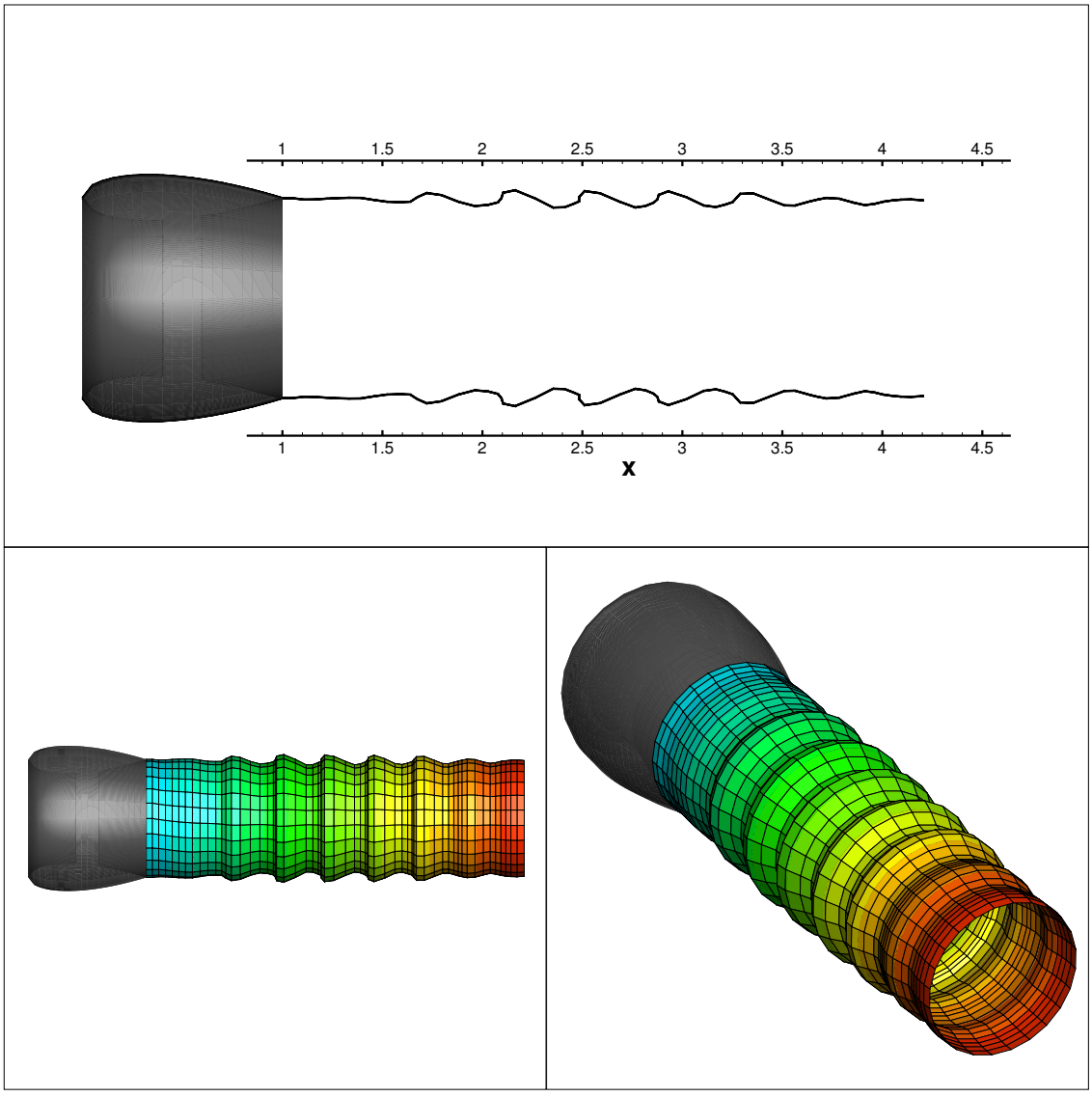

Figure 2.3: Jet column at $t = 5.0$

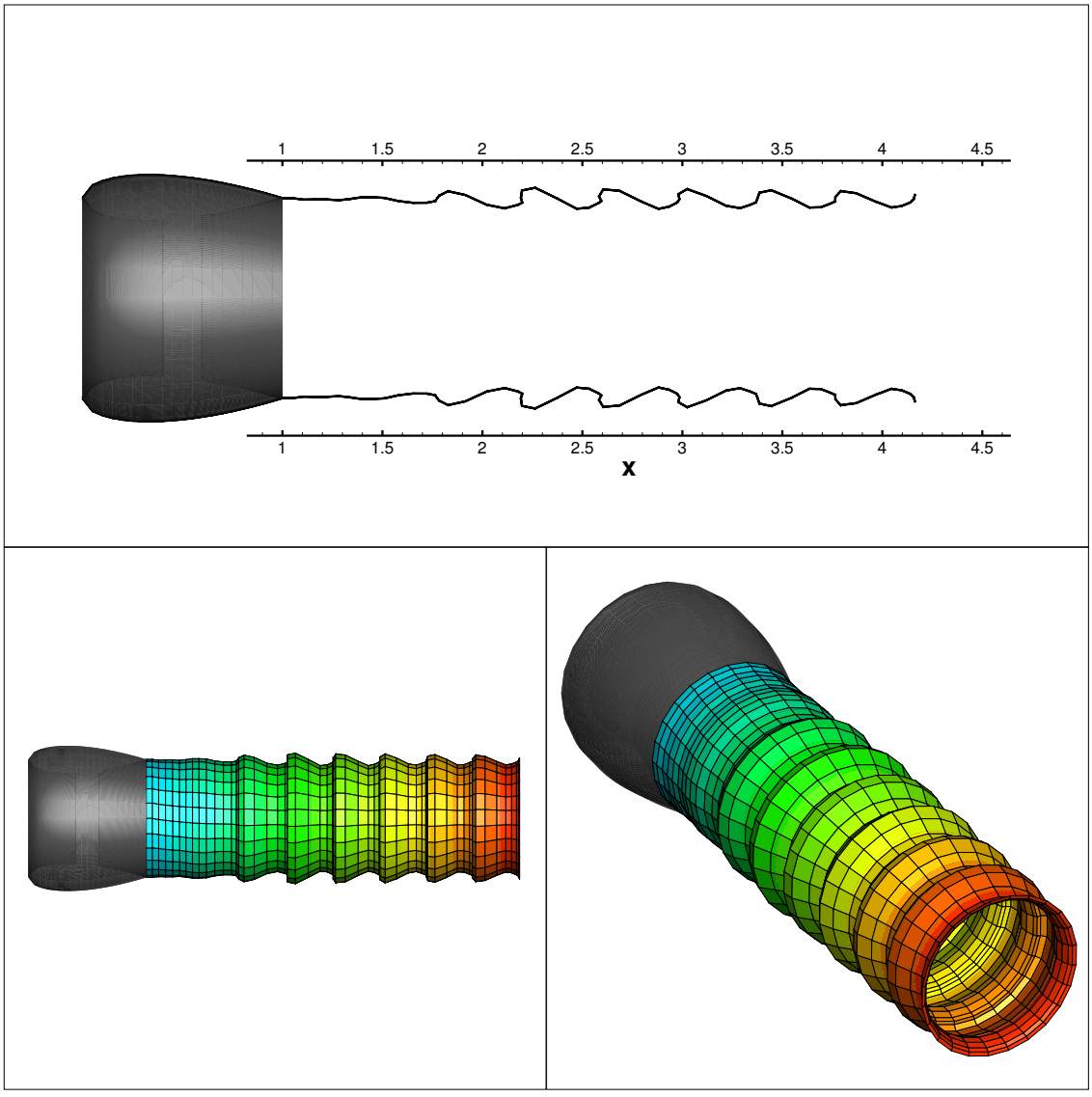

Figure 2.4: Jet column at $t = 6.25$

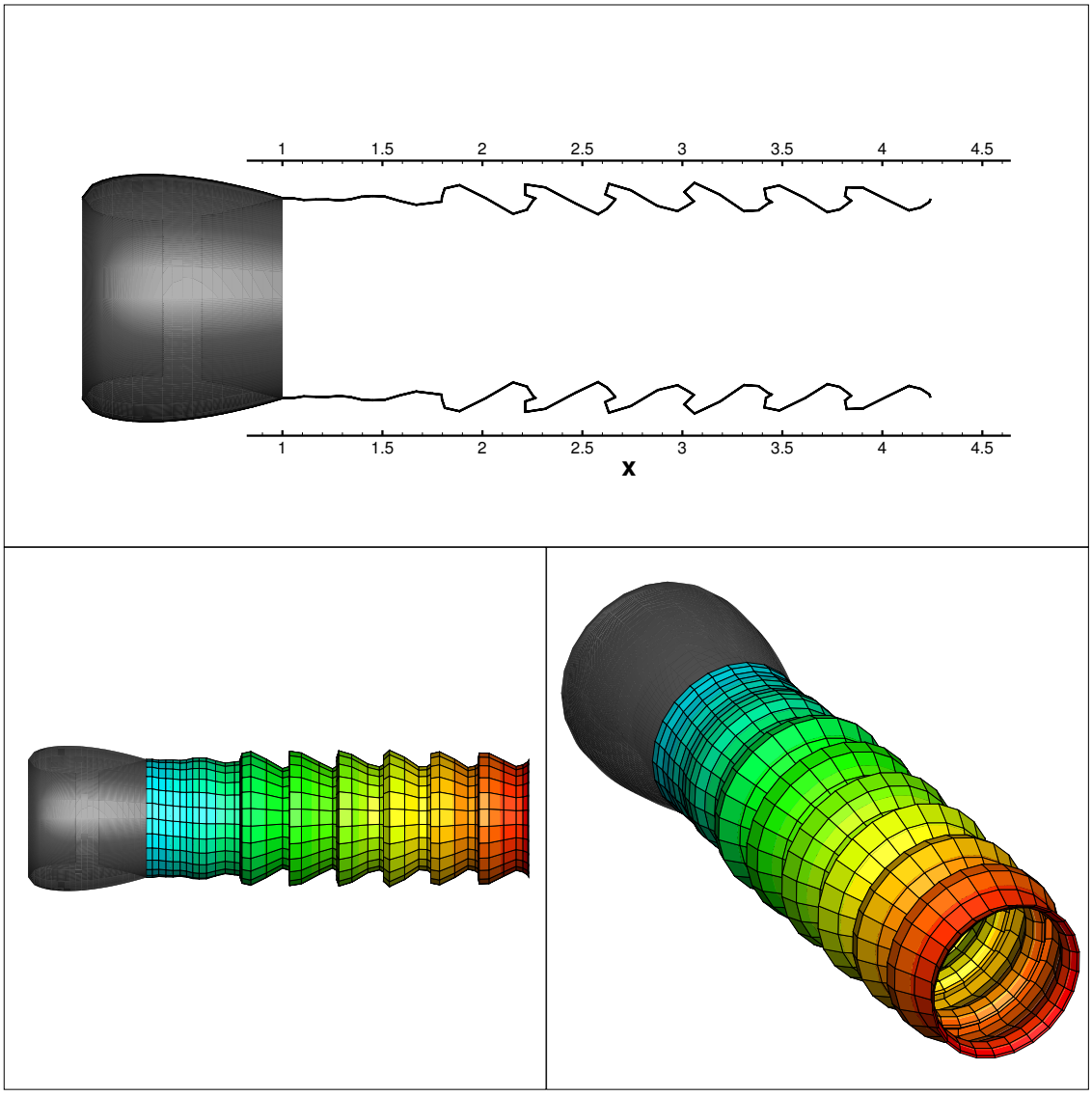

Figure 2.5: Jet column at $t = 9.0$

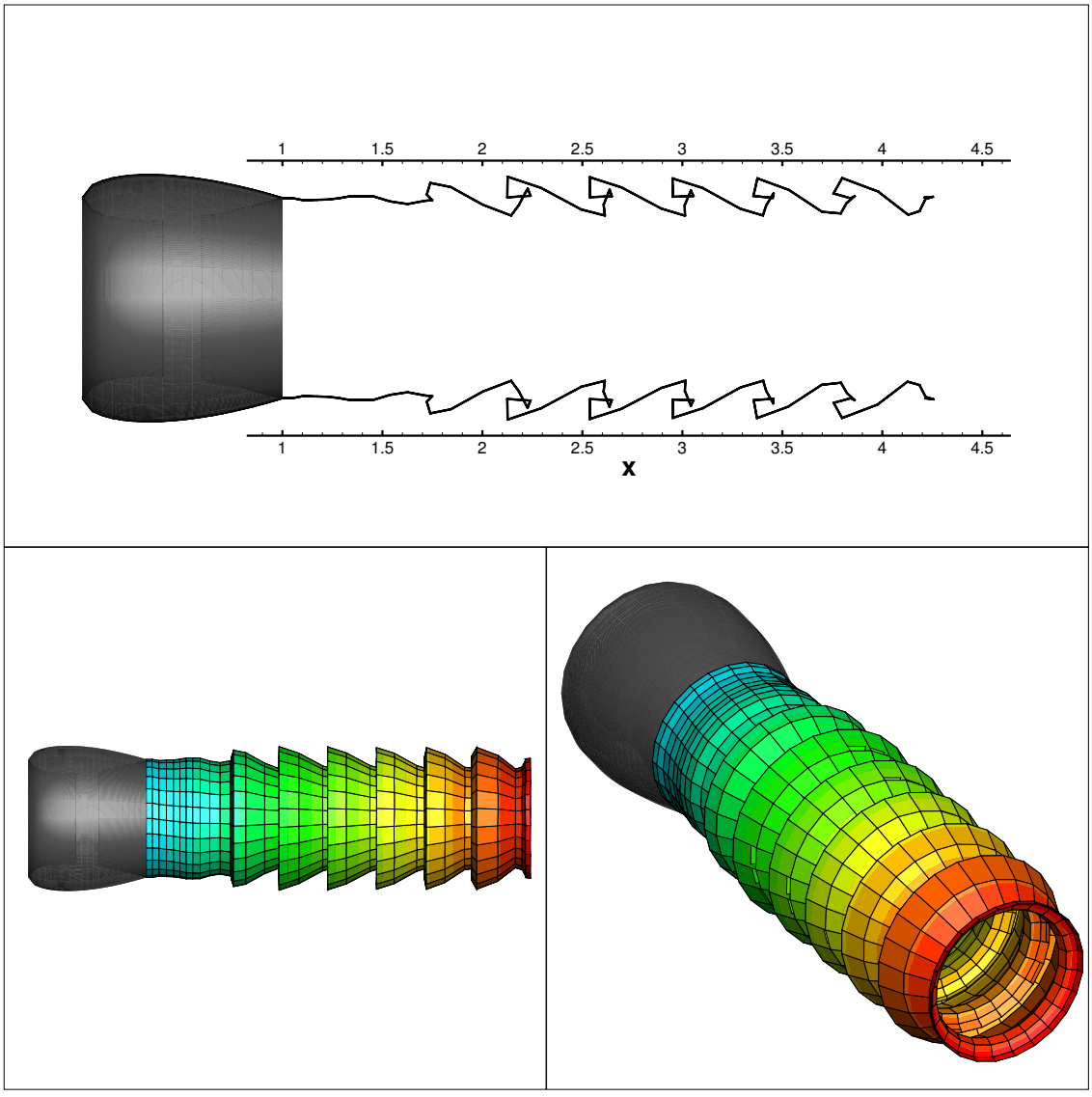

Figure 2.6: Jet column at $t = 12.5$

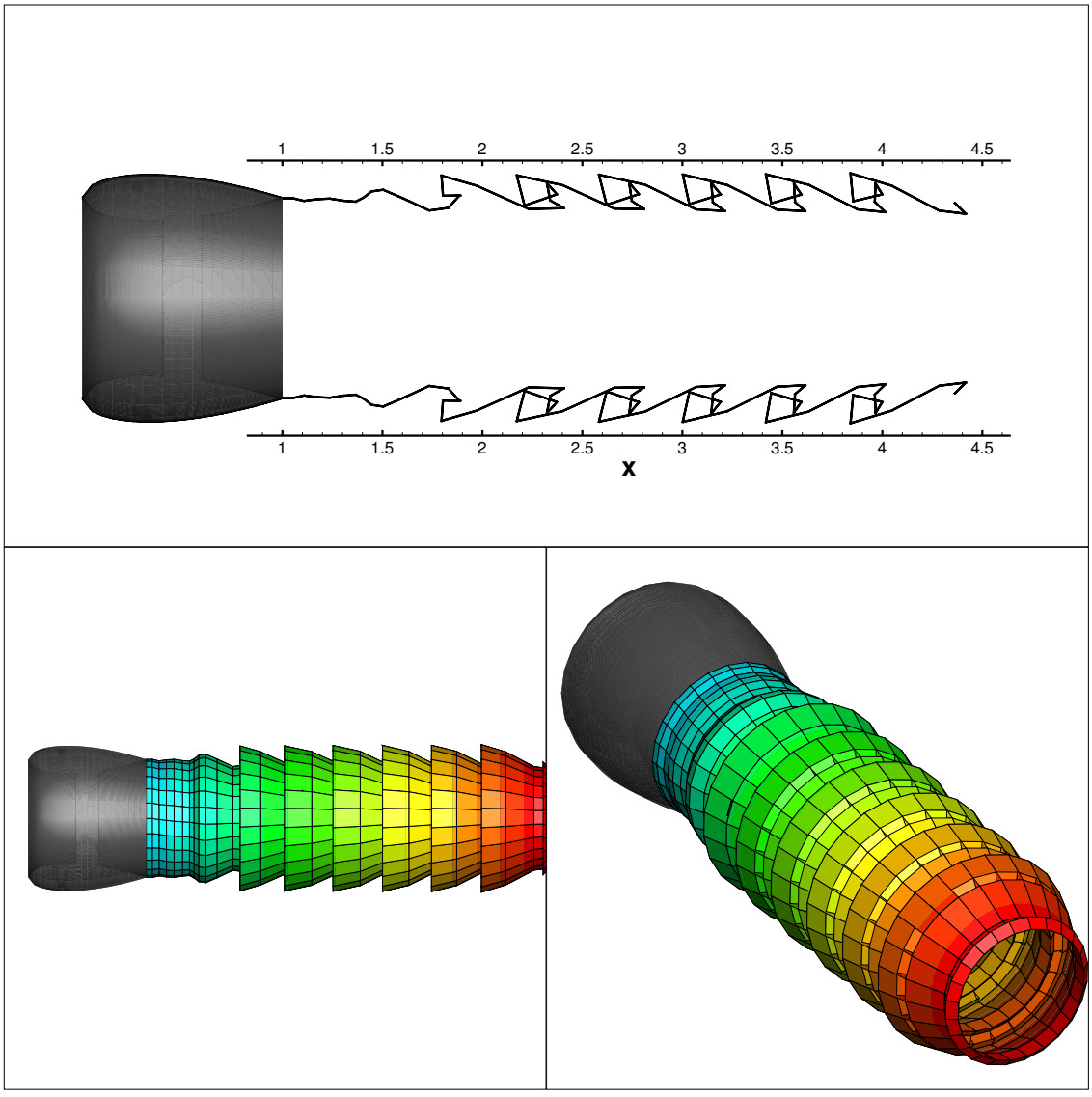

Figure 2.7: Jet column at $t = 17.0$

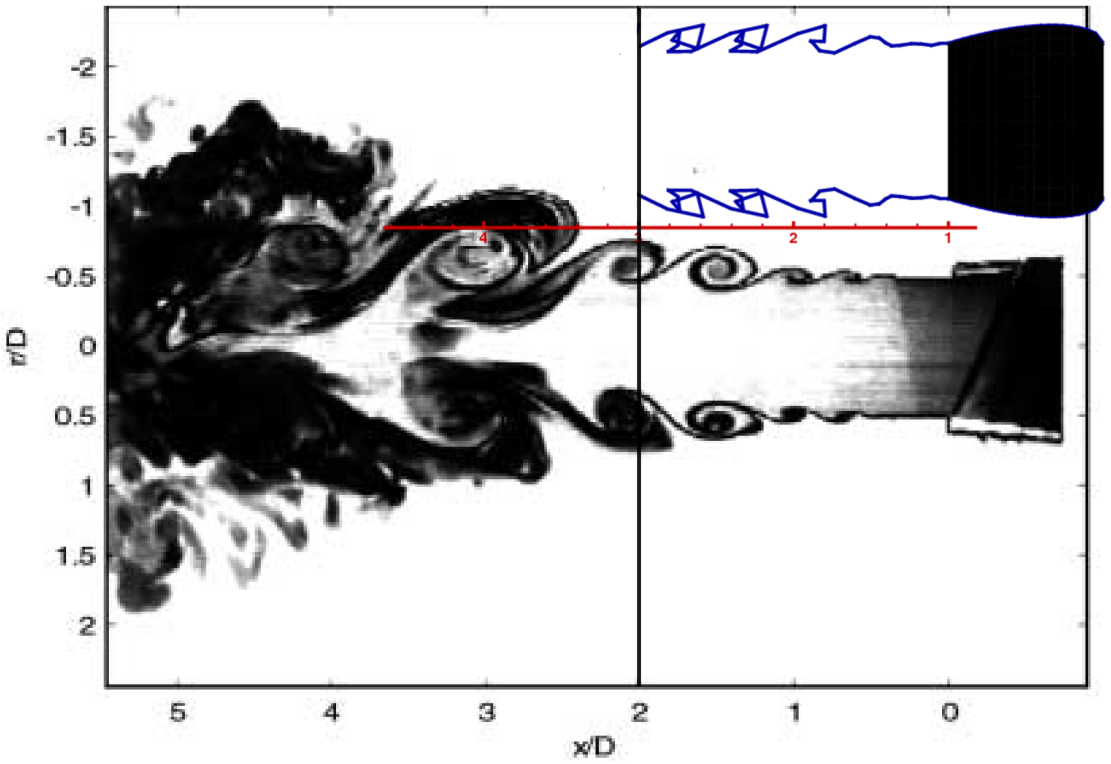

Figure 2.8: Comparison with experimental results by Romano, Ref. [45]

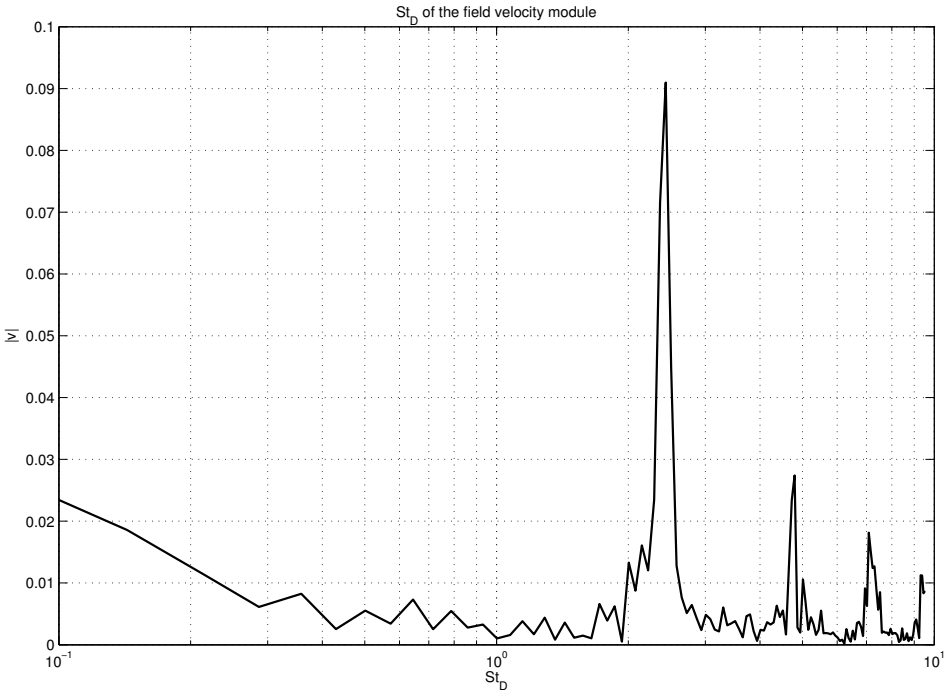

Figure 2.9: Field velocity Strouhal number (based on the nozzle diameter)

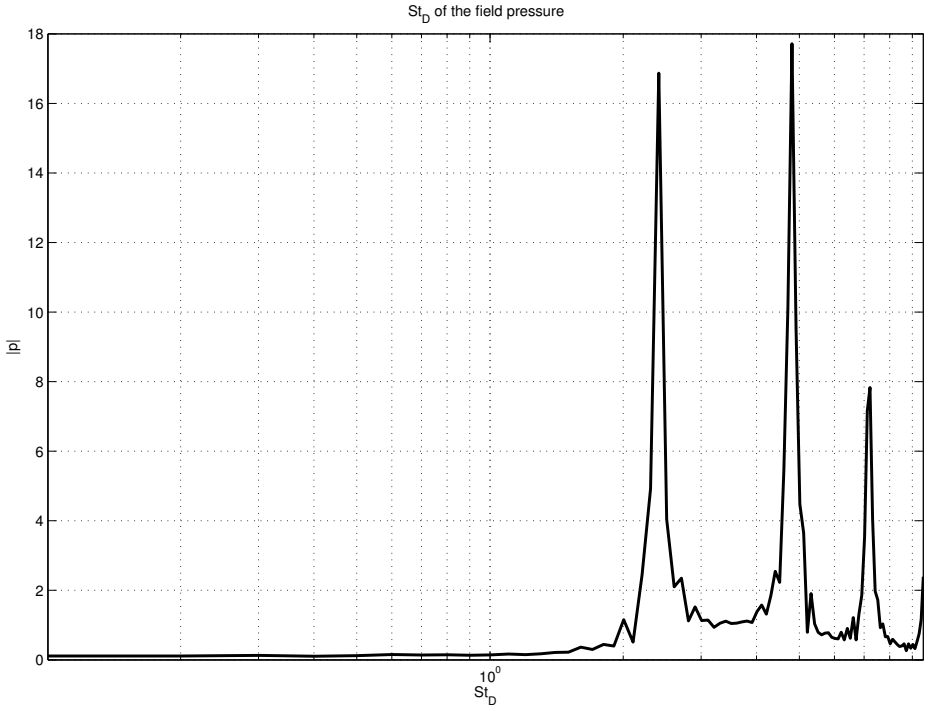

Figure 2.10: Field pressure Strouhal number (based on the nozzle diameter)

Chapter 3

Incompressible Euler flows

In this chapter, we consider unsteady incompressible Euler flows around a body $\mathcal{V}_{\text{B}}$. For these types of flows, we address a methodology based upon the vorticity evolution equation. Once the vorticity has been evaluated, the velocity field is obtained through the Biot–Savart law (Serrin, Ref. [49], p. 165).[1] This methodology is particularly useful when the vorticity is spatially bounded inside a well determined region (*i.e.*, a vortex tube). The formulation is presented for the general problem, namely the unsteady three–dimensional flow around a body having arbitrary shape and motion. As stated in the introduction, in order to study the vorticity evolution, we used the fact that the material contravariant components of the vorticity remain constant in time (see Serrin, Ref. [49], Eq. 17.5, p. 152). As an application, we address the evolution of a vortex ring, for which interesting results are available in the literature.

3.1 Proposed formulation

Here, we present a synthesis of the formulation of Ref. [24] (which is valid for compressible viscous flows), for the limited case of incompressible Euler flows. These flows are governed by the continuity equation for incompressible flows, namely

$$\nabla \cdot \mathbf{v} = 0, \tag{3.1}$$

and the Euler equation, namely (using the Lagrange expression for the acceleration)

$$\frac{\mathrm{D}\mathbf{v}}{\mathrm{D}t} = \frac{\partial \mathbf{v}}{\partial t} + (\mathbf{v} \cdot \nabla)\mathbf{v} = \frac{\partial \mathbf{v}}{\partial t} + \frac{1}{2}\nabla v^2 + \boldsymbol{\zeta} \times \mathbf{v} = -\frac{\nabla p}{\rho}, \tag{3.2}$$

where $\boldsymbol{\zeta}$ denotes the vorticity

$$\boldsymbol{\zeta} = \nabla \times \mathbf{v}. \tag{3.3}$$

Next, let us consider the equation governing the vorticity evolution. Taking the curl of Eq. 3.2, one obtains

$$\nabla \times \frac{\partial \mathbf{v}}{\partial t} + \frac{1}{2}\nabla \times \nabla v^2 + \nabla \times (\boldsymbol{\zeta} \times \mathbf{v}) = -\nabla \times \frac{\nabla p}{\rho}, \tag{3.4}$$

Then, recalling the following vector identity

$$\nabla \times \nabla a = 0, \tag{3.5}$$

[1] It may be of interest to know that the most computationally expensive part of this methodology is the evaluation of the coefficients for the Biot–Savart law. Indeed, this has to be performed at each time step since the formulation is Lagrangian and the geometry of the vortex ring varies.

one obtains the *vorticity transport equation*

$$\frac{\partial \boldsymbol{\zeta}}{\partial t} + \nabla \times (\boldsymbol{\zeta} \times \mathbf{v}) = \mathbf{0} \tag{3.6}$$

In order to simplify this equation, recall the following vector identity

$$\nabla \times (\mathbf{a} \times \mathbf{b}) = \mathbf{a}(\nabla \cdot \mathbf{b}) - \mathbf{b}(\nabla \cdot \mathbf{a}) + (\mathbf{b} \cdot \nabla)\mathbf{a} - (\mathbf{a} \cdot \nabla)\mathbf{b}, \tag{3.7}$$

which yields

$$\nabla \times (\boldsymbol{\zeta} \times \mathbf{v}) = \boldsymbol{\zeta}(\nabla \cdot \mathbf{v}) - \mathbf{v}(\nabla \cdot \boldsymbol{\zeta}) - (\boldsymbol{\zeta} \cdot \nabla)\mathbf{v} + (\mathbf{v} \cdot \nabla)\boldsymbol{\zeta} = (\mathbf{v} \cdot \nabla)\boldsymbol{\zeta} - (\boldsymbol{\zeta} \cdot \nabla)\mathbf{v}. \tag{3.8}$$

Hence, Eq. 3.6 may be rewritten as

$$\frac{\partial \boldsymbol{\zeta}}{\partial t} + (\mathbf{v} \cdot \nabla)\boldsymbol{\zeta} - (\boldsymbol{\zeta} \cdot \nabla)\mathbf{v} = 0, \tag{3.9}$$

or, recalling the definition of *substantial derivative* (namely $\mathrm{D}/\mathrm{D}t = \partial/\partial t + \mathbf{v} \cdot \nabla$),

$$\frac{\mathrm{D}\boldsymbol{\zeta}}{\mathrm{D}t} = (\boldsymbol{\zeta} \cdot \nabla)\mathbf{v}, \tag{3.10}$$

Next, we formulate the problem using a Lagrangian point of view, namely by following the material points. To this end, let us introduce a so–called *system of material curvilinear coordinates*, ξ^α. This is a coordinate system that identifies a material point, namely such that the location of a material is defined as follows

$$\mathbf{x} = \mathbf{x}(\xi^\alpha, t). \tag{3.11}$$

We can now introduce the so–called *covariant base vectors*, which are defined by

$$\mathbf{g}_\alpha = \frac{\partial \mathbf{x}}{\partial \xi^\alpha}, \tag{3.12}$$

and express the vorticity using the above set as a basis:

$$\boldsymbol{\zeta} = \zeta^\alpha \mathbf{g}_\alpha, \tag{3.13}$$

where ζ^α are the so–called *contravariant components* of the vorticity.

Next, note that

$$\frac{\mathrm{D}\mathbf{g}_\alpha}{\mathrm{D}t} = \frac{\partial^2 \mathbf{x}}{\partial t \, \partial \xi^\alpha} = \frac{\partial \mathbf{v}}{\partial \xi^\alpha}. \tag{3.14}$$

Therefore, we have

$$\frac{\mathrm{D}\boldsymbol{\zeta}}{\mathrm{D}t} = \frac{\mathrm{D}}{\mathrm{D}t}(\zeta^\alpha \mathbf{g}_\alpha) = \frac{\mathrm{D}\zeta^\alpha}{\mathrm{D}t}\, \mathbf{g}_\alpha + \zeta^\alpha \frac{\partial \mathbf{v}}{\partial \xi^\alpha}. \tag{3.15}$$

In addition, we have

$$(\boldsymbol{\zeta} \cdot \nabla)\mathbf{v} = \zeta^\alpha \frac{\partial \mathbf{v}}{\partial \xi^\alpha}. \tag{3.16}$$

Combining the last two equations with Eq. 3.10 yields[2]

$$\frac{\mathrm{D}\zeta^\alpha}{\mathrm{D}t} = 0. \tag{3.17}$$

[2] Note that for viscous flows, Eq. 3.10 would be modified by the addition of the viscous term $\nu\nabla^2\boldsymbol{\zeta}$; accordingly, Eq. 3.17 would be modified by the addition of the term $\nu\mathbf{g}^\alpha \cdot \nabla^2\boldsymbol{\zeta}$ (see Ref. [24], for details, as well as the extension to compressible flows).

Equation 3.17 states that the contravariant components of the vorticity remain constant in time, by following a material point, namely[3]

$$\boldsymbol{\zeta}(\mathbf{x},t) = \zeta^{\alpha}(\xi^{\alpha},t)\,\mathbf{g}_{\alpha}(\xi^{\alpha},t) = \zeta^{\alpha}(\xi^{\alpha},0)\,\mathbf{g}_{\alpha}(\xi^{\alpha},t) \tag{3.18}$$

In other words, in order to solve the vorticity evolution equation for an incompressible inviscid flow, we need to find the evolution of the material covariant base vectors $\mathbf{g}_{\alpha}$.[4]

Once these are obtained we may evaluate the vorticity (and hence the velocity), anywhere in the field, at any time, through the Biot–Savart law, given by

$$\begin{aligned}\mathbf{v}(\mathbf{x},t) &= \nabla_{\mathbf{x}} \times \int_{\mathcal{V}} G(\mathbf{x},\mathbf{y})\,\boldsymbol{\zeta}(\mathbf{y},t)\,\mathrm{d}\mathcal{V}(\mathbf{y}) \\ &= \int_{\mathcal{V}} \nabla_{\mathbf{x}} G(\mathbf{x},\mathbf{y}) \times \boldsymbol{\zeta}(\mathbf{y},t)\,\mathrm{d}\mathcal{V}(\mathbf{y}) \\ &= -\int_{\mathcal{V}} \nabla_{\mathbf{y}} G(\mathbf{x},\mathbf{y}) \times \boldsymbol{\zeta}(\mathbf{y},t)\,\mathrm{d}\mathcal{V}(\mathbf{y}),\end{aligned} \tag{3.19}$$

where $G(\mathbf{x},\mathbf{y}) = \dfrac{-1}{4\pi r}$ and $r = \|\mathbf{x}-\mathbf{y}\|$.

3.2 Application: Inviscid vortex ring

The above formulation has been applied to the study of a vortex ring. The corresponding numerical formulation used is obtained as follows: the volume integral is discretized considering the vorticity to be piece–wise constant. In order to evaluate successive position of the material points a predictor–corrector time–stepping method has been used (Section C.3).

The steady inviscid incompressible vortex ring model can be observed in Figure 3.1, p. 26. As previously mentioned this model is taken among the family of steady vortex rings studied by Norbury (Ref. [40]). Still according to Norbury, Ref. [40], in order for the vortex ring to be stable, the core boundary has to be described (in cylindrical coordinates) by

$$r = R(1 + s\cos\theta) \tag{3.20}$$

$$z = Rs\sin\theta \tag{3.21}$$

with $s = \displaystyle\sum_{n=0}^{\infty} a_n(\alpha)\cos n\theta$, where the parameter α is defined $\alpha = \sqrt{A_{\mathrm{c}}/\pi R^2}$ (A_{c} denotes the area of the core of the ring R is the vortex–ring radius); the values of the coefficients $a_n(\alpha)$ can be found in Ref. [40].[5] All the numerical results, are obtained for $\alpha = .1$.

Steady vortex ring

The steady evolution of the ring has been tested and a frame of the evolution is shown below in Figure 3.2, p. 27. The translation velocity for such ring has been found to be $V_{\mathrm{t}} = 0.013$, in agreement with Norbury, Ref. [40].

[3] According to Serrin, Ref. [49], Eq. 17.5, p. 152, "this beautiful result was obtained in 1815 by Cauchy".

[4] It may be noted that Eq. 3.18 provides us an elementary proof of the statement "vortex lines are material lines" (Helmholtz second vortex theorem, Serrin, Ref. [49], p. 163). Indeed, choosing the ξ^1-lines to be parallel to the vorticity at time $t = 0$, we have $\boldsymbol{\zeta}(\mathbf{x},0) = \zeta_0^1\,\mathbf{g}_1(0)$, namely $\zeta_0^2 = \zeta_0^3 = 0$. This implies $\boldsymbol{\zeta}(\mathbf{x},t) = \zeta_0^1\,\mathbf{g}_1(0)$, namely the ξ^1-lines are, at the same time, material lines and vortex lines, in agreement with the theorem.

[5] If the core is circular, we have $\alpha = a/R$, where a is the core radius. Thus, the parameter α represents the dimensionless mean vortex core.

Azimuthal perturbations of the vortex ring

Subsequently, in order to study the azimuthal instabilities, the ring has been initially perturbed and then its evolution has been observed. The parameter k indicates the wave–number of the azimuthal perturbations along the ring. In Figure 3.3, p. 28, the initial geometry of the ring with $k = 4$ and with $k = 6$ is shown. Finally, a frame of the evolution with $k = 4$ can be observed in Figure 3.4, p. 29. While the initial perturbation was in the plane of the vortex ring as shown in Figure 3.3, the deformation of the ring occurs both in the plane and outside of it, as it is possible to see in Figure 3.4. Such deformation increases in time thus showing how such perturbation makes the vortex ring unstable.

Core perturbations of the vortex ring

Finally, in order to study the core instability, perturbations have also been initially applied to the vortex core. The perturbations of the core have been implemented following, Ref. [18]:

$$r = R[1 + s\cos\theta(1 + \rho\cos m\theta)] \tag{3.22}$$

$$z = Rs\sin\theta(1 + \rho\cos m\theta) \tag{3.23}$$

The evolution of the unperturbed core is shown in Figure 3.5, p. 30. The perturbation amplitude has been fixed at $\rho = .05$ while two different perturbation wave have been reported. For each perturbation one can observe the evolution and (having translated the section back to its initial position) the movement of the core. In Figure 3.6, p. 31, it is possible to observe the perturbation of the core with $m = 2$ while in Figure 3.7, p. 32, the perturbation with $m = 4$ is shown. Both perturbations seem to maintain a stable position around the unperturbed core.

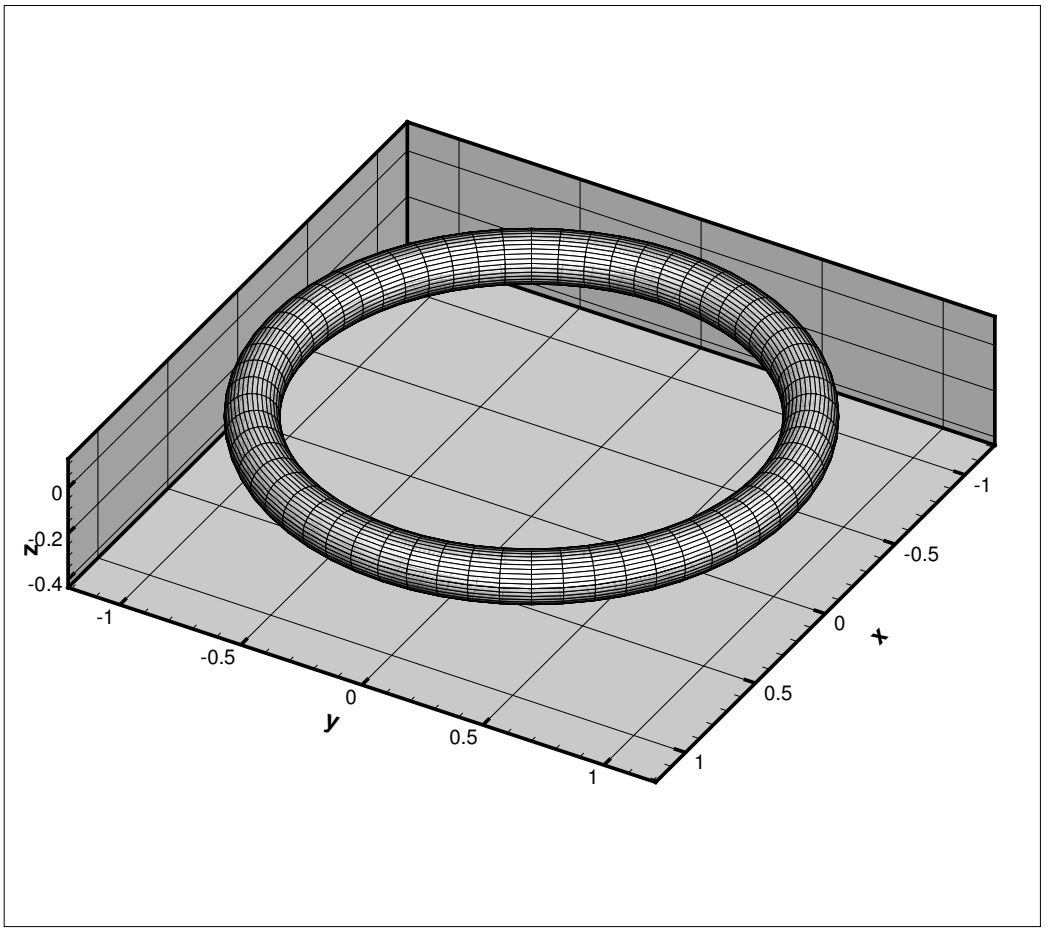

Figure 3.1: Vortex ring model

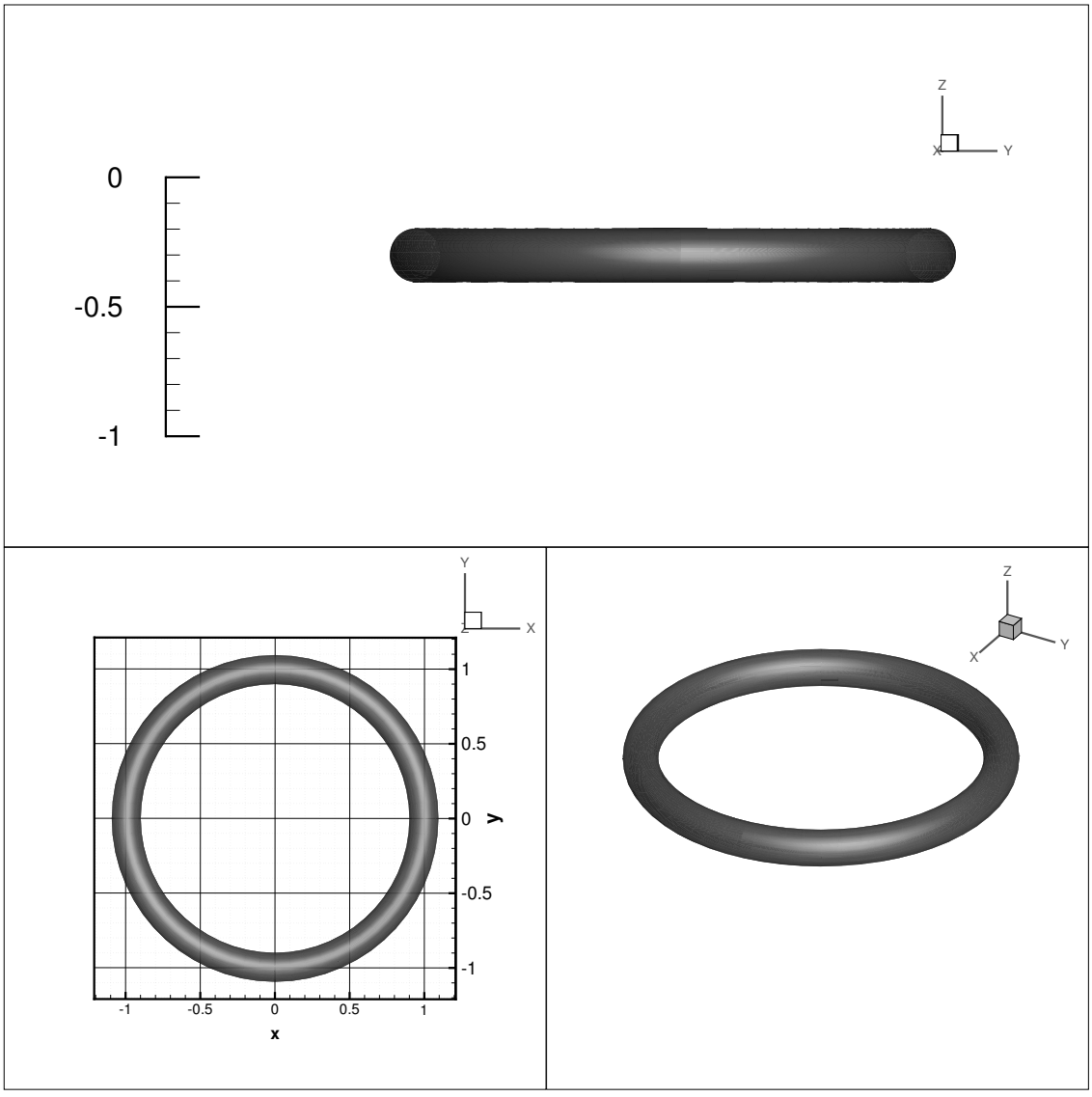

Figure 3.2: Steady vortex ring evolution

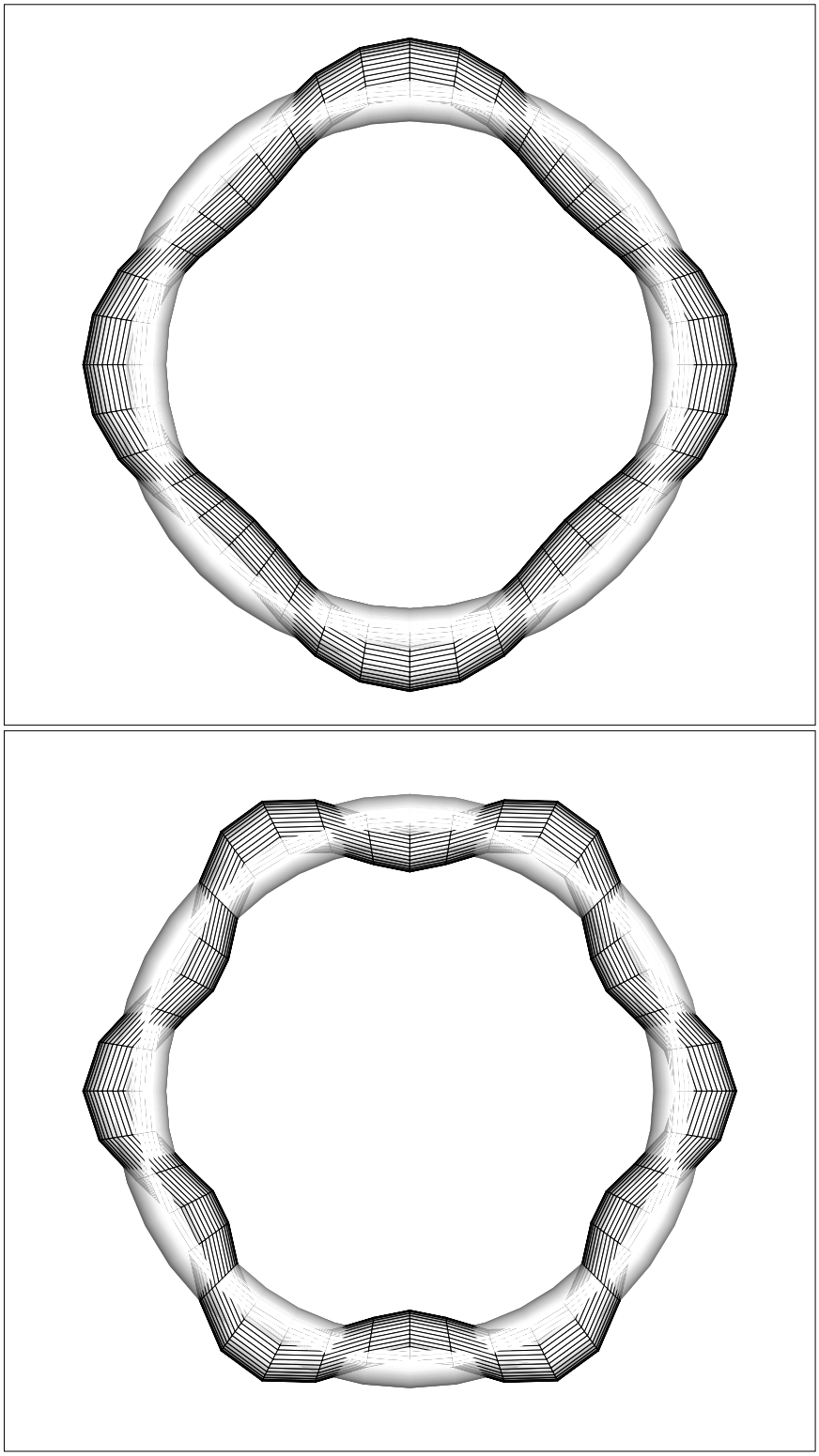

Figure 3.3: Initial azimuthal perturbation of the vortex ring with $k = 4$ and $k = 6$ over the unperturbed geometry (transparent)

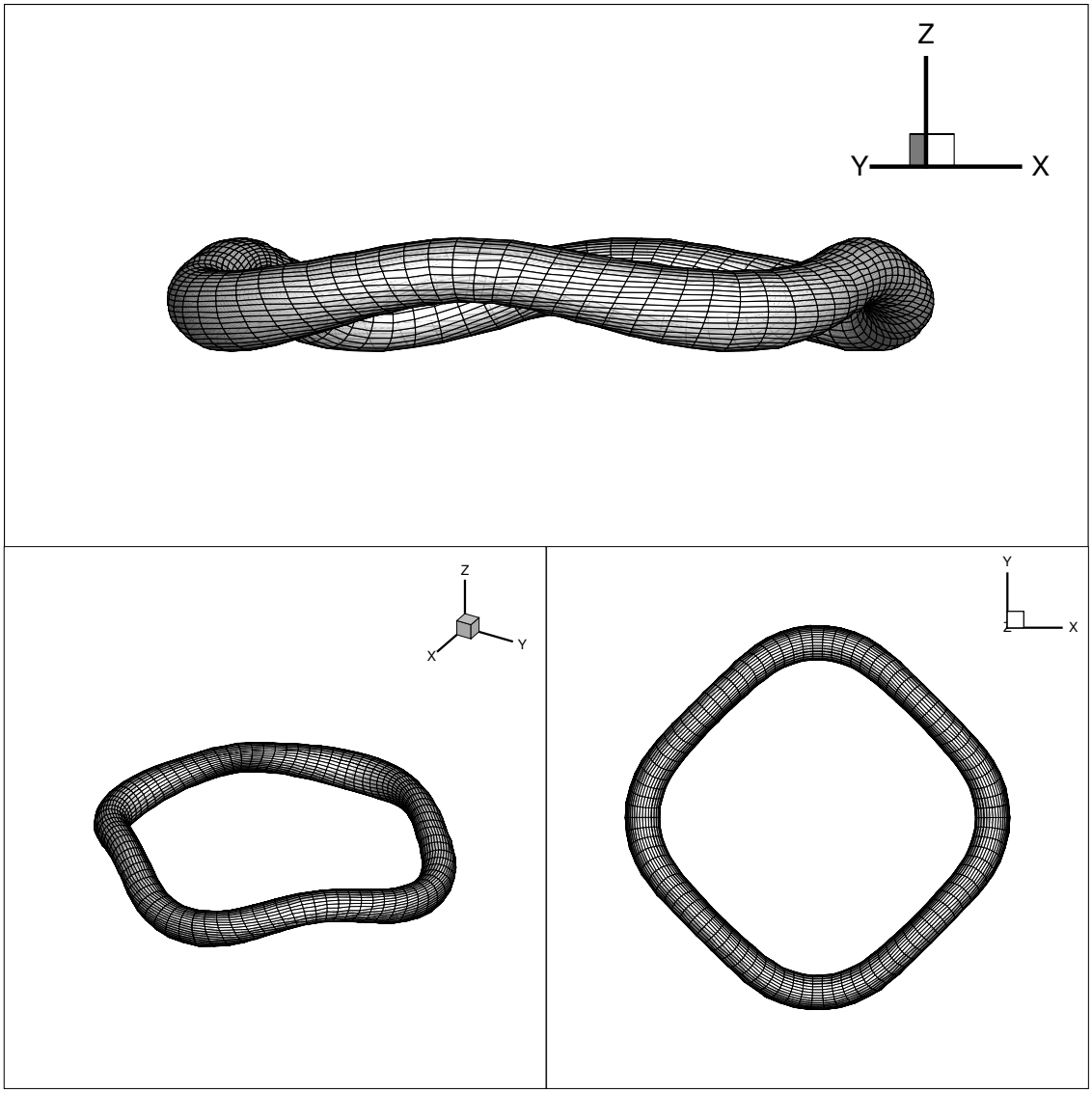

Figure 3.4: Evolution of the azimuthally perturbed vortex ring ($k = 4$)

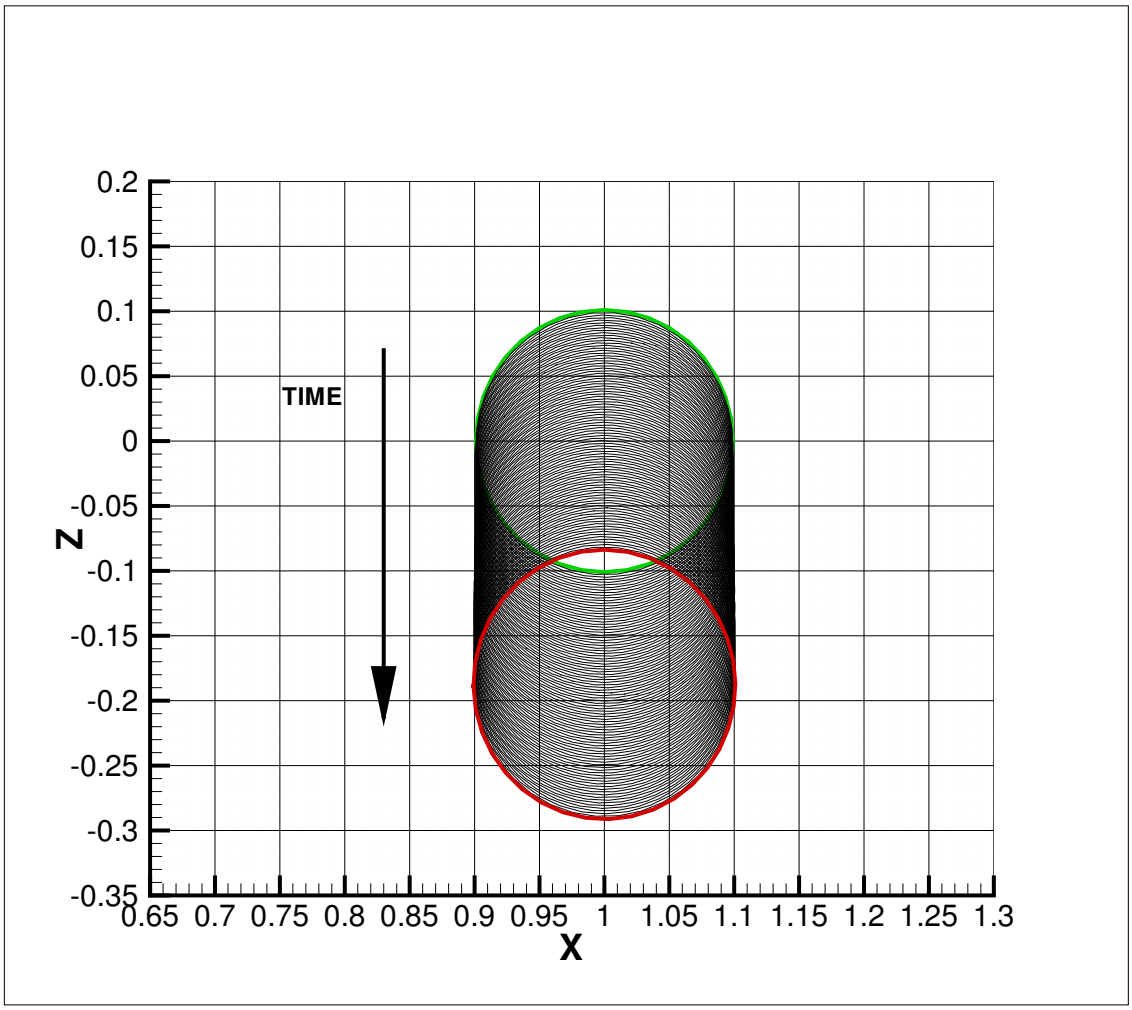

Figure 3.5: Evolution of the unperturbed core of a steady vortex ring from $t = 0.0$ (in green) to $t = 18.0$ (in red)

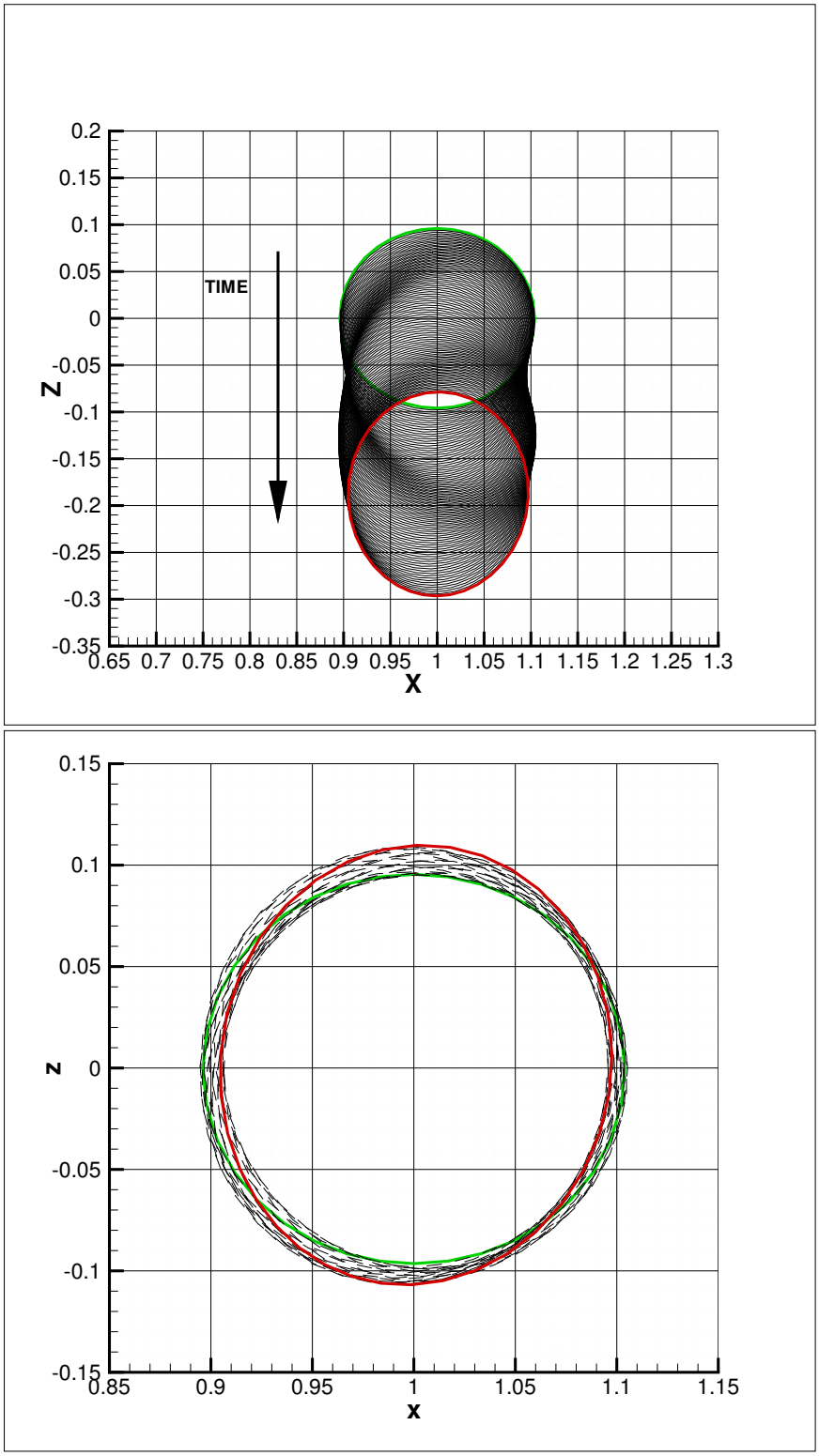

Figure 3.6: Evolution of the perturbed core ($m = 2$) from $t = 0.0$ (in green) to $t = 18.0$ (in red)

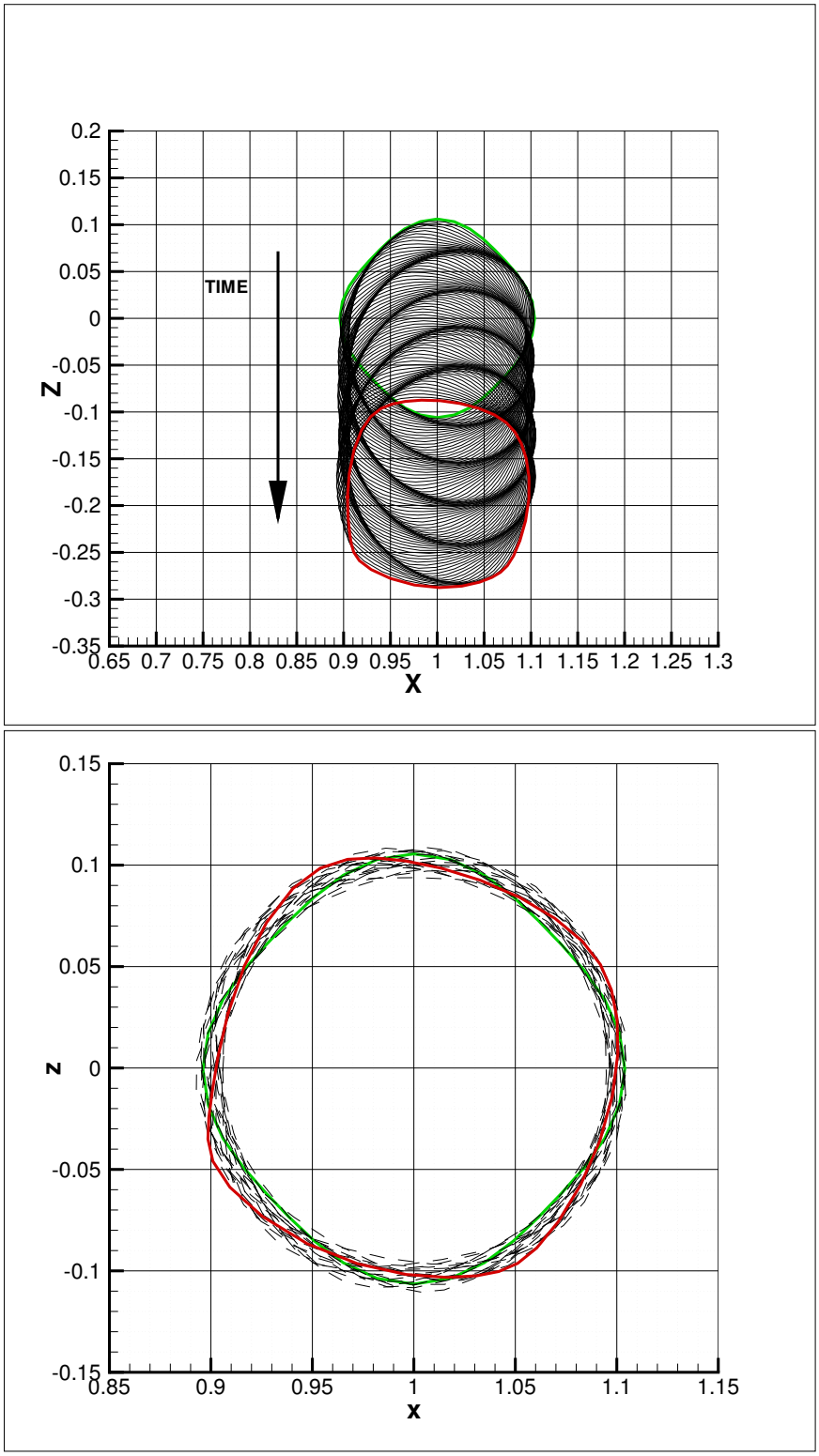

Figure 3.7: Evolution of the perturbed core ($m = 4$) from $t = 0.0$ (in green) to $t = 18.0$ (in red)

Chapter 4

Navier–Stokes flows

In this chapter, we consider unsteady incompressible Navier–Stokes flows around a body $\mathcal{V}_{\text{B}}$. For these types of flows, we address a methodology based upon the velocity decomposition for viscous compressible flows, introduced in Ref. [31], and there denoted as the "*natural velocity decomposition*".[1] Here, the formulation is presented for the generic incompressible–flow problem, namely the three–dimensional unsteady viscous incompressible flow around a body having arbitrary shape and motion. The validation however is limited to steady two–dimensional problems (albeit the results are obtained through a time–accurate transient); specifically, in order to validate the formulation, we apply it to the study the flow around an infinite circular cylinder.

4.1 The governing equations

Navier–Stokes flows are governed by the continuity equation and the Navier–Stokes equations, which for incompressible flows are given by, assuming for the sake of simplicity the forces per unit volume to be negligible,

$$\nabla \cdot \mathbf{v} = 0 \tag{4.1}$$

$$\partial_t \mathbf{v} + \mathbf{v} \cdot \nabla \mathbf{v} + \frac{1}{\rho} \nabla p = \nu \nabla^2 \mathbf{v}, \tag{4.2}$$

where ν denotes the dynamic viscosity coefficient, here assumed to be constant, again for the sake of simplicity.[2]

Next, consider the boundary conditions. For the Navier–Stokes equations, the standard no–slip boundary condition is used on the boundary surface $\mathcal{S}_{\text{B}} = \partial\mathcal{V}_{\text{B}}$

$$\mathbf{v}(\mathbf{x}, t) = \mathbf{v}_{\text{B}}(\mathbf{x}, t) = \text{prescribed} \qquad (\mathbf{x} \in \mathcal{S}_{\text{B}}). \tag{4.3}$$

The boundary conditions at infinity are given by

$$\mathbf{v} = \mathbf{0} \quad \text{and} \quad p = p_\infty \qquad (\|\mathbf{x}\| = \infty). \tag{4.4}$$

For the sake of simplicity, we assume the initial condition to be homogeneous, namely

$$\mathbf{v}(\mathbf{x}, 0) = \mathbf{0} \qquad (\mathbf{x} \in \mathcal{V}). \tag{4.5}$$

[1] Recently obtained theoretical results on the natural velocity decomposition are presented in Appendices A and B.

[2] For notational simplicity, we use ν. However, throughout the work it is tacitly understood that all the variables are dimensionless. Thus, ν denotes the reciprocal of the Reynolds number, and is assumed to be small.

4.2 The natural velocity decomposition

Here, we introduce a generic decomposition of the velocity field into a portion that is irrotational (that is, potential) and one that is rotational, namely

$$\mathbf{v}(\mathbf{x},t) = \mathbf{v}_{\text{P}}(\mathbf{x},t) + \mathbf{w}(\mathbf{x},t), \tag{4.6}$$

with

$$\mathbf{v}_{\text{P}}(\mathbf{x},t) = \nabla\varphi(\mathbf{x},t). \tag{4.7}$$

Combining with Eq. 4.1, one obtains, respectively

$$\nabla^2\varphi + \nabla\cdot\mathbf{w} = 0 \tag{4.8}$$

$$\nabla\Big[\partial_t\varphi + p/\rho + \varpi - \nu\,\nabla^2\varphi\Big] + \partial_t\mathbf{w} + \mathbf{v}\cdot\nabla\mathbf{v} - \nabla\varpi - \nu\,\nabla^2\mathbf{w} = \mathbf{0}, \tag{4.9}$$

where ϖ is a function that may be arbitrarily chosen and whose role is illustrated below.

Next, let us introduce the *key feature of the methodology under consideration.* Note that the use of the decomposition in Eq. 4.6 has replaced three unknowns (the three components of $\mathbf{v}$), with four (the three components of $\mathbf{w}$ as well as φ). Accordingly, we need four equation (a scalar one and a vector one). In order to achieve this, we split Eq. 4.9, and obtain two equations from one. Specifically, we impose[3]

$$\nabla\Big[\partial_t\varphi + p/\rho + \varpi - \nu\,\nabla^2\varphi\Big] = \mathbf{0}, \tag{4.10}$$

$$\partial_t\mathbf{w} + \mathbf{v}\cdot\nabla\mathbf{v} - \nabla\varpi = \nu\,\nabla^2\mathbf{w}. \tag{4.11}$$

The corresponding boundary conditions at infinity are given by (again, in the air frame)

$$\varphi = 0, \qquad \mathbf{w} = \mathbf{0}, \qquad \text{and} \qquad p = p_\infty \qquad\qquad (\|\mathbf{x}\| = \infty). \tag{4.12}$$

The boundary conditions on $\mathcal{S}_{\text{B}}$ and the initial conditions are addressed in Subsection 4.2.2.

4.2.1 A convenient choice for ϖ

Next, note that

$$\mathbf{v}\cdot\nabla\mathbf{v} = \mathbf{v}\cdot\nabla(\mathbf{w}+\mathbf{v}_{\text{P}}) = \mathbf{v}\cdot\nabla\mathbf{w} + \mathbf{w}\cdot\nabla\mathbf{v}_{\text{P}} + \frac{1}{2}\,\nabla v_{\text{P}}^2. \tag{4.13}$$

Therefore, a convenient choice for ϖ is[4]

$$\varpi = \frac{1}{2}\,v_{\text{P}}^2 = \frac{1}{2}\,\|\nabla\varphi\|^2. \tag{4.14}$$

[3] It should be pointed out that the formulation presented here is based upon the following choices: (*i*) to set $\mathbf{v}(\mathbf{x},t) = \mathbf{v}_{\text{P}}(\mathbf{x},t) + \mathbf{w}(\mathbf{x},t)$, Eq. 4.6, and (*ii*) to set the first and second parts in Eq. 4.9 separately equal to zero, so as to obtain Eqs. 4.10 and 4.11. Here, these choices appear to be completely arbitrary, albeit convenient. However, as shown in Ref. [31], these choices stem "naturally" from (namely, as a direct consequence of) the standard utilization of the boundary integral equation method for systems of differential equations. Specifically, using such an approach, one obtains Eq. 4.6, as well as Eqs. 4.10 and 4.11 – hence, the name "natural velocity decomposition". However, such an approach (namely the utilization of the boundary integral equation method for systems of differential equations) requires lengthy mathematical manipulations that obscure the simplicity of the end result (see Ref. [31], Section 3, for incompressible viscous flows). Accordingly, here we have preferred to use the present approach, referring the reader to Ref. [31], for the details of the proof of the "ineluctability" of the above choices.

[4] This is the choice in Ref. [31], which is addressed in this chapter. An alternate, equally convenient (and only recently introduced), choice is discussed in Appendix B. Some comments appear in order. As we can see from Eq. 4.17, for inviscid flows the above choice for ϖ yields $\mathbf{w}(\mathbf{x},t) = \mathbf{0}$, *for all the material points with* $\mathbf{w}(\mathbf{x},0) = \mathbf{0}$ (the same holds true for the alternate choice discussed in Appendix B). The effect of the viscosity is to broaden the region (akin to what happens to the vorticity); however, the decay at infinity is exponential. This is a considerable advantage, because the computational region may be reduced considerably. Other choices for ϖ might give $\mathbf{w} \neq \mathbf{0}$ even for those material points for which initially we have $\mathbf{w} = \mathbf{0}$, with decay that is not exponential (this is true in particular for the choice $\varpi = 0$).

In this way, Eq. 4.10, integrated, yields, using Eq. 4.12,

$$\partial_t \varphi + \frac{1}{2} \|\nabla \varphi\|^2 + \frac{p}{\rho} - \nu \nabla^2 \varphi = \frac{p_\infty}{\rho}, \tag{4.15}$$

which is an *extension of Bernoulli's theorem to incompressible viscous flows*. Note the similarity of Eq. 4.15 with the Bernoulli theorem for incompressible potential flows,

$$\partial_t \phi + \frac{1}{2} \|\nabla \phi\|^2 + \frac{p}{\rho} = \frac{p_\infty}{\rho}. \tag{4.16}$$

The difference is only due to the term $-\nu \nabla^2 \varphi$. Note that $\nabla^2 \varphi = -\nabla \cdot \mathbf{w}$, Eq. 4.8. Therefore, in those points where $\mathbf{w} = \mathbf{0}$, Eq. 4.15 reduces to the Bernoulli theorem for incompressible potential flows.

On the other hand, Eq. 4.11 yields

$$\frac{\mathrm{D}\mathbf{w}}{\mathrm{D}t} + \mathbf{w} \cdot \nabla \mathbf{v}_{\mathrm{P}} = \nu \nabla^2 \mathbf{w}, \tag{4.17}$$

where $\mathrm{D}/\mathrm{D}t := \partial_t + \mathbf{v} \cdot \nabla$ denotes the substantial derivative.

For future reference, we rewrite Eq. 4.17 as

$$\partial_t \mathbf{w} = \mathbf{g}(t, \mathbf{w}, \mathbf{v}_{\mathrm{P}}), \tag{4.18}$$

where

$$\mathbf{g}(t, \mathbf{w}, \mathbf{v}_{\mathrm{P}}) := -\mathbf{v} \cdot \nabla \mathbf{w} - \mathbf{w} \cdot \nabla \mathbf{v}_{\mathrm{P}} + \nu \nabla^2 \mathbf{w}. \tag{4.19}$$

4.2.2 Boundary and initial conditions

We now have four unknowns, $\varphi(\mathbf{x}, t)$ and $w_k(\mathbf{x}, t)$ $(k = 1, 2, 3)$, to describe the velocity. Correspondingly, we have four coupled equations, namely Eq. 4.8 (which, as we will see, can be treated as an equation for φ, with σ known), and Eq. 4.17 (which can be treated as an equation for $\mathbf{w}$, with $\mathbf{v}_{\mathrm{P}} = \nabla \varphi$ known).

As a consequence, we need to add a fourth boundary condition to the three we already have, namely $\mathbf{v}(\mathbf{x}, t) = \mathbf{v}_{\mathrm{B}}(\mathbf{x}, t)$, Eq. 4.3. In order to obtain a fourth boundary condition, we split the normal component of Eq. 4.3 into two. Specifically, we choose the following boundary condition for the normal component of $\mathbf{w}$:

$$\mathbf{w} \cdot \mathbf{n} = 0 \qquad (\mathbf{x} \in \mathcal{S}_{\mathrm{B}}). \tag{4.20}$$

Correspondingly, Eq. 4.3 yields

$$\frac{\partial \varphi}{\partial n} = \chi := \mathbf{v}_{\mathrm{B}} \cdot \mathbf{n} \qquad (\mathbf{x} \in \mathcal{S}_{\mathrm{B}}). \tag{4.21}$$

On the other hand, for the tangential components, we use Eq. 4.3 as such, namely, combining with Eq. 4.6,

$$\mathbf{w} \cdot \mathbf{t}_k + \frac{\partial \varphi}{\partial s_k} = \mathbf{v}_{\mathrm{B}} \cdot \mathbf{t}_k \qquad (\mathbf{x} \in \mathcal{S}_{\mathrm{B}}). \tag{4.22}$$

where $\mathbf{t}_k$ $(k = 1, 2)$ denotes two different tangential unit vectors, whereas $\partial / \partial s_k$ denotes the directional derivative along the direction $\mathbf{t}_k$.

Finally, in reference to the initial conditions, we set

$$\mathbf{w}(\mathbf{x}, 0) = \mathbf{0} \qquad (\mathbf{x} \in \mathcal{V}). \tag{4.23}$$

which implies $\varphi(\mathbf{x}, 0) = 0$, as already stated in Eq. 4.12.

4.3 Method of solution

Here, we summarize the results obtained in the preceding subsections and discuss how the formulation thereby obtained may be implemented from a computational point of view. As shown above, the velocity may decomposed into two terms, as $\mathbf{v} = \mathbf{w} + \nabla\varphi$ (Eq. 4.6), where $\mathbf{w}$ satisfies Eq. 4.17 (which however depends upon φ, through $\mathbf{v}_{\text{P}}$); on the other hand, φ satisfies Eq. 4.8, which may be written as (Poisson equation)

$$\nabla^2\varphi = \sigma_\varphi \tag{4.24}$$

which however depends upon $\mathbf{w}$, since

$$\sigma_\varphi = -\nabla\cdot\mathbf{w} \tag{4.25}$$

Boundary integral formulation for φ

In the following, we will use the standard boundary integral equation method for the Poisson equation (see Subsection 2.1.1), we have, for $\mathbf{x}\in\mathcal{V}$, the boundary integral representation, namely

$$\varphi(\mathbf{x},t) = \oint_{\mathcal{S}_{\text{B}}} \left(\chi\, G - \varphi\,\frac{\partial G}{\partial n}\right) \mathrm{d}\mathcal{S}(\mathbf{y}) + \int_{\mathcal{V}} \sigma_\varphi\, G\,\mathrm{d}\mathcal{V}(\mathbf{y}). \tag{4.26}$$

As $\mathbf{x}$ tends to $\mathcal{S}$, Eq. 4.26 yields a boundary integral equation, namely

$$\frac{1}{2}\,\varphi(\mathbf{x},t) = \oint_{\mathcal{S}_{\text{B}}} \left(\chi\, G - \varphi\,\frac{\partial G}{\partial n}\right) \mathrm{d}\mathcal{S}(\mathbf{y}) + \int_{\mathcal{V}} \sigma_\varphi\, G\,\mathrm{d}\mathcal{V}(\mathbf{y}). \tag{4.27}$$

This provides a linear relationship between $\varphi(\mathbf{x},t)$ and $\chi(\mathbf{x},t)$ on $\mathcal{S}_{\text{B}}$ and $\sigma_\varphi(\mathbf{x},t) = -\nabla\cdot\mathbf{w}$ in $\mathcal{V}$. Recall that $\chi(\mathbf{x},t) = \partial\varphi/\partial n$ on $\mathcal{S}_{\text{B}}$ is known from $\chi(\mathbf{x},t) := \mathbf{v}_{\text{B}}\cdot\mathbf{n}$, Eq. 4.21. Hence, Eq. 4.27 may be used to obtain $\varphi(\mathbf{x},t)$ on $\mathcal{S}_{\text{B}}$, provided that $\sigma(\mathbf{x},t)$ in $\mathcal{V}$ is known. Once φ on $\mathcal{S}_{\text{B}}$ is known, Eq. 4.26 may be used to obtain φ (and hence $\mathbf{v}_{\text{P}}$, as well as p) everywhere in $\mathcal{V}$, of course provided again that σ in $\mathcal{V}$ is known.

Time discretization

Consider first the discretization with respect to time. Let $t_r = r\,\Delta t$, with $r = 0, 1, \ldots$, denote the generic time step. We begin with the fact that $\mathbf{w}(\mathbf{x},t_0) = \mathbf{w}(x,0) = \mathbf{0}$ is known (see Eq. 4.23), and show how to obtain $\mathbf{w}(\mathbf{x},t_1)$ and, from this, $\mathbf{w}(\mathbf{x},t_2)$. Of course, in the same way we can then obtain $\mathbf{w}(\mathbf{x},t_3)$, and then $\mathbf{w}(\mathbf{x},t_4)$, and so on.

Indeed, from $\mathbf{w}(\mathbf{x},t_0) = \mathbf{0}$, we have $\sigma(\mathbf{x},t_0) = 0$. Hence, Eq. 4.27 may be used to obtain $\varphi(\mathbf{x},t_0)$ on $\mathcal{S}_{\text{B}}$, since $\chi(\mathbf{x},t_0)$ on $\mathcal{S}_{\text{B}}$ and $\sigma(\mathbf{x},t_0)$ in $\mathcal{V}$ are known (indeed, $\chi(\mathbf{x},t_0) = \mathbf{v}_{\text{B}}\cdot\mathbf{n}$, Eq. 4.21, whereas $\sigma(\mathbf{x},t_0) = 0$). Then, Eq. 4.26 may be used to obtain $\varphi(\mathbf{x},t_0)$ (and hence $\mathbf{v}_{\text{P}}(\mathbf{x},t_0)$) everywhere in $\mathcal{V}$, again because $\chi(\mathbf{x},t_0)$ on $\mathcal{S}_{\text{B}}$ and $\sigma(\mathbf{x},t_0)$ in $\mathcal{V}$ are known.

Next, consider Eq. 4.18. Using the Euler explicit integration scheme, this may be discretized into[5]

$$\mathbf{w}^{(r+1)} = \mathbf{w}^{(r)} + \Delta t\,\mathbf{g}(t_r, \mathbf{w}^{(r)}, \mathbf{v}_{\text{P}}^{(r)}) \tag{4.28}$$

This allows us to obtain $\mathbf{w}(\mathbf{x},t_1)$.

[5] Of course, the Euler explicit scheme is used here simply for the sake of simplicity in order to illustrate the step–by–step procedure. Other schemes (such as Runge–Kutta and/or implicit schemes) may be used as well. The scheme used for the numerical results (namely the semi–implicit Euler scheme, also known as Crank–Nicolson scheme, applied only to the linear portion of the equation) is discussed in Appendix C (see Section C.4, without corrector).

It should be noted that from $\mathbf{w}(\mathbf{x}, t_1)$ we may now evaluate $\sigma(\mathbf{x}, t_1)$. Hence, using the same sequence of operations used in the first time step, we can obtain, $\varphi(\mathbf{x}, t_1)$ on $\mathcal{S}_{\text{B}}$, then $\varphi(\mathbf{x}, t_1)$ (and hence $\mathbf{v}_{\text{P}}(\mathbf{x}, t_1)$) everywhere in $\mathcal{V}$. Therefore, Eq. 4.28, with $r = 1$, allows us to obtain $\mathbf{w}(\mathbf{x}, t_2)$. In this way we may proceed and obtain the solution for the velocity for any time t_r.

Space discretization

It goes goes without saying that the space discretization is also required. Equations 4.26 and 4.27 are discretized by boundary element approach (specifically, a third order discretization for the surface integrals and a first order discretization for the volume integral). On the other hand, the expression for $\mathbf{g}(t, \mathbf{w}, \mathbf{v}_{\text{P}})$, in Eq. 4.19, is approximated by central finite differences; these are also used for $\mathbf{v}_{\text{P}} = \nabla\varphi$ and $\sigma = \nabla \cdot \mathbf{w}$.

Comments

Note that, from the discussion presented in the preceding section, we may infer that the resulting system of equations needs to be solved only in the vortical region, $\mathcal{V}_{\zeta}$. Note that $\mathbf{w}$ vanishes exponentially at infinity; hence, it may be neglected beyond a suitable outer boundary, that surrounds body and wake; the boundary condition on such a boundary is $\mathbf{w} = \mathbf{0}$. Also, the method does not appear to be affected by well–known complexities of other schemes – such as those related to the solenoidality of $\mathbf{v}$ for the incompressible Navier-Stokes equations, or that of $\boldsymbol{\zeta}$ for the vorticity transport equation, or those related to the boundary conditions for $\boldsymbol{\zeta}$.

Pressure field

Finally, note that, again from the discussion presented in the preceding section, we may observe that the velocity field may be obtained independently of the pressure field. In addition, once the velocity field has been obtained using the above procedure, the pressure may be evaluated by using the *generalized Bernoulli theorem for viscous incompressible fields*, which for $\mathbf{x} \in \mathcal{V}$ is given by, again in the air frame, Eq. 4.15.

4.4 Validation and assessment

The natural velocity decomposition has been introduced only recently, hence the primary objective has been the validation and assessment of the formulation.

As mentioned in the introduction, Chapter 1, a very preliminary validation of the methodology has been presented in Ref. [17]. A more exhaustive formulation is presented here. To accomplish this, the natural decomposition has been applied to the study of the flow around an infinite cylinder, since this case has been extensively examined in the past and therefore many results are available in the literature.

A polar grid has been generated around a cylinder of unit radius positioned in the center of the grid (Figure 4.1, p. 38). A stretch has been applied in the radial direction in order to increase the resolution close to the body surface. In Figure 4.2, p. 39, it is possible to observe such stretch as well has the scale factor along the radial direction. Then, we have assumed a constant body velocity of $\mathbf{v} = -\mathbf{i}$. The implementation scheme is reported in Figure 4.3, p. 39, where it is possible to note how the various steps described in the preceding theoretical section follow one another. The details of the various time–stepping integration methods used for the solution of the $\mathbf{w}$ equation (Eq. 4.17) are addressed in Appendix C.[6]

[6]Here, we would only like to mention that we have used both the explicit (Section C.1) and the semi–implicit scheme (Section C.2), albeit limited to the linear portion of Eq. 4.18 (namely the viscous term, $\nu\nabla^2\mathbf{w}$ (see also

Several Reynolds numbers (between 10 and 40, hence below the critical Reynolds number) we have tested. The results obtained are in good agreement with those available in the literature. The recirculation bubble's length is compared in Figure 4.4, p. 40, while the separation angle comparison can be found in Figure 4.5, p. 41. Moreover, for the case of $Re_{\text{D}} = 30$, we present several interesting results. The evolution of the velocity magnitude (Figure 4.6, p. 42) as well as the final steady–state velocity vectors and velocity magnitude (Figure 4.7, p. 42). The convergence of the length of the recirculation bubble (Figure 4.8, p. 43). Also, the **w** vectors (Figure 4.9, p. 43) and the vorticity contours (Figure 4.10, p. 44) are shown. It is possible to notice two counter-rotating vortices close to the trailing edge of the cylinder. Those vortices eventually become unstable and are those leading to the von Kármán instability.

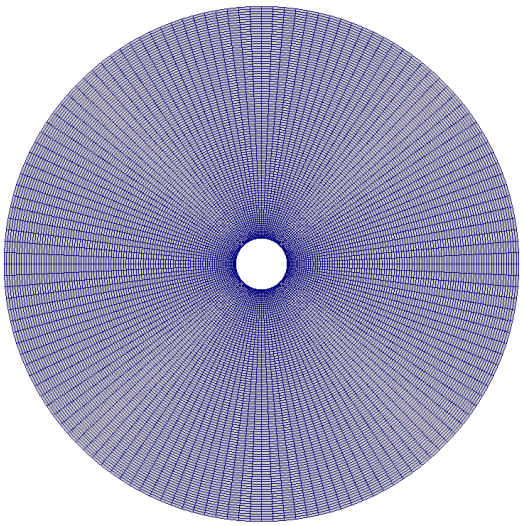

Figure 4.1: Mesh around the infinite cylinder

Footnote 5, p. 36). Although these schemes are both adequately stable and provide a good accuracy, it may be worth noting that considerable computing–time reduction may be obtained with the use of the ADI (alternate direction implicit) scheme (Section C.5); indeed, the resulting matrices are block diagonal (this is true even if one does not take advantage of the fact that they are tridiagonal). Moreover, the amount of memory necessary is largely reduced if we take into consideration that instead of having to invert the matrix of the Laplacian for the whole domain, one can work with a single radius and a single azimuth matrix, since all the radius are similar while all the azimuth are simply scaled.

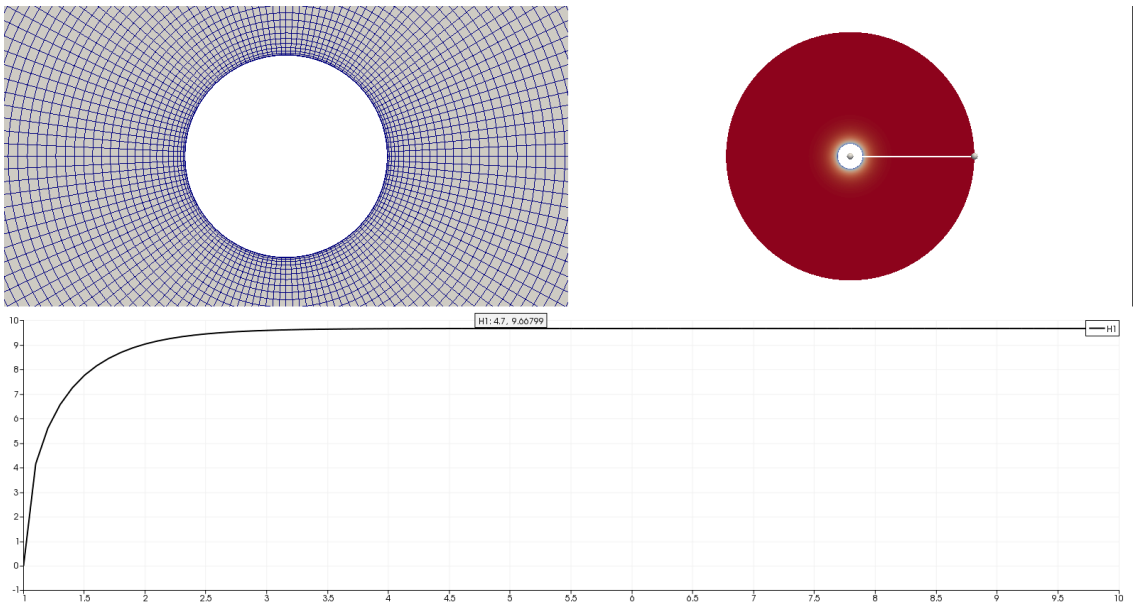

Figure 4.2: Grid stretching in the radial direction

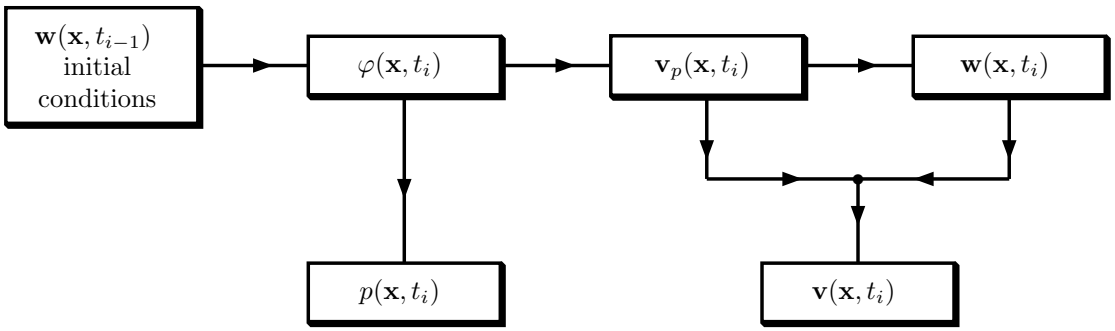

Figure 4.3: Natural decomposition implementation scheme

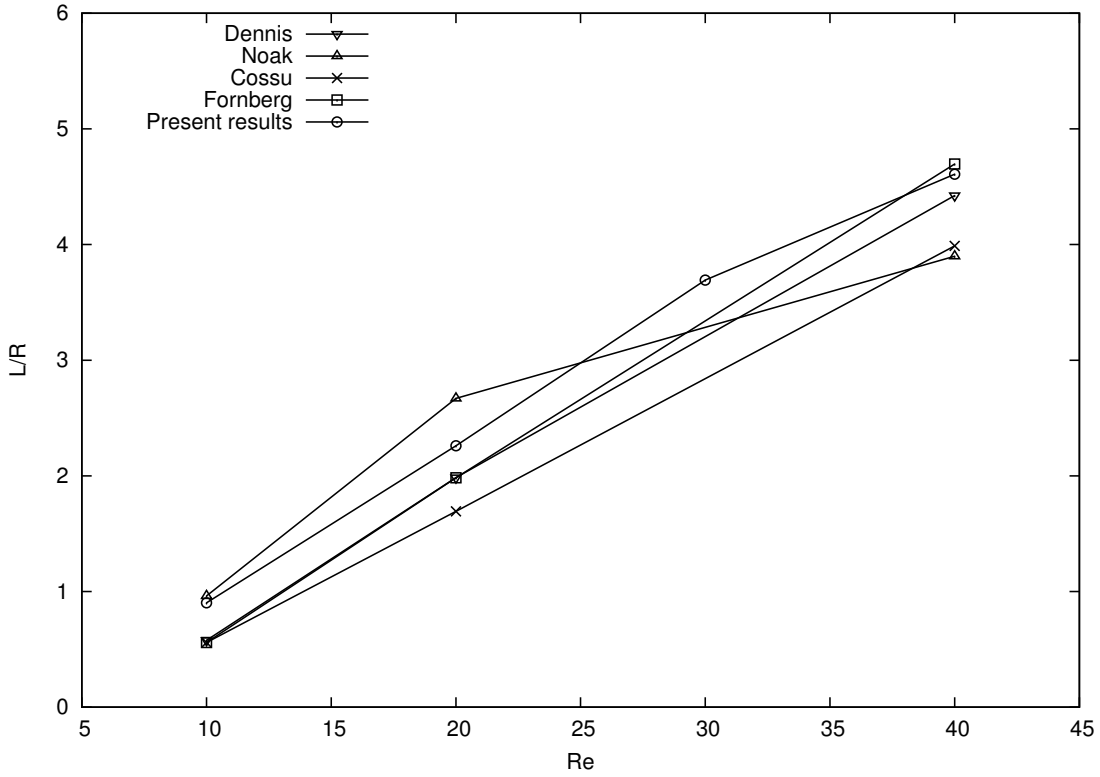

Figure 4.4: Length of recirculation bubble

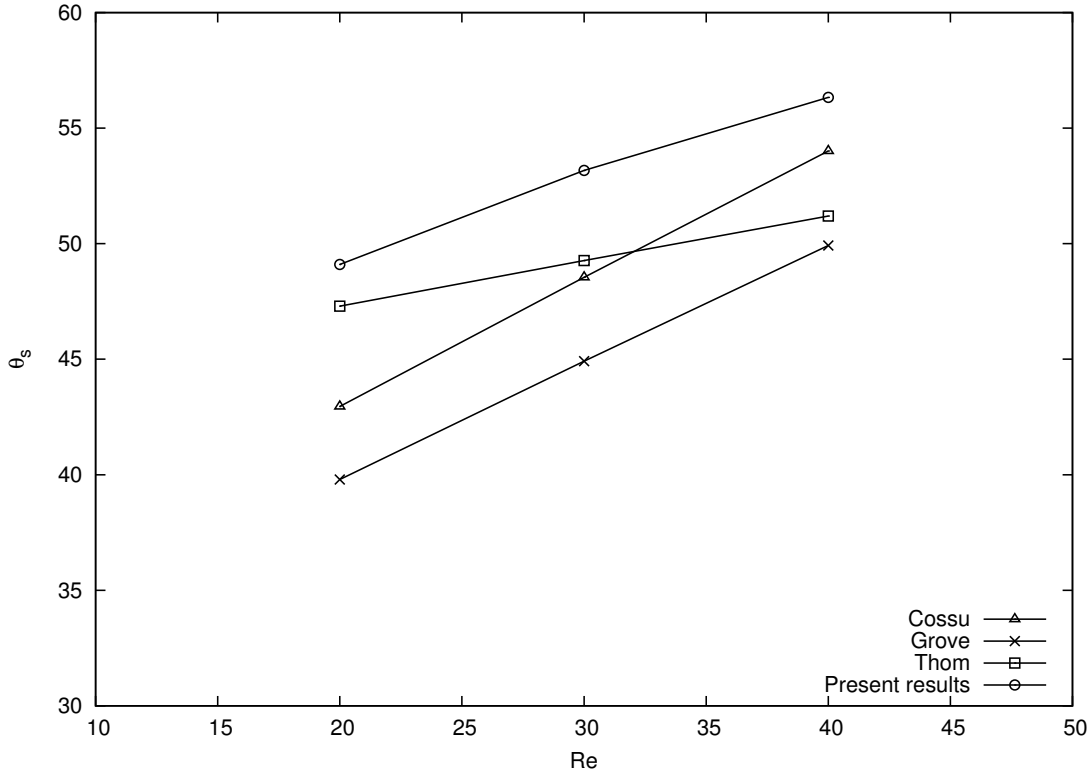

Figure 4.5: Separation angle

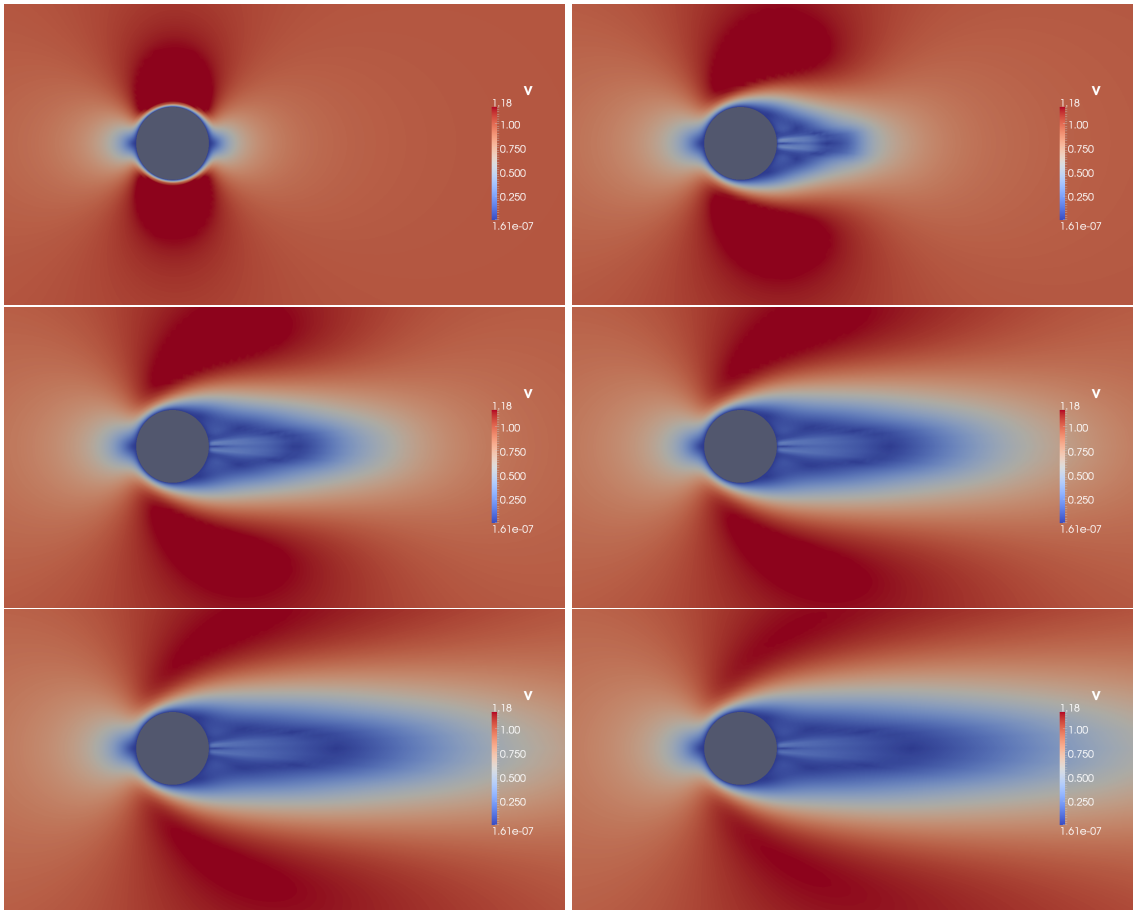

Figure 4.6: Evolution of the velocity around the cylinder at $Re_{\mathrm{D}} = 30$ (from right-to-left and top-to-bottom) after 0, 600, 1200, 1800, 2400 and 3000 timesteps

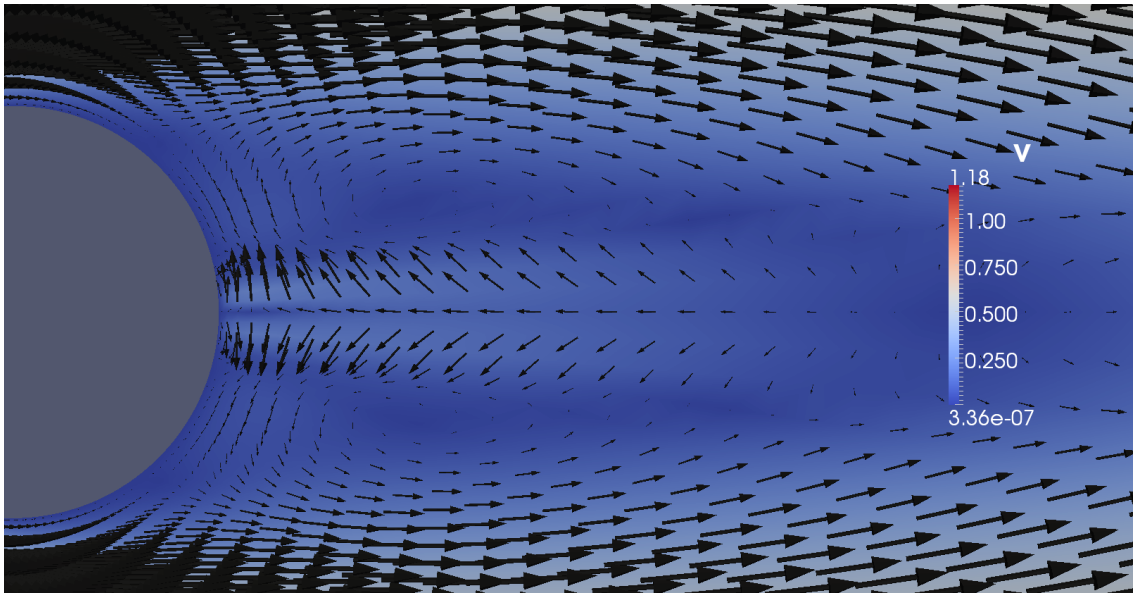

Figure 4.7: Steady velocity vectors behind the cylinder at $Re_{\mathrm{D}} = 30$

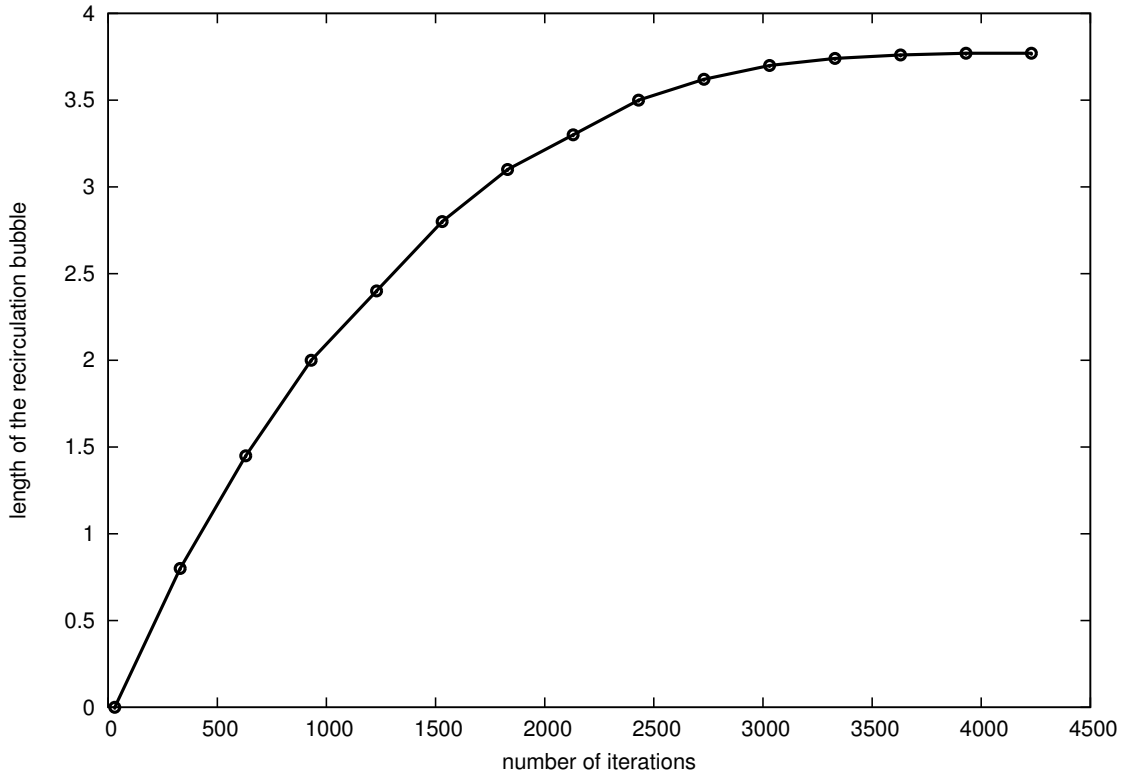

Figure 4.8: Convergence of the recirculation bubble's length at $Re_{\text{D}} = 30$

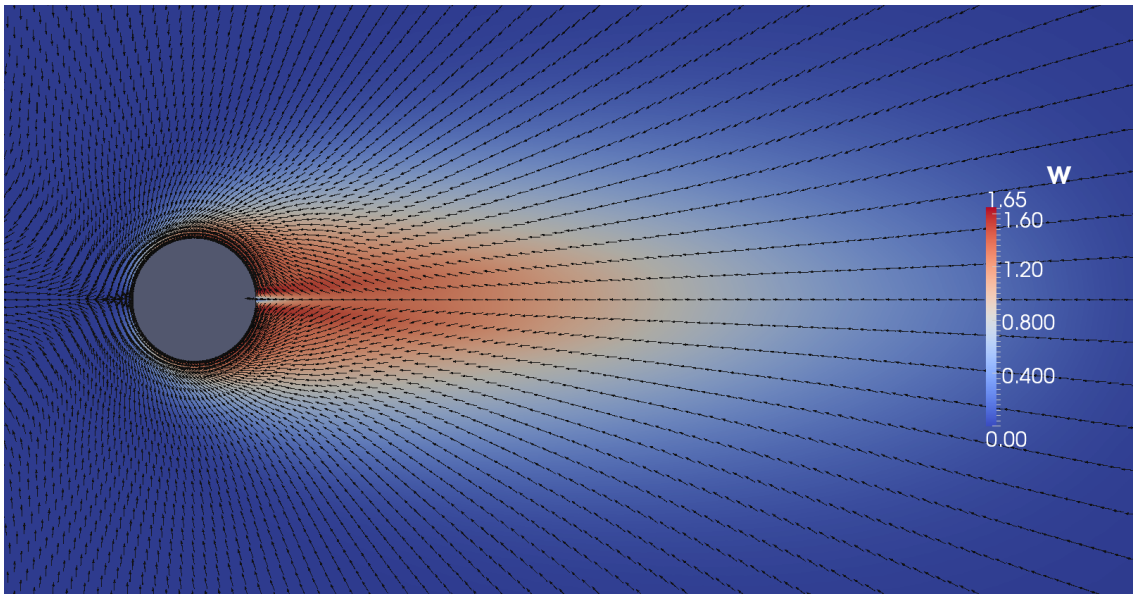

Figure 4.9: Steady $\mathbf{w}$ vectors around the cylinder at $Re_{\text{D}} = 30$

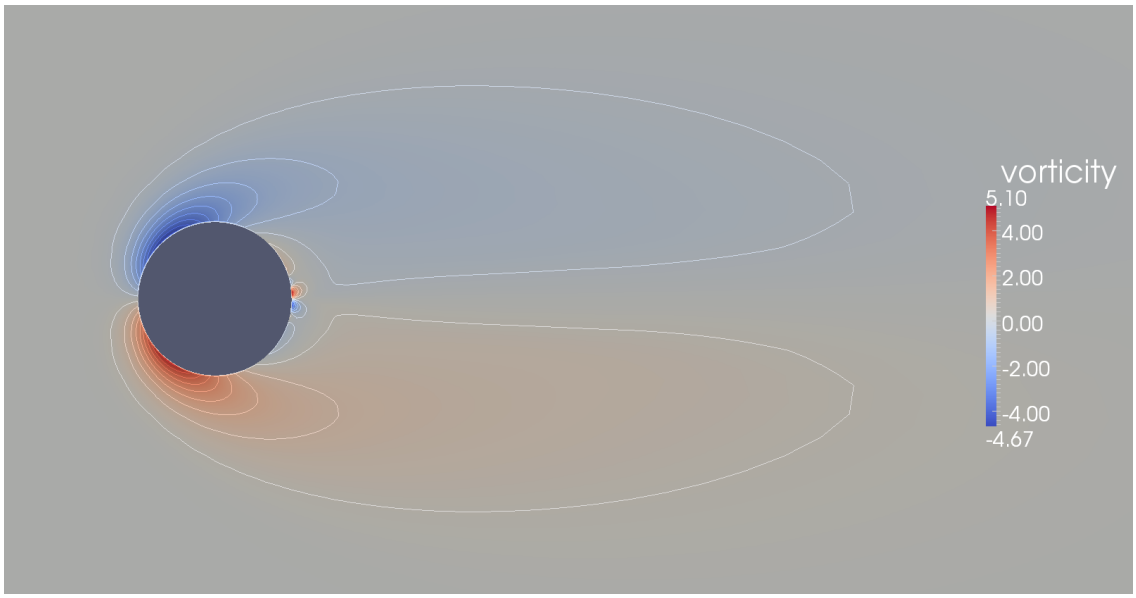

Figure 4.10: Steady vorticity contour around the cylinder at $Re_{\mathrm{D}} = 30$

Chapter 5

Concluding remarks

Here, we present a summary of the work presented in the main body of this thesis. In addition, we provide comments related to Appendices A and B.

5.1 Summary of work

Vortex flows have been analyzed through the use of three different methodologies. By focusing on the aerodynamic and aeroacoustic study of a jet, we were able to identify three distinct vortical regions. A region where the vorticity is found to be concentrated in a thin layer, a region where the vorticity is distributed into a spatially bounded volume and finally a region (more precisely two regions, see Chapter 1) where viscosity plays a major role thus the vorticity is diffused in the field.

Then, specific methodologies have been introduced to analyze each of the three regions. A quasi–potential formulation has been used to study the first vortex–layer flows. A methodology based on the time–invariance of the contravariant component of the vorticity in Euler flows has was chosen to examine the second region, where the vorticity is distributed yet confined. Finally, the natural velocity decomposition was adopted to examine problems where viscosity effects cannot be neglected.

Within the framework of aeronautical jets, the aim of the first part of this work is to capture the phenomenon occurring in the area just downstream of a jet nozzle utilizing a quasi–potential formulation. In that region, the difference between the jet velocity and the outer flow velocity leads to the well known Kelvin–Helmholtz instability. The quasi–potential formulation used here is closely related to that already extensively exploited for the study of both fixed and rotating wings. Thus, after having briefly discussed its standard theoretical approach, details of its tuning to the novel application have been given. Afterwards, the extended quasi–potential formulation has been used to analyze the incompressible flow around a three–dimensional axisymmetric jet. To this end, a non–permeable nacelle–like body containing two inner permeable surfaces (inlet and outlet) has been modelled. The results obtained have been successfully compared to some experimental ones thereby proving that the Kelvin–Helmholtz instability is mainly governed by the convection of the vorticity. Velocity and pressure have been measured in a field point located outside the jet and their respective Strouhal number has been evaluated.

The second methodology, based on the time invariance of the material contravariant component of the vorticity in Eulerian flows, may be used to model any inviscid vortex flow where the vorticity spatial distribution is bounded. Accordingly, a steady inviscid vortex ring has been modelled and examined. Such vortex ring model stems from a well known family of stable vortex rings that are described by the parameter α that represents the mean dimensionless radius of the

ring core. The model has been validated by the evaluation of the translation velocity of a stable vortex ring. In order to better understand the second region of a typical jet, where coherent structures similar to vortex rings appear, become unstable and break down, the vortex ring has been subjected to different perturbations. Both azimuthal and core perturbations have been studied and the evolution of the unperturbed and perturbed ring are presented.

Finally in order to complete the study of an aeronautical jet, a third methodology was introduced. This methodology enables the analysis of incompressible viscous flows. Such methodology is based upon the novel *natural velocity decomposition* and has several advantages among which: the absence of the pressure in the evaluation of the velocity, the use of computational domain for the analysis of the rotational part of the decomposition limited to the rotational region, the use of a boundary element for the potential part and the use of a primitive variable formulation (not requiring the evaluation of the vorticity). Before applying this formulation to the analysis of jets, a validation is required. In order to validate this methodology, the incompressible flow around an infinite cylinder was examined. Results such has the length of the re–circulation bubble and the separation angle were evaluated for several Reynolds numbers and compared with results available in the literature. Due to the accuracy of the obtained results, the methodology is considered as validated.

The three methodology introduced in this work have given very encouraging results, thereby showing their effectiveness in the study of vortex flows. Each methodology has its own strength and is particularly suited to the study of its corresponding vortex flow.

5.2 Comments

The positive results obtained so far should encourage further developments of the three methodologies to either improve or extent their current application.

The main advantage of the first methodology is its efficiency in the modelling of the Kelvin–Helmholtz instability of an incompressible jet. An improvement could be obtained by increasing the order of accuracy of the solution. Indeed a third–order solution would enable to obtain both a smoother surface and removing some numerical singularities present in the zeroth–order formulation used here. Another improvement could be obtained by using a more efficient integration scheme, such as the a predictor–corrector scheme (discussed in Section C.4) or even a Runge–Kutta scheme.

Regarding the second methodology used, to further investigate the instability of the coherent structures, typically found in jets, it would be possible to include the effects of viscosity. The theoretical approach has already been discussed (see Footnote 2, p. 23), but not yet implemented. Here as well, improvements could be obtained by using the linearly–implicit predictor–corrector scheme discussed in Section C.4. Additional improvements are discussed below, in relationship with the material presented in Appendix B (see Section 5.3).

The computational time of the third methodology could be reduced considerably by using different grids in the solution of the potential and rotational parts. Indeed, the evaluation of the field integral in the analysis of potential part is required only in the region where the divergence of $\mathbf{w}(\mathbf{x}, t)$, $\sigma(\mathbf{x}, t)$, is not negligible (see Figures 5.1, pp. 47); this happens to be much smaller than the region where $\mathbf{w}$ is not negligible. This is especially true if a third–order discretization is introduced in the evaluation of the field integrals, since in this case the fact that σ varies smoothly also plays an important role. An additional improvement of the efficiency of the formulation may be obtained by the use of the ADI (Alternating Direction Implicit) method, discussed in Section C.5. Moreover, the formulation has only been tested in a two–dimensional domain and a extension to a three-dimensional application, such as a sphere, would be in order before its usage for the study of more complicated phenomenons like an aeronautical jet (or even airframe noise). One last remark has to be made on the possibility of using this methodology to study compressible flows; indeed, even though the natural decomposition has been applied, in this work, to an incompressible

flow, this methodology is also valid for compressible flows (see Ref. [31], Section 5).

5.3 A unified approach

Finally, we want to discuss how the material presented in Appendix A and B may be used to provided a unified approach for the solution of the three stages of the jet development, as proposed in Ref. [37].

In Appendix A, we discuss how the quasi–potential flow formulation of Chapter 2 may be obtained from the natural decomposition in the limit as the vortex–layer thickness tends to zero. This would provide a unified formulation for the first, second and fourth stage of the jet development.

In Appendix B, an alternate choice for the function ϖ is presented and, akin two the second formulation with vorticity, it is discussed how, in an inviscid flow, the material covariant components of the rotational part remain constant in time. This applies also to the material presented in Appendix A. The promising results obtained in Appendix B have led us to believe that any future development of the present work will follow the direction depicted in the appendices (see, for instance, Ref. [37]).

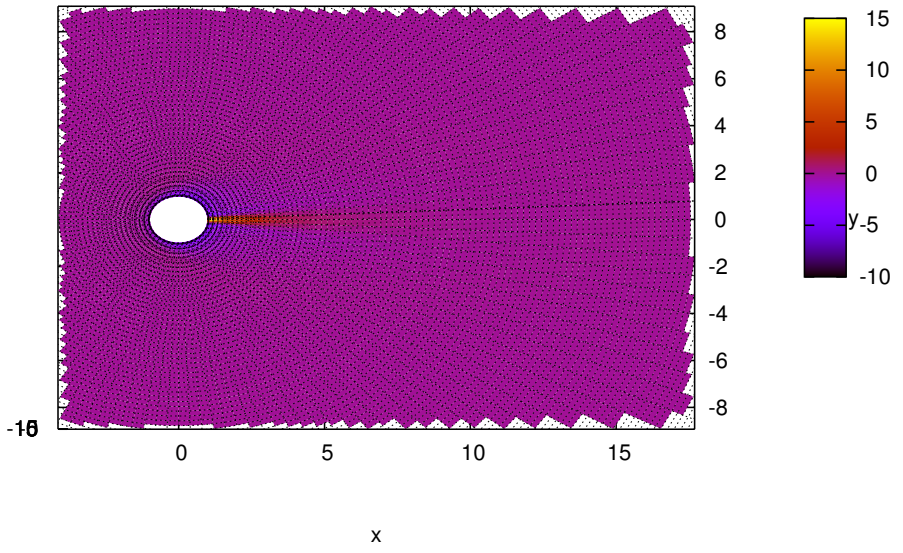

Figure 5.1: Extention of σ in the case of $Re_{\text{D}} = 30$

Bibliography

[1] Batchelor, G.K., *An Introduction to Fluid Dynamics*, Cambridge University Press, Cambridge, UK, 1967.

[2] Casciola, C.M., Piva, R., *A Lagrangian approach for vorticity intensification in swirling rings*, Computational Mechanics, 21, pp. 276–282, 1998.

[3] Chorin, A.J., Marsden, J.E., *A Mathematical Introduction to Fluid Mechanics*, 2nd Ed., Springer Verlag, New York, NY, 1990.

[4] Chorin, A.J., *Vorticity and Turbulence*, Applied Mathematical Sciences, Springer, 1994.

[5] Crank, J., Nicolson, P., *A practical method for numerical evaluation of solutions of partial differential equations of the heat conduction type*, Proc. Camb. Phil. Soc., 43(1), pp. 50–67, 1947.

[6] Crow, S.C., Champagne, F.H., *Orderly structure in jet turbulence*, Journal of Fluid Mechanics, 48(03), pp. 547–591, 1971.

[7] Dessi, D., Mastroddi, F., Morino, L., *Normal–Form Analysis of Hopf Bifurcation Beyond the Center Manifold Approximation*, Euromech Colloqium, 2004.

[8] Fraenkel, L. E., *Examples of steady vortex rings of small cross–section in an ideal fluid*, Journal of Fluid Mechanics, 51, pp. 119–135, 1972.

[9] Helmholtz, H., *ber Integrale der hydrodynamischen Gleiehungen, welche den Wirbelwegungen entsprechen*, J. Reine Angew. Math, 55, pp. 25–55, 1858.

[10] Hess, J., Smith, A.M.O., *Calculation of Non–Lifting Potential Flow About Arbitrary Three–Dimensional Bodies*, Journal of Ship Research, Vol. 8, No. 2, pp. 22–44, 1964.

[11] Howe, M.S., *Theory of vortex sound*, Cambridge University Press, 2003.

[12] Kellog, O.D., *Foundations of Potential Theory*, Fredrick Ugar, New York, NY, 1929 (also available as Dover Ed., 1953).

[13] Kambe, T., *Vortex sound with special reference to vortex rings: theory, computer simulations, and experiments.* International Journal of Aeroacoustics, 35(1), pp. 488–89, 2010.

[14] Kop'ev, V.F., Chernyshev, S.A., *Vortex ring eigen–oscillations as a source of sound*, Journal of Fluid Mechanics, 341, pp. 19–57, 1997.

[15] Kop'ev, V.F., Chernyshev, S.A., *Vortex ring oscillations, the development of turbulence in vortex rings and generation of sound*, Physics–Uspekhi, 43(7), pp. 663–690, 2000.

[16] Kress, R., *Linear Integral Equations*, Springer, New York, NY, 1989.

[17] Leotardi, C. , *An Innovative Decomposition of the Velocity Field with the Corresponding Generalized Bernoulli Theorem for Viscous Flows*, Doctoral Thesis, Università Roma Tre, Scuola Dottorale di Ingegneria, Sezione di Ingegneria Meccanica, 2011.

[18] Leung, R.C.K., Ko, N.W.M., *A Study of Inviscid Vortex Ring Core Instability using Contour Dynamics*, Proc. of the 4th World Congress on Computational Mechanics, Idelsohn, S., Oñate, E., Dvorkin, E., CIMNE, Barcelona, 1998.

[19] Lighthill, M.J., *On Displacement Thickness*, Journal of Fluid Mechanics, Vol. 4, pp. 383–392, 1958.

[20] Lim, T.T., Nickels, T.B., *Vortex rings*, Fluid Vortices, in S. I. Green, Kluwer, 1995.

[21] Maxworthy, T., *The structure and stability of vortex rings*, Journal of Fluid Mechanics, 51(1), pp. 15–32, 1972.

[22] Maxworthy, T., *Some experimental studies of vortex rings*, Journal of Fluid Mechanics, 81(3), pp. 465–495, 1977.

[23] Morino, L., *A General Theory of Unsteady Compressible Potential Aerodynamics*, NASA CR–2464, 1974.

[24] Morino, L., *Material Contravariant Components: Vorticity Transport and Vortex Theorems*, AIAA Journal, 24(3), pp. 526–528, 1986.

[25] Morino, L., *Helmholtz Decomposition Revisited: Vorticity Generation and Trailing Edge Condition, Part 1: Incompressible Flows*, Computational Mechanics, Vol. 1, No. 1, pp. 65–90, 1986.

[26] Morino, L., *Helmholtz and Poincaré Potential–Vorticity Decompositions for the Analysis of Unsteady Compressible Viscous Flows*, Boundary Element Methods in Nonlinear Fluid Dynamics, Vol. 6 of Developments in Boundary Element Methods, in P. K. Banerjee and L. Morino (Eds.), Elsevier Applied Science, 1990.

[27] Morino, L. *Boundary Integral Equations in Aerodynamics*, Applied Mechanics Reviews, Vol. 46, No. 8, pp. 445–466, 1993.

[28] Morino, L., *Is There a Difference Between Aeroacoustics and Aerodynamics? An Aeroelastician's Viewpoint*, AIAA Journal, 41(7), pp. 1209–1223, 2003.

[29] Morino, L., *Boundary Elements in Primitive Variables and FWH Equation Revisited – Viscosity Effect*, 10th AIAA/CEAS Aeroacoustics Conference, Manchester, UK, AIAA Paper 2004–2890, 2004.

[30] Morino, L., *From Primitive–Variable Boundary–Integral Formulation to FWH Equation*, 12th AIAA/CEAS Aeroacoustics Conference, Cambridge, MA, AIAA Paper 2006–2485, 2006.

[31] Morino, L., *A Primitive–Variable Boundary Integral Formulation Unifying Aeroacoustics and Aerodynamics, and a Natural Velocity Decomposition for Vortical Fields*, International Journal of Aeroacoustics, 10(2–3), pp. 295–400, 2011.

[32] Morino, L., Bernardini, G., *Singularities in BIE's for the Laplace equation; Joukowski trailing–edge conjecture revisited,* Engineering Analysis with Boundary Elements, Vol. 25, pp. 805–818, 2001.

[33] Morino, L., Bernardini, G., Caputi-Gennaro, G., *A vorticity formulation for computational fluid dynamic and aeroelastic analyses of viscous flows*, Journal of Fluids and Structures, 25(8), pp. 1282–1298, 2009.

[34] Morino, L., Camussi, R., Bernardini, G., Gradassi, P., Onori, M., *A simple, but efficient aeroacoustic model of jets*, 18th AIAA/CEAS Aeroacoustics Conference, Colorado Springs, CO, AIAA Paper 2012–2164 2012.

[35] Morino, L., Corbelli, A., Tseng, K., *A Primitive Variable Boundary Element Formulation for the Euler Equations in Aeroacoustics of Rotors and Propellers*, 5th AIAA/CEAS Aeroacoustics Conference, Bellevue, WA, AIAA Paper 99–0399, 1999.

[36] Morino, L., Gennaretti, M., *Boundary Integral Equation Methods for Aerodynamics*, Computational Nonlinear Mechanics in Aerospace Engineering, in S. N. Atluri (Ed.), Progress in Aeronautics and Astronautics, Vol. 146, American Institute of Aeronautics and Astronautics, pp. 279–321, 1992.

[37] Morino, L., Gradassi, G., *Vorticity generated sound and jet noise*, to be presented at the

19th AIAA/CEAS Aeroacoustics Conference, Berlin, GE, 2013.

[38] Morino, L., Salvatore, F., Gennaretti, M., *A New Velocity Decomposition for Viscous Flows: Lighthill's Equivalent–Source Method Revisited*, Computer Methods in Applied Mechanics and Engineering, 173(3–4), pp. 317–336, 1999.

[39] Morino, L., Tseng, K., *A General Integral Formulation for Unsteady Compressible Potential Flows with Applications to Airplanes and Rotors*, Boundary Element Methods in Nonlinear Fluid Dynamics, Vol. 6 of Developments in Boundary Element Methods, in P.K. Banerjee and L. Morino (eds.), Elsevier Applied Science, pp. 183–246, 1990.

[40] Norbury, J. *A family of steady vortex rings*, Journal of Fluid Mechanics, 57(3), pp. 417–431, 1973.

[41] Peaceman, D.W., Rachford, H.H. Jr., *The numerical solution of elliptic and parabolic differential equations*, J. Soc. Indust. Appl. Math., 3, pp. 28–41, 1955.

[42] Piva, R., Morino, L., *Vector Green's Function Method for Unsteady Navier–Stokes Equations*, Meccanica, Vol. 22, 1987, pp. 76–85.

[43] Piva, R., Morino, L., *A Boundary Integral Formulation in Primitive Variable for Unsteady Viscous Flows*, Boundary Element Methods in Nonlinear Fluid Dynamics, Vol. 6 of Developments in Boundary Element Methods, in P.K. Banerjee and L. Morino (eds.), Elsevier Applied Science, pp. 117–150, 1990.

[44] Ran, H., Colonius, T., *Numerical simulation of the sound radiated from a turbulent vortex ring*, International Journal of Aeroacoustics, 8(4), pp. 317–336, 2009.

[45] Romano, G.P., *The effect of boundary conditions by the side of the nozzle of a low Reynolds number jet*, Experiments in Fluids, 33(2), pp. 323–333, 2002.

[46] Saffman, P.G., *Vortex Dynamics*, Cambridge University Press, 1995.

[47] Shariff, K., Leonard, A., *Vortex rings*, Annual Review of Fluid Mechanics, 24, pp. 235–279, 1992.

[48] Shariff, K., Verzicco, R., Orlandi, P., *A numerical study of three–dimensional vortex ring instabilities: viscous corections and early nonlinear stage*, Journal of Fluid Mechanics, 279, pp. 351–375, 1994.

[49] Serrin, J., *Mathematical Principles of Classical Fluid Mechanics*, Encyclopedia of Physics, in S. Flügge (ed.), Vol. VIII/1, Springer–Verlag, Berlin, pp. 125–263, 1959.

[50] Smith, A.M.O., Pierce, J., *Exact–Solution of the Neumann Problem. Calculation of Non–Circulatory Plane and Axially Symmetric Flows about or within Arbitrary Boundaries*, Proceedings of the Third U.S. National Congress of Applied Mechanics, Brown University, 1958.

[51] Truesdell, C., *The Kinematics of Vorticity*, Indiana University Press, Bloomington, IN, 1954.

[52] Widnall, S.E., *The structure and dynamics of vortex filaments*, Annual Review of Fluid Mechanics, 7, pp. 141–165, 1975.

[53] Widnall, S.E., Bliss, D.B., Tsai, C.-Y., *The instability of short waves on a vortex ring*, Journal of Fluid Mechanics, 66(1), pp. 35–47, 1974.

[54] Widnall, S.E., Tsai, C.-Y., *The Instability of the Thin Vortex Ring of Constant Vorticity*, Philosophical Transactions of the Royal Society A: Mathematical, Physical and Engineering Sciences, 287(1344), pp. 273–305, 1977.

Appendix A

Quasi–potential flow *vs* almost potential flows

In this appendix, we discuss the relationship between quasi–potential flows and almost potential flows.[1]

A.1 Quasi–potential flows

In order to address this relationship let us start by reviewing quasi–potential flows, presented in Chapter 2. The velocity field is given by

$$\mathbf{v} = \nabla\phi, \tag{A.1}$$

where ϕ satisfies the Laplace equation

$$\nabla^2\phi = 0 \qquad \text{for } \mathbf{x} \in \mathcal{V}\backslash\mathcal{S}_{\text{W}}, \tag{A.2}$$

where $\mathcal{S}_{\text{W}}$ denotes the wake surface. The boundary conditions on the body surface $\mathcal{S}_{\text{B}}$ are

$$\frac{\partial\phi}{\partial n} = \mathbf{v}_{\text{B}} \cdot \mathbf{n}, \tag{A.3}$$

whereas, on the wake surface $\mathcal{S}_{\text{W}}$, we have

$$\Delta\,\frac{\partial\phi}{\partial n} = 0 \qquad \text{and} \qquad \frac{\mathrm{D}_{\text{W}}\phi}{\mathrm{D}t} = \frac{\partial\phi}{\partial t} + \mathbf{v}_{\text{W}} \cdot \nabla\phi = 0, \tag{A.4}$$

where $\mathbf{v}_{\text{W}} = \dfrac{1}{2}(\mathbf{v}_1 + \mathbf{v}_2)$ is by definition the velocity of a wake point (1 and 2 denote the two sides of the wake); finally, at infinity, we have

$$\phi = 0. \tag{A.5}$$

As shown in Chapter 2, the solution of the above equations admits the following integral representation

$$\phi(\mathbf{x}, t) = \oint_{\mathcal{S}_{\text{B}}} \left(\chi\, G - \phi\,\frac{\partial G}{\partial n}\right) \mathrm{d}\mathcal{S}(\mathbf{y}) + \int_{\mathcal{S}_{\text{W}}} \Delta\phi\, G\, \mathrm{d}\mathcal{S}(\mathbf{y}), \tag{A.6}$$

[1] As stated in Footnote 3, p. 1, we follow Chorin and Marsden, Ref. [3], p. 60, who define an *almost potential flow* as "a flow in which vorticity is concentrated in some thin layers of fluid".

where $G = 1/(4\pi\|\mathbf{x}-\mathbf{y}\|)$, whereas $\mathbf{x} \in \mathcal{V}$. All the quantities on the right side are known (see above boundary conditions), except for ϕ on $\mathcal{S}_{\text{B}}$. This is obtained from the following boundary integral equation (obtained as the limit of Eq. A.6, as $\mathbf{x} \in \mathcal{V}$ tends to a point on $\mathcal{S}_{\text{B}}$)

$$\frac{1}{2}\,\phi(\mathbf{x},t) = \oint_{\mathcal{S}_{\text{B}}} \left(\chi\, G - \phi\,\frac{\partial G}{\partial n}\right) \mathrm{d}\mathcal{S}(\mathbf{y}) + \int_{\mathcal{S}_{\text{W}}} \Delta\phi\, G\, \mathrm{d}\mathcal{S}(\mathbf{y}), \tag{A.7}$$

where now $\mathbf{x} \in \mathcal{S}_{\text{B}}$. Once Eq. A.7 has been solved for ϕ on $\mathcal{S}$, the value of ϕ (and hence that of $\mathbf{v} = \nabla\phi$) anywhere on $\mathcal{V}$ is given by Eq. A.6.

Finally, the pressure is given by the Bernoulli theorem for potential incompressible flows, Eq. 4.16, namely

$$\partial_t\phi + \frac{1}{2}\,\|\nabla\phi\|^2 + \frac{p}{\rho} = \frac{p_\infty}{\rho}, \tag{A.8}$$

in the air–frame.

A.2 Viscous correction; Lighthill equivalent sources

In order to shed further light on the relationship between quasi–potential flow and almost potential flows, it is convenient to review the widely–used *equivalent source* method by Lighthill, Ref. [19], as reformulated in Ref. [38].[2]

Some differential geometry

In order to formulate this method, let us introduce a set of curvilinear coordinates ξ^α ($\alpha = 1, 2$) over $\mathcal{S}$, so that $\mathbf{x} = \mathbf{p}(\xi^\alpha)$ describes the surface $\mathcal{S}$. Consider an infinitesimal quadrilateral surface elements, bounded by two coordinate segments (namely segment along the coordinate lines $\xi^\beta =$ constant)

$$\mathbf{x}_1 = \frac{\partial \mathbf{x}}{\partial \xi^1}\,\mathrm{d}\xi^1 = \mathbf{a}_1\,\mathrm{d}\xi^1 \qquad \text{and} \qquad \mathbf{x}_2 = \frac{\partial \mathbf{x}}{\partial \xi^2}\,\mathrm{d}\xi^2 = \mathbf{a}_2\,\mathrm{d}\xi^2, \tag{A.9}$$

where

$$\mathbf{a}_\alpha = \frac{\partial \mathbf{x}}{\partial \xi^\alpha} \qquad (\alpha = 1, 2) \tag{A.10}$$

are known as the *surface covariant vectors*. We have

$$\mathrm{d}\mathcal{S} = \|\mathrm{d}\mathbf{x}_1 \times \mathrm{d}\mathbf{x}_2\| = \|\mathbf{a}_1 \times \mathbf{a}_2\|\,\mathrm{d}\xi^1\,\mathrm{d}\xi^2. \tag{A.11}$$

Recalling the *Binet–Cauchy identity*,

$$\mathbf{a}\times\mathbf{b}\cdot\mathbf{c}\times\mathbf{d} = (\mathbf{a}\cdot\mathbf{c})\,(\mathbf{b}\cdot\mathbf{d}) - (\mathbf{a}\cdot\mathbf{d})\,(\mathbf{b}\cdot\mathbf{c}), \tag{A.12}$$

we have

$$\begin{aligned}\|\mathbf{a}_1 \times \mathbf{a}_2\|^2 &= \mathbf{a}_1\times\mathbf{a}_2\cdot\mathbf{a}_1\times\mathbf{a}_2 = \mathbf{a}_1\cdot\mathbf{a}_1\;\mathbf{a}_2\cdot\mathbf{a}_2 - \big(\mathbf{a}_1\cdot\mathbf{a}_2\big)^2 \\ &= a_{11}a_{22} - a_{12}^2 = \big|a_{\alpha\beta}\big| =: a,\end{aligned} \tag{A.13}$$

where $a_{\alpha\beta} = \mathbf{a}_\alpha \cdot \mathbf{a}_\beta$ are known as the covariant components of the surface first metric tensor. Hence, we can use the traditional notations

$$\mathrm{d}\mathcal{S} = \sqrt{a}\,\mathrm{d}\xi^1\,\mathrm{d}\xi^2. \tag{A.14}$$

[2]The method is also known as the *transpiration velocity* method, and is closely related to the *displacement thickness* method, also by Lighthill, Ref. [19].

Next, let us introduce a mapping $\mathbf{x}(\xi^1, \xi^2, \eta)$, where ξ^1 and ξ^2 coincide with the surface coordinates introduced above, whereas η is the coordinate along the normal $\mathbf{n}$ (the origin of the η coordinate is on $\mathcal{S}$, so that for $\eta = 0$, we recover the equation of the surface). For instance, we may use the mapping[3]

$$\mathbf{x}(\xi^1, \xi^2, \eta) = \mathbf{p}(\xi^1, \xi^2) + \eta\, \mathbf{n}(\xi^1, \xi^2) \qquad\qquad \eta \in [0, \delta], \tag{A.15}$$

where δ denotes the boundary–layer thickness, whereas

$$\mathbf{n}(\xi^1, \xi^2) = \frac{\mathbf{a}_1 \times \mathbf{a}_2}{\|\mathbf{a}_1 \times \mathbf{a}_2\|} \tag{A.16}$$

is the unit normal to the surface, and hence η is the arclength along the normal direction. In addition, δ denotes the value of η just outside the boundary layer.

Similarly, we have

$$\mathrm{d}\mathcal{V} = J\, \mathrm{d}\xi^1\, \mathrm{d}\xi^2\, \mathrm{d}\eta, \tag{A.17}$$

where J is the Jacobian of the mapping $\mathbf{x}(\xi^1, \xi^2, \eta)$, given by

$$J(\xi^1, \xi^2, \eta) = \frac{\partial(x_1, x_2, x_3)}{\partial(\xi^1, \xi^2, \eta)} = \mathbf{g}_1 \times \mathbf{g}_2 \cdot \mathbf{n}, \tag{A.18}$$

with

$$\mathbf{g}_\alpha = \frac{\partial \mathbf{x}}{\partial \xi^\alpha} \qquad\qquad (\alpha = 1, 2). \tag{A.19}$$

Note that $\mathbf{g}_\alpha\big|_{\eta=0} = \mathbf{a}_\alpha$. Hence, for $\eta = 0$ we have

$$J_0 = J\Big|_{\eta=0} = \frac{\partial(x_1, x_2, x_3)}{\partial(\xi^1, \xi^2, \eta)}\bigg|_{\eta=0} = \mathbf{a}_1 \times \mathbf{a}_2 \cdot \mathbf{n} = \|\mathbf{a}_1 \times \mathbf{a}_2\| = \sqrt{a}. \tag{A.20}$$

Lighthill equivalent source method

As mentioned above, the Lighthill equivalent source method is widely used to provide a viscous–flow correction to the results of a potential (or quasi–potential) flow analysis, so as to take into account the effects of the boundary layer presence.

The method consists of the following procedure. Let us consider a potential flow and modify its boundary condition, by replacing the potential–flow boundary condition, $\partial\phi/\partial n = \chi$, with

$$\frac{\partial \phi}{\partial n} = \chi + \check{\chi}_{\mathrm{B}}, \tag{A.21}$$

where the *equivalent source* term, $\check{\chi}_{\mathrm{B}}$, is given by[4]

$$\check{\chi}_{\mathrm{B}} = \frac{-1}{\sqrt{a}} \frac{\partial}{\partial \xi^\alpha} \int_0^\delta \left[J\big(v^\alpha - v_{\mathrm{E}}^\alpha\big) \right] \mathrm{d}\eta, \tag{A.22}$$

with v_{E}^α denoting the contravariant components of $\mathbf{v}_{\mathrm{E}}$, where $\mathbf{v}_{\mathrm{E}}$ is the "*irrotational and solenoidal continuation*" into the vortical region $\mathcal{V}_\zeta$ of the velocity $\mathbf{v}$ (which is irrotational and solenoidal outside the vortical region $\mathcal{V}_\zeta$).

[3] It is well known that this mapping may be used only if the thickness of the vortical region is smaller than the (smallest) radius of curvature of the surface (with outward concavity). However, it is useful (and adequate) for the discussion presented here. If this is not the case, one may use a similar mapping where the condition that η be the arclength along the normal is true only for $\eta = 0$.

[4] The Einstein summation convention on repeated indices is adopted throughout the paper; Latin letters are used when the range is from 1 to 3, Greek letters are used when the range is from 1 to 2.

Indeed, following Ref. [38], set $\mathbf{v} = \mathbf{v}_{\scriptscriptstyle E} + \check{\mathbf{w}}$, where $\mathbf{v}$ and $\mathbf{v}_{\scriptscriptstyle E} = \nabla\phi$ are both solenoidal, so that the "defect velocity" $\check{\mathbf{w}}$ is also solenoidal and hence $\nabla \cdot \check{\mathbf{w}} = 0$. The boundary condition, $\mathbf{v} \cdot \mathbf{n} = \mathbf{v}_{\scriptscriptstyle B} \cdot \mathbf{n} := \chi$, yields $\partial\phi/\partial n = \chi_{\scriptscriptstyle B} + \check{\chi}_{\scriptscriptstyle B}$, Eq. A.21, with

$$\check{\chi}_{\scriptscriptstyle B} = -\check{\mathbf{w}} \cdot \mathbf{n} = -\check{w}^3, \tag{A.23}$$

since $\check{w}^3 = \check{\mathbf{w}} \cdot \mathbf{n}$.

Next, recall that $\nabla \cdot \check{\mathbf{w}} = 0$ and use the curvilinear–coordinate expression for the divergence of a generic vector field, $\mathbf{b}(\mathbf{x})$,

$$\nabla \cdot \mathbf{b} = \frac{1}{J}\,\frac{\partial\,(Jb^k)}{\partial\xi^k}. \tag{A.24}$$

This yields, using Eqs. A.20 and A.23,

$$\big[J\,\check{w}^3\big]_{\eta=0} = \frac{\partial}{\partial\xi^\alpha}\,\int_0^\delta J\,\check{w}^\alpha\,\mathrm{d}\eta, \tag{A.25}$$

in agreement with Eq. A.22.[5]

Lighthill equivalent source method in presence of wake

Here, we are interested in the flow around a wing. In three dimensions, the presence of lift is connected with the fact that the vortical region is not limited to the boundary layer. Indeed, this is the reason to introduce quasi–potential flows (as distinct from potential flows). In this case, the preceding formulation must be slightly modified, as follows: the surface $\eta = 0$ corresponds to the limit of a surface that surrounds $\mathcal{S}_{\scriptscriptstyle B}$ and $\mathcal{S}_{\scriptscriptstyle W}$, as the distance tends to zero. In other words, $\mathcal{S}$ is the union of; (i) the (closed) body surface, $\mathcal{S}_{\scriptscriptstyle B}$, and (ii) the two sides of the (open) wake surface, $\mathcal{S}_{\scriptscriptstyle W}$, namely $\mathcal{S} = \mathcal{S}_{\scriptscriptstyle B} \cup \mathcal{S}_{\scriptscriptstyle W_1} \cup \mathcal{S}_{\scriptscriptstyle W_2}$, Eq. 2.29.

The result is

$$\phi(\mathbf{x},t) = \oint_{\mathcal{S}_{\scriptscriptstyle B}} \left((\chi + \check{\chi}_{\scriptscriptstyle B})\,G - \phi\,\frac{\partial G}{\partial n} \right) \mathrm{d}\mathcal{S}(\mathbf{y}) + \int_{\mathcal{S}_{\scriptscriptstyle W}} \left(\check{\chi}_{\scriptscriptstyle W}\,G - \Delta\phi\,\frac{\partial G}{\partial n} \right) \mathrm{d}\mathcal{S}(\mathbf{y}), \tag{A.26}$$

where

$$\check{\chi}_{\scriptscriptstyle W} = \check{\chi}_{\scriptscriptstyle W_1} + \check{\chi}_{\scriptscriptstyle W_2}, \tag{A.27}$$

with

$$\check{\chi}_{\scriptscriptstyle W_k} = \frac{-1}{\sqrt{a}}\,\frac{\partial}{\partial\xi^\alpha}\int_0^{\delta_k} \big[J\big(v^\alpha - v_{\scriptscriptstyle E}^\alpha\big)\big]\,\mathrm{d}\eta, \tag{A.28}$$

where δ_1 and δ_2 denote the thicknesses of the vortical layers on the two sides of the wake.

A.3 Almost potential flows

In order to analyze almost potential flows, let us focus our attention on an attached high–Reynolds–number flow around an isolated thin wing. Let us introduce the wake mid–surface (better defined below) and a mapping $\mathbf{x}(\xi^1, \xi^2, \eta)$ similar to that introduced at the end of the the preceding section (the only difference is that the quasi–potential wake surface is replaced by the wake mid–surface).

[5] The expression in Eq. A.22 is virtually identical to the equivalent–source term of Lighthill [19], where $\mathbf{v}_{\scriptscriptstyle E}$ denotes the velocity just outside the boundary layer (by definition independent of η, an unnecessary restriction). Indeed, Eq. A.22 is exact. Note that the boundary–layer approximations used by Lighthill, Ref. [19], have not been utilized.

Then, using the curvilinear–coordinate expression for the divergence of a generic vector field $\mathbf{b}(\mathbf{x})$, Eq. A.24, we have

$$\nabla \cdot \mathbf{w} = \frac{1}{\sqrt{a}} \frac{\partial \sqrt{a} w^\alpha}{\partial \xi^\alpha} + \frac{\partial w^3}{\partial \eta}. \tag{A.29}$$

Thus, Eq. 4.26 may be written as (using $\mathrm{d}\mathcal{V} = \mathrm{d}\mathcal{S}\,\mathrm{d}\eta$)

$$\begin{aligned} \varphi(\mathbf{x},t) = & \oint_{\mathcal{S}_{\mathrm{B}}} \left(\chi\, G - \varphi \frac{\partial G}{\partial n} \right) \mathrm{d}\mathcal{S}(\mathbf{y}) \\ & - \int_{\mathcal{S}_{\mathrm{V}}} \int_0^\delta \frac{1}{\sqrt{a}} \frac{\partial \sqrt{a}\, w^\alpha}{\partial \xi^\alpha} G \,\mathrm{d}\eta \,\mathrm{d}\mathcal{S}(\mathbf{y}) - \int_{\mathcal{S}_{\mathrm{V}}} \int_0^\delta \frac{\partial w^3}{\partial \eta} G \,\mathrm{d}\eta \,\mathrm{d}\mathcal{S}(\mathbf{y}), \end{aligned} \tag{A.30}$$

or, using Eq. A.14 and performing an integration by parts on the last integral,

$$\begin{aligned} \varphi(\mathbf{x},t) = & \oint_{\mathcal{S}_{\mathrm{B}}} \left(\chi\, G - \varphi \frac{\partial G}{\partial n} \right) \mathrm{d}\mathcal{S}(\mathbf{y}) \\ & - \int_{\mathcal{S}_{\mathrm{V}}} \int_0^\delta \frac{\partial \sqrt{a} w^\alpha}{\partial \xi^\alpha} G \,\mathrm{d}\eta \,\mathrm{d}\xi_1 \,\mathrm{d}\xi_2 + \int_{\mathcal{S}_{\mathrm{V}}} \int_0^\delta w^3 \frac{\partial G}{\partial \eta} \,\mathrm{d}\eta \,\mathrm{d}\mathcal{S}(\mathbf{y}). \end{aligned} \tag{A.31}$$

Next, recall that we are addressing almost potential flows, namely flows in which δ is very small. Therefore, we may assume G and $\partial G/\partial \eta$ to be independent of η, provided of course that the point $\mathbf{x}$ is suitably distant from each dummy point of integration $\mathbf{y}$ (namely that $\|\mathbf{x}-\mathbf{y}\| \gg \delta$). Then, neglecting higher order terms, we have

$$\varphi(\mathbf{x},t) = \oint_{\mathcal{S}_{\mathrm{B}}} \left((\chi + \check{\chi}_{\mathrm{B}})\, G - (\varphi + \Delta\varphi) \frac{\partial G}{\partial n} \right) \mathrm{d}\mathcal{S}(\mathbf{y}) + \int_{\mathcal{S}_{\mathrm{W}}} \left(\check{\chi}_{\mathrm{W}}\, G - \Delta\varphi \frac{\partial G}{\partial n} \right) \mathrm{d}\mathcal{S}(\mathbf{y}), \tag{A.32}$$

where, on $\mathcal{S}_{\mathrm{B}}$, we have

$$\check{\chi}_{\mathrm{B}} = \frac{-1}{\sqrt{a}} \frac{\partial}{\partial \xi^\alpha} \int_0^\delta \sqrt{a} w^\alpha \,\mathrm{d}\eta, \tag{A.33}$$

whereas, on $\mathcal{S}_{\mathrm{W}}$, we have $\check{\chi}_{\mathrm{W}} = \check{\chi}_{\mathrm{W}_1} + \check{\chi}_{\mathrm{W}_2}$ (as in Eq. A.27), with

$$\check{\chi}_{\mathrm{W}_k} = \frac{-1}{\sqrt{a}} \frac{\partial}{\partial \xi^\alpha} \int_0^{\delta_k} \sqrt{a} w^\alpha \,\mathrm{d}\eta, \tag{A.34}$$

where δ_1 and δ_2 denote the thicknesses of the vortical layers on the two sides of the wake. In addition, we have, on $\mathcal{S}_{\mathrm{B}}$

$$\Delta\varphi(\mathbf{x},t) = -\int_0^\delta w^3 \,\mathrm{d}\eta, \tag{A.35}$$

whereas, on $\mathcal{S}_{\mathrm{W}}$

$$\Delta\varphi(\mathbf{x},t) = \Delta\varphi_1(\mathbf{x},t) + \Delta\varphi_2(\mathbf{x},t), \tag{A.36}$$

with

$$\Delta\varphi_k(\mathbf{x},t) = -\int_0^{\delta_k} w^3 \,\mathrm{d}\eta. \tag{A.37}$$

Comparison with Lighthill equivalent source method

Let us compare the boundary integral representation for quasi–potential flows with viscous correction, Eq. A.26 and that for almost potential flows, Eq. A.32. They are derived in quite a different way: the velocity field $\mathbf{v} = \nabla\phi$, with ϕ in Eq. A.26 is solenoidal, whereas the velocity field $\mathbf{v}_{\text{P}} = \nabla\varphi$, with φ in Eq. A.32 is not. In spite of this fact, the two equations are very similar. The main difference is that $\varphi + \Delta\varphi$ in Eq. A.32 takes the place of φ in Eq. A.26. However, this should not be a cause for alarm. For, $\varphi + \Delta\varphi$ in Eq. A.32 is the value of the potential outside the boundary layer, whereas φ is the value of the potential inside the boundary layer. Hence, the boundary integral equation in the two cases are fully equivalent: for quasi–potential flows with viscous correction, we have

$$\frac{1}{2}\,\phi(\mathbf{x},t) = \oint_{\mathcal{S}_{\text{B}}} \left((\chi + \check{\chi}_{\text{B}})\, G - \phi\, \frac{\partial G}{\partial n} \right) \mathrm{d}\mathcal{S}(\mathbf{y}) + \int_{\mathcal{S}_{\text{W}}} \left(\check{\chi}_{\text{W}}\, G - \Delta\phi\, \frac{\partial G}{\partial n} \right) \mathrm{d}\mathcal{S}(\mathbf{y}) \tag{A.38}$$

whereas for viscous flows, we have

$$\begin{aligned} \frac{1}{2}\,\varphi_{\text{E}}(\mathbf{x},t) = \oint_{\mathcal{S}_{\text{B}}} & \left((\chi + \check{\chi}_{\text{B}})\, G - \varphi_{\text{E}}\, \frac{\partial G}{\partial n} \right) \mathrm{d}\mathcal{S}(\mathbf{y}) \\ & + \int_{\mathcal{S}_{\text{W}}} \left(\check{\chi}_{\text{W}}\, G - \Delta\varphi\, \frac{\partial G}{\partial n} \right) \mathrm{d}\mathcal{S}(\mathbf{y}) \end{aligned} \tag{A.39}$$

where

$$\varphi_{\text{E}} := \varphi(\mathbf{x},t) + \Delta\varphi(\mathbf{x},t) \tag{A.40}$$

is the exterior value of the potential φ, namely the value of the potential outside the boundary layer. For, in taking the limit, one obtains $\varphi_{\text{E}}(\mathbf{x},t)$ and not $\varphi(\mathbf{x},t)$, since the discontinuity is not captured by the operation of limit.

Appendix B

An alternate choice for ϖ

In Chapter 4, specifically in Subsection 4.2.1, we introduced a convenient choice for φ, namely $\varpi = \frac{1}{2}\, v_{\text{P}}^2$, Eq. 4.14. Here, we want to address an alternate choice, namely

$$\varpi = \frac{1}{2}\, v_{\text{P}}^2 - \frac{1}{2}\, w^2. \tag{B.1}$$

B.1 The natural decomposition under the alternate choice

Using Eq. B.1, Eq. 4.10, integrated, yields, using Eq. 4.12,

$$\dot{\varphi} + \frac{1}{2}\, \|\nabla\varphi\|^2 + p - \frac{1}{2}\, \|\mathbf{w}\|^2 - \nu\, \nabla^2\varphi = p_\infty, \tag{B.2}$$

which is an *alternate extension of the Bernoulli theorem to incompressible viscous flows.*[1]

Next, note that for any vector $\mathbf{b}$ we have

$$\frac{1}{2}\, \partial_k b^2 = b_{j,k}\, b_j = b_{k,j}\, b_j + \big(b_{j,k} - b_{k,j}\big)\, b_j \tag{B.3}$$

which in tensor notation, corresponds to the following identity

$$\frac{1}{2}\, \nabla b^2 = \mathbf{C}^{\intercal}\mathbf{b} = \mathbf{C}\mathbf{b} - \big(\mathbf{C} - \mathbf{C}^{\intercal}\big)\, \mathbf{b} \tag{B.4}$$

where $\mathbf{C} = \nabla\mathbf{b}$ is the tensor whose Cartesian components are $c_{jk} = b_{j,k} = \partial b_j/\partial x_k$ (the comma denotes partial differentiation). On the other hand, using vector notations, we have

$$\frac{1}{2}\, \nabla b^2 = \mathbf{b}\cdot\nabla\mathbf{b} - \mathbf{c}\times\mathbf{b} \tag{B.5}$$

where $\mathbf{c} = \nabla\times\mathbf{b}$.

In particular, we have

$$\frac{1}{2}\, \nabla w^2 = \mathbf{w}\cdot\nabla\mathbf{w} - \boldsymbol{\zeta}\times\mathbf{w}, \tag{B.6}$$

where $\boldsymbol{\zeta} = \nabla\times\mathbf{w} = \nabla\times\mathbf{v}$ denotes the vorticity. Therefore, Eq. 4.11 yields

$$\frac{\mathrm{D}\mathbf{w}}{\mathrm{D}t} = \partial_t + \mathbf{v}\cdot\nabla\mathbf{w} = -\mathbf{w}\cdot\nabla\mathbf{v} + \boldsymbol{\zeta}\times\mathbf{w} + \nu\,\nabla^2\mathbf{w}. \tag{B.7}$$

[1] Recall that $\nabla^2\varphi = -\nabla\cdot\mathbf{w}$, Eq. 4.8. Therefore, here as well, in those points where $\mathbf{w} = \mathbf{0}$, Eq. 4.15 reduces to the Bernoulli theorem for incompressible potential flows, $\dot{\varphi} + \frac{1}{2}\, \|\nabla\varphi\|^2 + p = p_\infty$.

A comparison of the two approaches

Equation B.7 appears to be more complicated that Eq. 4.17. However, if we use indicial or tensor notations, the difference becomes irrelevant. Indeed, Eq. 4.17 may be written as (compare Eqs. B.4 and B.5)

$$\frac{\mathrm{D}\mathbf{w}}{\mathrm{D}t} + \mathbf{P}^{\intercal}\mathbf{w} = \nu\,\nabla^2\mathbf{w}. \tag{B.8}$$

where $\mathbf{P} = \nabla\mathbf{v}_{\mathrm{P}} = \mathbf{P}^{\intercal}$, whereas Eq. B.7 may be written as (compare again Eqs. B.4 and B.5)

$$\frac{\mathrm{D}\mathbf{w}}{\mathrm{D}t} + \mathbf{Q}^{\intercal}\mathbf{w} = \nu\,\nabla^2\mathbf{w}. \tag{B.9}$$

where $\mathbf{Q} = \nabla\mathbf{v} \neq \mathbf{Q}^{\intercal}$. Thus, computationally, the two approaches are similar – all is needed is simply to replace $\mathbf{P}$ with $\mathbf{Q}$.

B.2 Material covariant components of w

In analogy to what we did in Chapter 3 for the equation governing the contravariant components of $\boldsymbol{\zeta}$, we can obtain a convenient equation governing the covariant components of $\mathbf{w}$.

Let $\mathbf{x} = \mathbf{x}(\xi^\alpha, t)$ denote the transformation from the ξ^α space into the $\mathbf{x}$ space, as the field evolves in time. Assuming that the Jacobian of the transformation does not vanish, we can invert the transformation to obtain $\xi^\alpha = \xi^\alpha(\mathbf{x}, t)$. Next, introduce the material covariant and contravariant base vector given respectively by:[2]

$$\mathbf{g}_\alpha = \frac{\partial\mathbf{x}}{\partial\xi^\alpha} \qquad\qquad \mathbf{g}^\alpha = \nabla\xi^\alpha \tag{B.10}$$

A useful formula

Here, we prove that

$$\frac{\mathrm{D}\mathbf{g}^\alpha}{\mathrm{D}t} = -\mathbf{Q}^{\intercal}\,\mathbf{g}^\alpha \tag{B.11}$$

namely

$$\frac{\mathrm{D}}{\mathrm{D}t}\left(\frac{\partial\xi^\alpha}{\partial x_j}\right) = -\frac{\partial v_k}{\partial x_j}\frac{\partial\xi^\alpha}{\partial x_k} \tag{B.12}$$

In order to show this let us begin with the identity:

$$\frac{\partial x_k}{\partial\xi^\beta}\,\frac{\partial\xi^\beta}{\partial x_j} = \frac{\partial x_k}{\partial x_j} = \delta^j_k \tag{B.13}$$

Note that

$$\frac{\mathrm{D}}{\mathrm{D}t}\left(\frac{\partial x_k}{\partial\xi^\beta}\right) = \frac{\partial}{\partial t}\left[\frac{\partial x_k}{\partial\xi^\beta}\right]_{\xi^\alpha=\text{constant}} = \frac{\partial^2 x_k(\xi^\alpha, t)}{\partial\xi^\alpha\,\partial t} = \frac{\partial v_k}{\partial\xi^\beta} \tag{B.14}$$

Thus, taking the material derivative of Eq. B.13 and using Eq. B.14, one obtains

$$\frac{\mathrm{D}}{\mathrm{D}t}\left(\frac{\partial\xi^\beta}{\partial x_j}\right)\frac{\partial x_k}{\partial\xi^\beta} = -\frac{\mathrm{D}}{\mathrm{D}t}\left(\frac{\partial x_k}{\partial\xi^\beta}\right)\frac{\partial\xi^\beta}{\partial x_j} = -\frac{\partial v_k}{\partial\xi^\beta}\frac{\partial\xi^\beta}{\partial x_j} = -\frac{\partial v_k}{\partial x_j} \tag{B.15}$$

[2]The term material indicates that the vectors $\mathbf{g}_\alpha$ evolve in time and are always tangent to the material ξ^α–line. Similarly, the contravariant base vector $\mathbf{g}^\alpha$ are always normal to the surface ξ^α = constant.

Using $\partial x_k/\partial\xi^\beta \partial\xi^\alpha/\partial x_k = \delta^\alpha_\beta$

$$\frac{\partial v_k}{\partial x_j}\frac{\partial \xi^\alpha}{\partial x_k} = -\frac{\mathrm{D}}{\mathrm{D}t}\left(\frac{\partial \xi^\beta}{\partial x_j}\right)\frac{\partial x_k}{\partial \xi^\beta}\frac{\partial \xi^\alpha}{\partial x_k} = -\frac{\mathrm{D}}{\mathrm{D}t}\left(\frac{\partial \xi^\beta}{\partial x_j}\right)\delta^\alpha_\beta = -\frac{\mathrm{D}}{\mathrm{D}t}\left(\frac{\partial \xi^\alpha}{\partial x_j}\right) \tag{B.16}$$

in agreement with Eq. B.12.

Equation for w_α

Let us express $\mathbf{w}$ in terms of its material covariant components w_α, as

$$\mathbf{w} = w_\alpha(\xi^\beta, t)\,\mathbf{g}^\alpha(\xi^\beta, t), \tag{B.17}$$

Taking the material time derivative and combining the result with B.11 we have:

$$\frac{\mathrm{D}\mathbf{w}}{\mathrm{D}t} = \frac{\mathrm{D}w_\alpha}{\mathrm{D}t}\mathbf{g}^\alpha + w_\alpha\frac{\mathrm{D}\mathbf{g}^\alpha}{\mathrm{D}t} = \frac{\mathrm{D}w_\alpha}{\mathrm{D}t}\mathbf{g}^\alpha - w_\alpha\mathbf{Q}^\intercal\,\mathbf{g}^\alpha = \frac{\mathrm{D}w_\alpha}{\mathrm{D}t}\mathbf{g}^\alpha - \mathbf{Q}^\intercal\,\mathbf{w} \tag{B.18}$$

Substituting into Eq. B.9, we have

$$\frac{\mathrm{D}w_\alpha}{\mathrm{D}t}\,\mathbf{g}^\alpha = \nu\,\nabla^2\mathbf{w}, \tag{B.19}$$

or

$$\frac{\mathrm{D}w_\alpha}{\mathrm{D}t} = \nu\,\mathbf{g}_\alpha\cdot\nabla^2\mathbf{w}. \tag{B.20}$$

For inviscid flows ($\nu = 0$), we have

$$\frac{\mathrm{D}w_\alpha}{\mathrm{D}t} = 0 \tag{B.21}$$

or w_α constant following a material point, namely

$$w_\alpha(\xi^\beta, t) = w_\alpha(\xi^\beta, 0). \tag{B.22}$$

This implies (see Eq. B.17)[3]

$$\mathbf{w}(\xi^\alpha, t) = w_\alpha(\xi^\beta, 0)\,\mathbf{g}^\alpha(\xi^\beta, t) \tag{B.23}$$

On the other hand, for viscous flows, $\mathbf{w}$ is given by Eq. B.17, with

$$w_\alpha(\xi^\beta, t) = w_\alpha(\xi^\beta, 0) + \nu\int_0^t \mathbf{g}_\alpha(\xi^\beta, t)\cdot\nabla^2\mathbf{w}(\xi^\beta, t)\mathrm{d}t \tag{B.24}$$

B.3 Preliminary results

Some encouraging, albeit very preliminary, results have been obtained applying Eq. B.9 to the infinite cylinder presented in Chapter 4. In Figure B.1, p. 60, one can observe how the length of the recirculation bubble obtained using the new formulation has bee found to be comparable to the previous results. Moreover, streamlines obtained with this present formulation at $Re_{\mathrm{D}} = 20$ are shown in Figure B.2, p. 60.

[3] This is analogous to the "beautiful result was obtained in 1815 by Cauchy" (Serrin, Ref. [49], Eq. 17.5, p. 152), for the material contravariant components of the vorticity, Eq. 3.18.

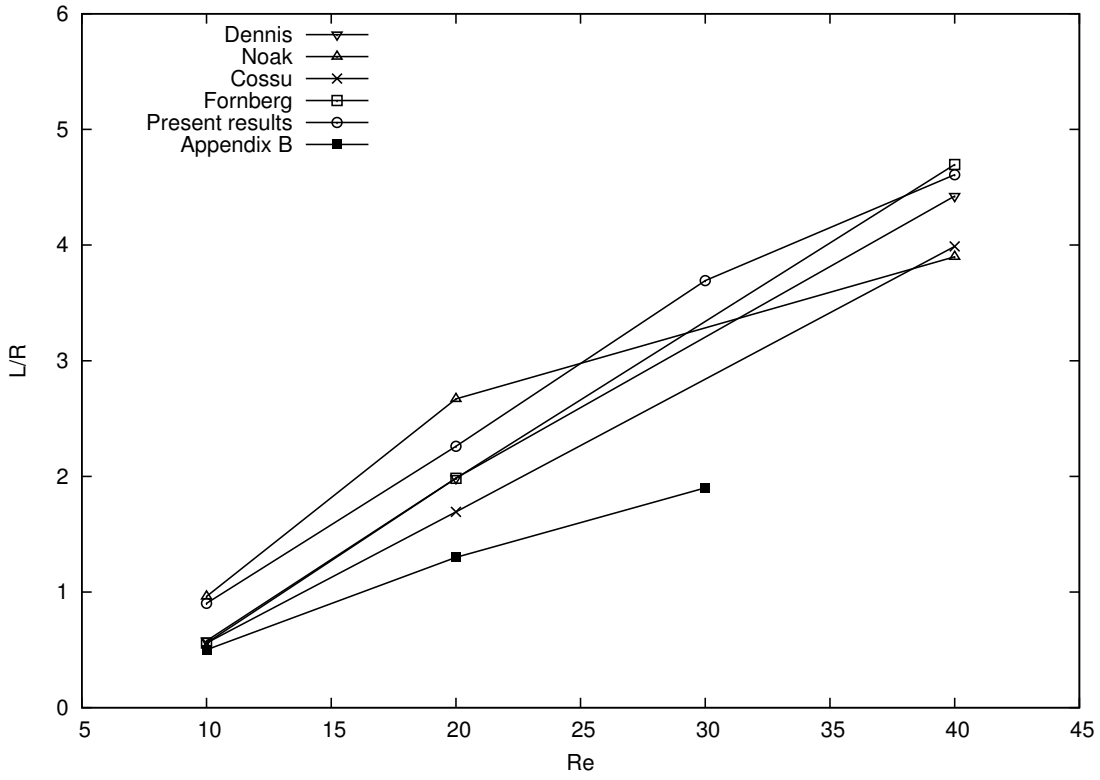

Figure B.1: Length of recirculation bubble

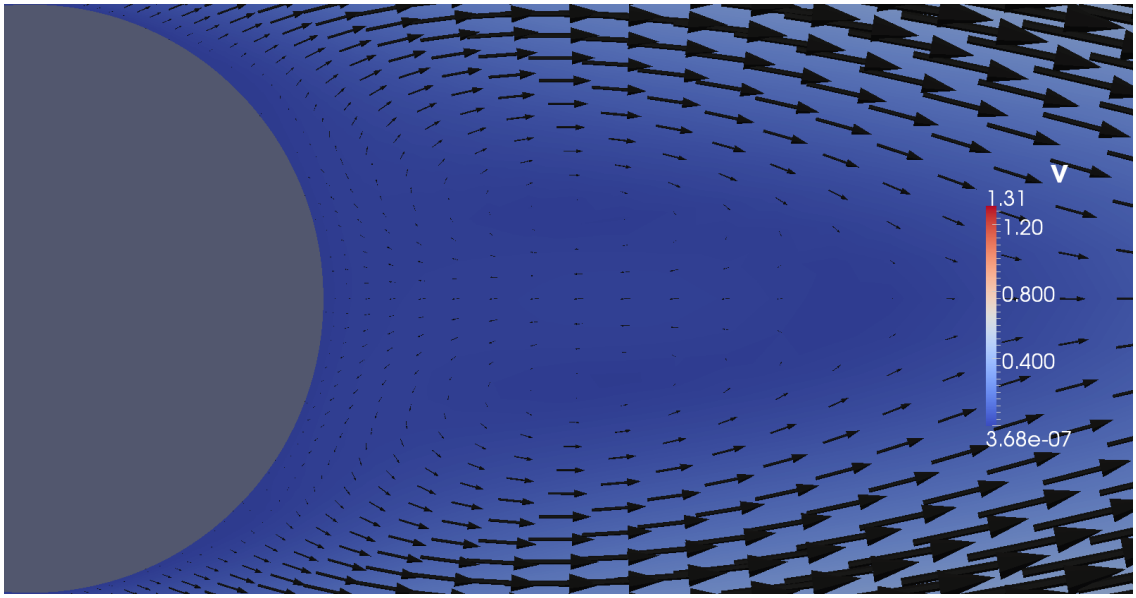

Figure B.2: Velocity field at $Re_{\text{D}} = 20$ with the new formulation

Appendix C

Time-stepping methods

For the sake of completeness, all the details of the various time-stepping methods utilized, or simply discussed, in this work are presented in this appendix.

Let us consider an initial problem represented by a system of ordinary differential equations:

$$\dot{\mathsf{x}} = \mathsf{g}(\mathsf{x}, t) \qquad \text{with } \mathsf{x}(0) = \mathsf{x}_0. \tag{C.1}$$

The solution of this problem is unique, provided that the function $\mathsf{g}(\mathsf{x}, t)$ satisfies suitable regularity conditions (which are typically satisfied in practice). Unfortunately, in several problems of practical interest, it is not possible to obtain explicit solutions. In these cases, however, one may utilize numerical solution.

All the numerical methods for the integration of systems of differential equations consist of the following procedure: from x_0 obtain $\mathsf{x}_1 = \mathsf{x}(h)$, where h is suitable time step (which is determined by considerations of accuracy and stability, see below). Once we have x_1, we may used this as the initial condition to obtain x_2, by proceeding as in the first step. In general, we can use x_n to obtain $\mathsf{x}_{n+1} = \mathsf{x}[(n+1)h]$. In this way, we may obtain the solution for time $t = t_p$ as large as we wish – provided of course that the solution exists, and that it is within the upper limits of the computer utilized (every computer has a highest number that it can handle; if the number evaluated is above this limit, the computer said to be *in overflow*). This approach is known as *step-by-step integration*.

Let us now introduce the concepts of accuracy and stability.

Accuracy

We can assess the accuracy of the various schemes, by comparing their result with the exact solution of Eq. C.3 when the function g is given by

$$\mathsf{g}(\mathsf{x}, t) = \mathsf{A}\mathsf{x} + \mathsf{f}(t), \tag{C.2}$$

namely,

$$\dot{\mathsf{x}} = \mathsf{A}\,\mathsf{x} + \mathsf{f}(t) \qquad \text{with } \mathsf{x}(0) = \mathsf{x}_0, \tag{C.3}$$

with A constant. The solution is given by

$$\mathsf{x}(t) = \mathrm{e}^{\mathsf{A}t}\,\mathsf{x}_0 + \int_0^t \mathrm{e}^{\mathsf{A}(t-\tau)}\,\mathsf{f}(\tau)\,\mathrm{d}\tau. \tag{C.4}$$

In particular, we have

$$\mathsf{x}_1 = \mathrm{e}^{\mathsf{A}h}\,\mathsf{x}_0 + \int_0^h \mathrm{e}^{\mathsf{A}(t-\tau)}\,\mathsf{f}(\tau)\,\mathrm{d}\tau, \tag{C.5}$$

and, in general,

$$\mathsf{x}_{k+1} = \mathrm{e}^{\mathsf{A}h}\,\mathsf{x}_k + \int_{t_k}^{t_{k+1}} \mathrm{e}^{\mathsf{A}(t_{k+1}-\tau)}\,\mathsf{f}(\tau)\,\mathrm{d}\tau, \tag{C.6}$$

where $t_k = kh$ $(k = 0, 1, \dots)$.

Stability

We have the following definitions

- A numerical integration scheme is called *unstable*, iff it yields a solution x_k that grows without limits as k tends to infinity.
- A numerical scheme is called *conditionally stable*, iff it is stable only for bounded values of the time step h.
- A numerical scheme is called *unconditionally stable*, iff it is stable for any value of the time step h.
- A numerical scheme is said to introduce *artificial damping*, iff the numerical solution is damped, even when the exact solution is not.

In order to address the *stability* of the time stepping methods, we consider again the linear problem with constant coefficients, Eq. C.3. In addition, we limit our analysis to homogeneous problems. In addition, for simplicity, let us assume that the matrix A be diagonalizable, thus, instead of Eq. C.3, we can study

$$\dot{y} = \lambda y, \tag{C.7}$$

where λ is any of the eigenvalues of the matrix A. The above equation is stable iff

$$\Re(\lambda) \leq 0. \tag{C.8}$$

C.1 Explicit Euler method

The simplest and most intuitive way to integrate systems of ordinary differential equations is to approximate, in Eq. C.1, $\dot{\mathsf{x}}_k$ with its forward finite difference approximation, namely

$$\dot{\mathsf{x}}_k = \frac{\mathsf{x}_{k+1} - \mathsf{x}_k}{h} + \mathcal{O}(h). \tag{C.9}$$

Thus, setting $\mathsf{f}_k = \mathsf{f}(\mathsf{x}_k, t_k)$ and multiplying by h, Eq. C.9 yields[1]

$$\mathsf{x}_{k+1} = \mathsf{x}_k + h\,\mathsf{f}_k + \mathcal{O}\big(h^2\big). \tag{C.10}$$

Neglecting the term $\mathcal{O}(h^2)$, one may obtain x_{k+1} from x_k, with $k = 0, 1, \dots$, namely obtain $\mathsf{x}_1, \mathsf{x}_2, \dots$ starting from x_0.

Note that Eq. C.10 defines x_{k+1} explicitly: hence the name *Explicit Euler method*. This method is used in Chapter 2 to integrate the wake evolution equation, $\dot{\mathbf{x}}_\mathrm{w} = \mathbf{v}_\mathrm{w}(\mathbf{x}_\mathrm{w})$, Eq. 2.31 (see Eq. 2.34).

Accuracy analysis

In order to assess the *accuracy* of the scheme, let us compare Eq. C.10 with the exact solution, Eq. C.6, of the linear problem with constant coefficients, Eq. C.3. Had we not neglected the term

[1] The scheme obtained by neglecting the term $\mathcal{O}(h^2)$ is called *accurate to the order h*.

$\mathcal{O}(h^2)$, instead of Eq. C.10, Eq. C.9, with $\mathsf{g}_k = \mathsf{A}\mathsf{x}_k + \mathsf{f}_k$, would have given us

$$\mathsf{x}_{k+1} = \big(\mathsf{I} + h\mathsf{A}\big)\,\mathsf{x}_k + h\,f_k + \mathcal{O}(h^2). \tag{C.11}$$

This is in agreement with the power series expansion of Eq. C.6, that is (recall that $\mathrm{e}^{h\mathsf{A}} = \mathsf{I} + h\mathsf{A} + \dots$),

$$\mathsf{x}_{k+1} = \big(\mathsf{I} + h\mathsf{A} + \dots\big)\,\mathsf{x}_k + h\,\mathsf{f}_k + \dots. \tag{C.12}$$

Thus, the two approaches yield the same result. This confirms that the accuracy of the solution is to order h.

Stability analysis

Unfortunately, the method is affected by a problem known as *numerical instability*. This consists in the fact that, as mentioned above, a dynamical system with a stable solution, may have an unstable numerical solution. In order to address the *stability* of the explicit Euler scheme, consider Eq. C.7. Using Eq. C.10, Eq. C.7 yields

$$y_{k+1} = \rho\, y_k, \tag{C.13}$$

where

$$\rho = 1 + \lambda\, h. \tag{C.14}$$

Equation C.13 implies $\mathsf{x}_k = \rho^k\,\mathsf{x}_0$. Hence, the solution is stable if and only if

$$|\rho| < 1; \tag{C.15}$$

otherwise, $\lim_{k\to\infty} \|\mathsf{x}_k\| = \infty$, namely the numerical solution is unstable.

Real eigenvalues: Consider first the case in which $\lambda = -\beta$ is real (note that, for the stability of the differential equation, we must have $\beta = -\lambda \geq 0$, Eq. C.8). In this case Eq. C.15 is satisfied only if

$$h < \frac{2}{\beta} \qquad\qquad \text{with } \beta \geq 0. \tag{C.16}$$

Thus, the scheme is conditionally stable even if the differential equation is stable.

Of course if we have a system of equations, instead of a single one, the instability constraint must be satisfied for all the eigenvalues. Hence, the most restrictive stability constraint (which gives the maximum allowed value for h, corresponds to the highest eigenvalue. In other words, the numerical scheme is stable, if and only if h does not exceeds its maximum allowed value, namely for

$$h < \frac{2}{\beta_{\text{Max}}}, \qquad\qquad \text{where } \beta_{\text{Max}} = \max_r\, \beta_r. \tag{C.17}$$

Finally, note that for $h > 2/\beta$, we have $\rho < -1$. This implies that the numerical solution of Eq. C.7 oscillates (as it grows). This is a typical sign of numerical instability.

Imaginary eigenvalues: Next, consider the case in which λ is purely imaginary: $\lambda = \imath\omega$. In this case, using Eq. C.10, we still have Eq. C.13 (that is, $y_{k+1} = \rho y_k$), where now $\rho = 1 + \imath\omega h$. Hence, $|\rho| = \sqrt{1 + \omega^2 h^2} > 1$, for all the values of h. Thus, in this case, the scheme is unconditionally unstable.

Complex eigenvalues: On the other hand, for a generic complex eigenvalue $\lambda = -\beta \pm \imath\omega$, with $\beta \geq 0$ (recall that, for the stability of the differential equation, we must have $\beta = -\lambda \geq 0$).

Now, we have $\rho = 1 + (-\beta \pm \imath\omega)h$, and $|\rho|^2 = (1 - \beta\, h)^2 + (\omega\, h)^2$. Imposing the condition $|\rho|^2 \leq 1$, one obtains $h\big[-2\beta + (\beta^2 + \omega^2)h\big] \geq 0$. This stability condition is satisfied only for $0 < h \leq 2\beta/(\beta^2 + \omega^2)$. Hence, the explicit Euler method is stable for

$$h \leq \frac{2\beta}{\beta^2 + \omega^2}, \tag{C.18}$$

with $\beta > 0$, as required for the stability of the differential equation. Note that for $\omega = 0$, we recover the expression in Eq. C.16. Note also that h is a decreasing function of ω.

Of course if we have a system of equation instead of a single one, the instability constraint must be satisfied for all the eigenvalues. The most restrictive stability constraint gives us

$$h \leq \max_r \left[\frac{2\beta_r}{\beta_r^2 + \omega_r^2} \right]. \tag{C.19}$$

Trade–off between accuracy and stability

Note that the fact accuracy and instability impose different types of constraints on $h = \Delta t$. Typically, the accuracy matters only for those modes that have low eigenvalues, whereas, as pointed out above, the instability constraint must be satisfied for all the eigenvalues. It is possible that the stability condition requires h to be so small that accuracy becomes irrelevant and *vice versa*.

The above issue is particularly important when the ratio between the lowest and the highest eigenvalue is very high. Systems with this characteristic are called *stiff*. In the vast majority of the cases, we are interested in the accuracy of the lowest eigenvalue. In this case, for conditionally stable systems the stability constraint is the dominant one. For, if this is satisfied, the accuracy connected with the lowest eigenvalue is largely adequate.

The method presented in the following section (semi–implicit Euler method) offer a remedy to this problem.

C.2 Semi–implicit Euler method

The semi–implicit Euler method consists of the approximations[2]

$$\dot{\mathsf{x}}_{k+\frac{1}{2}} = \frac{1}{h}\,(\mathsf{x}_{k+1} - \mathsf{x}_k) + \mathcal{O}(h^2) \tag{C.20}$$

$$\mathsf{g}_{k+\frac{1}{2}} = \frac{1}{2}\,(\mathsf{g}_{k+1} + \mathsf{g}_k) + \mathcal{O}(h^2). \tag{C.21}$$

This yields

$$\frac{1}{h}\,(\mathsf{x}_{k+1} - \mathsf{x}_k) = \frac{1}{2}\,(\mathsf{g}_{k+1} - \mathsf{g}_k) + \mathcal{O}(h^2). \tag{C.22}$$

Neglecting terms of order h^2 one obtains

$$\mathsf{x}_{k+1} - \frac{h}{2}\,\mathsf{g}(\mathsf{x}_{k+1}, t_{k+1}) = \mathsf{x}_k + \frac{h}{2}\,\mathsf{g}(\mathsf{x}_{k+1}, t_{k+1}). \tag{C.23}$$

The accuracy of this scheme is of order h^2.

[2]This method is also referred to as the method of Crank and Nicolson, Ref. [5].

Accuracy analysis

In order to assess the *accuracy* of the scheme, let us compare the semi–implicit Euler scheme, namely

$$\mathsf{x}_{k+1} = \left(\mathsf{I} - \frac{h}{2}\,\mathsf{A}\right)^{-1} \left[\left(\mathsf{I} + \frac{h}{2}\,\mathsf{A}\right)\mathsf{x}_k + h\,\frac{\mathsf{f}_k + \mathsf{f}_{k+1}}{2}\right], \tag{C.24}$$

with the exact solution of the linear problem with constant coefficients. Note that

$$\left(\mathsf{I} - \frac{h}{2}\,\mathsf{A}\right)^{-1} = \mathsf{I} + \frac{h}{2}\,\mathsf{A} + \frac{h^2}{4}\,\mathsf{A}^2 + \mathcal{O}(h^3). \tag{C.25}$$

Hence, Eq. C.24 yields

$$\mathsf{x}_{k+1} = \left(\mathsf{I} + h\,\mathsf{A} + \frac{h^2}{2}\,\mathsf{A}^2\right)\mathsf{x}_k + h\left(\mathsf{I} + \frac{h}{2}\,\mathsf{A}\right)\frac{\mathsf{f}_k + \mathsf{f}_{k+1}}{2} + \mathcal{O}(h^3). \tag{C.26}$$

This is in agreement with the power series expansion of the exact solution. In order to show this, note that, setting $\tau = t_k + \tau'$, we have

$$\int_{t_k}^{t_{k+1}} \mathrm{e}^{\mathsf{A}(t_{k+1}-\tau)}\,\mathsf{f}(\tau)\,\mathrm{d}\tau = \int_0^h \mathrm{e}^{\mathsf{A}(h-\tau')}\,\mathsf{f}(\tau')\,\mathrm{d}\tau'. \tag{C.27}$$

Next, noting that

$$\mathsf{f}(\tau) = \frac{1}{2}(\mathsf{f}_k + \mathsf{f}_{k+1}) + \frac{1}{h}(\mathsf{f}_{k+1} - \mathsf{f}_k)\left(\tau' - \frac{h}{2}\right) + \mathcal{O}(h^3), \tag{C.28}$$

and recalling that $\mathrm{e}^{h\mathsf{A}} = \mathsf{I} + h\,\mathsf{A} + \frac{1}{2}h^2\,\mathsf{A}^2 + \ldots$, one obtains, with a little patience,

$$\int_0^h \mathrm{e}^{\mathsf{A}(h-\tau')}\mathsf{f}(\tau')\,\mathrm{d}\tau' = h\left(\mathsf{I} + \frac{h}{2}\mathsf{A}\right)\frac{\mathsf{f}_k + \mathsf{f}_{k+1}}{2} + \mathcal{O}(h^3). \tag{C.29}$$

Finally, combining with $\mathsf{x}_{k+1} = \mathrm{e}^{\mathsf{A}h}\mathsf{x}_k + \displaystyle\int_{t_k}^{t_{k+1}} \mathrm{e}^{\mathsf{A}(t_{k+1}-\tau)}\mathsf{f}(\tau)\,\mathrm{d}\tau$, Eq. C.6, one obtains that indeed the accuracy of the scheme is of order h^2.

Stability analysis

In order to address the *stability* of the semi–implicit Euler scheme, again we limit our analysis to the homogeneous linear problem, with constant coefficients and assume again that the matrix A be diagonalizable. Thus we can study $\dot{y} = \lambda y$, where λ is any of the eigenvalues of the matrix A. Using Eq. C.23, we obtain again $y_{k+1} = \rho y_k$, Eq. C.13, where now

$$\rho = \frac{1 - \frac{1}{2}h\lambda}{1 + \frac{1}{2}h\lambda}. \tag{C.30}$$

The scheme is stable iff $|\rho| \leq 1$, that is, iff

$$|\rho| = \frac{\left|1 - \frac{1}{2}h\lambda\right|}{\left|1 + \frac{1}{2}h\lambda\right|} < 1. \tag{C.31}$$

This is true, for any value of h, whenever $\lambda_{\mathrm{R}} = -\beta < 0$. Thus, for stable differential equations, the implicit Euler scheme is *unconditionally stable*.

Note that, for imaginary eigenvalues ($\lambda = \imath\omega$, that is, $\lambda_{\text{R}} = 0$), we have[3]

$$|\rho| = \frac{\left|1 - \frac{1}{2}h\imath\omega\right|}{\left|1 + \frac{1}{2}h\imath\omega\right|} = 1. \tag{C.32}$$

Thus, the scheme is not affected by artificial damping.

C.3 Predictor-corrector method (classical)

The standard predictor–corrector algorithm consists of obtaining first an approximative calculation of the solution through an Euler explicit method, which is then corrected by an Euler semi–implicit method (the overall method is an explicit one). Accordingly, denoting by n the current time step, the $n+1$ prediction $\hat{\mathsf{x}}_{n+1}$ is obtained through

$$\frac{\hat{\mathsf{x}}_{n+1} - \mathsf{x}_n}{h} = \mathsf{g}(\mathsf{x}_n), \tag{C.33}$$

and the correction is consequently evaluated by taking the value of g in $\hat{\mathsf{x}}_{n+1}$

$$\frac{\mathsf{x}_{n+1} - \mathsf{x}_n}{h} = \frac{1}{2}\big[\mathsf{g}(\hat{\mathsf{x}}_{n+1}) + \mathsf{g}(\mathsf{x}_n\big]. \tag{C.34}$$

Accuracy and stability analysis

Assuming the system to be linear, diagonalized we would have $\mathsf{g}(y) = \lambda y$ (and stable $\lambda_{\text{R}} \leq 0$), we would then have

$$\hat{y}_{n+1} - y_n = \lambda y_n h, \tag{C.35}$$

$$y_{n+1} - y_n = \frac{h}{2}\lambda\left(\hat{y}_{n+1} + y_n\right) = \frac{h}{2}\lambda\left(2\,y_n + \lambda y_n h\right), \tag{C.36}$$

or

$$y_{n+1} = \left(1 + \lambda h + \frac{\lambda^2 h^2}{2}\right) y_n = y_n\,\mathrm{e}^{\lambda\Delta t} + o(h^3) \tag{C.37}$$

Thus, this method holds the same accuracy than an Euler semi–implicit one. Moreover, the accuracy would not be improved by increasing the corrector iterations.

Regarding the stability, consider, for the sake of simplicity, only real eigenvalues, $\lambda = -\beta$. The method is stable if and only if $|1 - \beta h + \beta^2 h^2/2| < 1$, namely, for $h \leq 2/\beta$, akin to the explicit Euler scheme, Eq. C.16.

C.4 Predictor–corrector method (linearly implicit)

Here, we assume that the right side of Eq. C.1, namely $\dot{\mathsf{x}} = \mathsf{g}(\mathsf{x}, t)$ is given by

$$\mathsf{g}(\mathsf{x}, t) = \mathsf{A}\mathsf{x} + \mathsf{f}(\mathsf{x}, t) \tag{C.38}$$

where this time f included all the nonlinear terms (compare to Eq. C.2, where we had $\mathsf{f} = \mathsf{f}(t)$), and A is time–independent. In other words, the differential equation under consideration is

$$\dot{\mathsf{x}} = \mathsf{A}\,\mathsf{x} + \mathsf{f}(\mathsf{x}, t) \qquad\qquad \text{with } \mathsf{x}(0) = \mathsf{x}_0 \tag{C.39}$$

[3]Recall that, for any complex number $z = x + \imath y = r\mathrm{e}^{\imath\theta}$, we have $|z/\overline{z}| = |r\mathrm{e}^{\imath\theta}/r\mathrm{e}^{-\imath\theta}| = |\mathrm{e}^{2\imath\theta}| = 1$.

The linearly implicit predictor–corrector scheme consists of the following: the semi-explicit Euler scheme is used for the linear term of the right side of the equation, whereas for the nonlinear term we use the explicit Euler scheme for the predictor and the semi–implicit Euler scheme for the corrector. Specifically, the predictor is given by (for simplicity, we assume $\mathsf{f} = \mathsf{f}(\mathsf{x})$)

$$\frac{1}{h}\left(\hat{\mathsf{x}}_{n+1} - \mathsf{x}_n\right) = \frac{1}{2}\,\mathsf{A}\left(\hat{\mathsf{x}}_{n+1} + \mathsf{x}_n\right) + \mathsf{f}(\mathsf{x}_n) \tag{C.40}$$

and the corrector

$$\frac{\mathsf{x}_{n+1} - \mathsf{x}_n}{h} = \frac{1}{2}\,\mathsf{A}\left(\mathsf{x}_{n+1} + \mathsf{x}_n\right) + \frac{1}{2}\left[\mathsf{f}(\hat{\mathsf{x}}_{n+1}) + \mathsf{f}(\mathsf{x}_n)\right]. \tag{C.41}$$

C.4.1 Accuracy and stability analyses

The accuracy and stability analyses are limited to the case in which the nonlinear terms may be approximated with linear ones $\mathsf{f}(\mathsf{x}) \simeq \mathsf{B}\mathsf{x}$ and that A and B can be diagonalized using the same transformation. Thus, we study the equation

$$\dot{y} = \lambda\, y + \mu\, y \qquad\qquad \text{with } y(0) = y_0 \tag{C.42}$$

where λ and μ denote, respectively, eigenvalues of A and B corresponding to the same eigenvector. The predictor is

$$\frac{1}{h}\left(\hat{y}_{n+1} - y_n\right) = \frac{1}{2}\,\lambda\left(\hat{y}_{n+1} + y_n\right) + \mu\, y_n \tag{C.43}$$

and the corrector is

$$\frac{1}{h}\left(y_{n+1} - y_n\right) = \frac{1}{2}\,\lambda\left(y_{n+1} + y_n\right) + \frac{1}{2}\,\mu\left(\hat{y}_{n+1} + y_n\right) \tag{C.44}$$

The overall scheme yields $y_{n+1} = \rho y_n$,

$$\rho = \frac{1}{1 - \check{\lambda}}\left(1 + \check{\lambda} + \check{\mu} + \check{\mu}\frac{1 + \check{\lambda} + 2\check{\mu}}{1 - \check{\lambda}}\right) \tag{C.45}$$

with $\check{\lambda} = \lambda h/2$ and $\check{\mu} = \mu h/2$.

Accuracy analysis

The accuracy of the method is obtained by using again $(1 - x)^{-1} = 1 + x + x^2 + \ldots$ and $\mathrm{e}^x = 1 + x + x^2/2 + \ldots$, to yield

$$\rho = 1 + (\lambda + \mu)h + \frac{1}{2}(\lambda + \mu)^2 h^2 + \cdots = \mathrm{e}^{(\lambda+\mu)h} + \mathcal{O}(h^3). \tag{C.46}$$

This confirms that the accuracy of the scheme is of order h^2.

Stability analysis

In order for this method to be stable we need $-1 \le \rho \le 1$. Thus, the stability boundary are

$$\frac{1 + \check{\lambda} + \check{\mu}}{1 - \check{\lambda}} + \check{\mu}\frac{1 + \check{\lambda} + 2\check{\mu}}{(1 - \check{\lambda})^2} = \pm 1 \tag{C.47}$$

or

$$(1 + \check{\lambda} + \check{\mu})(1 - \check{\lambda}) + \check{\mu}(1 + \check{\lambda} + 2\check{\mu}) = \pm(1 - \check{\lambda})^2 \tag{C.48}$$

C.5 The Alternating Direction Implicit method (ADI)

The ADI (Alternating Direction Implicit) method, introduced by Peaceman and Rachford, Ref. 41, in 1955, is a generalization of the semi–implicit Euler scheme, which avoids the problem of having to invert the whole matrix A at each time step. Assume that $\mathsf{A} = \mathsf{A}_1 + \mathsf{A}_2$. Then, Eq. C.3 may be written as[4]

$$\dot{\mathsf{x}} = (\mathsf{A}_1 + \mathsf{A}_2)\mathsf{x} + \mathsf{f}(t). \tag{C.49}$$

The ADI scheme consists of using two semi–steps: in the first one the term $\mathsf{A}_1\mathsf{x}$ is treated as implicit and $\mathsf{A}_2\mathsf{x}$ as explicit; in the second step, we reverse the roles. This yields

$$\begin{aligned} \frac{\mathsf{x}_n - \mathsf{x}_{n-1}}{h} &= \mathsf{A}_1\,\mathsf{x}_n + \mathsf{A}_2\,\mathsf{x}_{n-1} + \frac{1}{2}\big(\mathsf{f}_n + \mathsf{f}_{n-1}\big) \\ \frac{\mathsf{x}_{n+1} - \mathsf{x}_n}{h} &= \mathsf{A}_1\,\mathsf{x}_n + \mathsf{A}_2\,\mathsf{x}_{n+1} + \frac{1}{2}\big(\mathsf{f}_{n+1} + \mathsf{f}_n\big) \end{aligned} \tag{C.50}$$

or

$$\begin{aligned} \big(\mathsf{I} - h\,\mathsf{A}_1\big)\,\mathsf{x}_n &= \big(\mathsf{I} + h\,\mathsf{A}_2\big)\,\mathsf{x}_{n-1} + \frac{h}{2}\,\big(\mathsf{f}_n + \mathsf{f}_{n-1}\big) \\ \big(\mathsf{I} - h\,\mathsf{A}_2\big)\,\mathsf{x}_{n+1} &= \big(\mathsf{I} + h\,\mathsf{A}_1\big)\,\mathsf{x}_n + \frac{h}{2}\,\big(\mathsf{f}_{n+1} + \mathsf{f}_n\big) \end{aligned} \tag{C.51}$$

Combining, we have

$$\begin{aligned} \mathsf{x}_{n+1} = {} & \big(\mathsf{I} - h\,\mathsf{A}_2\big)^{-1}\big(\mathsf{I} + h\,\mathsf{A}_1\big)\,\big(\mathsf{I} - h\,\mathsf{A}_1\big)^{-1}\big(\mathsf{I} + h\,\mathsf{A}_2\big)\,\mathsf{x}_{n-1} \\ & + \big(\mathsf{I} - h\,\mathsf{A}_2\big)^{-1}\,\frac{h}{2}\,\big(\mathsf{f}_{n+1} + \mathsf{f}_n\big) \\ & + \big(\mathsf{I} - h\,\mathsf{A}_2\big)^{-1}\big(\mathsf{I} + h\,\mathsf{A}_1\big)\,\big(\mathsf{I} - h\,\mathsf{A}_1\big)^{-1}\,\frac{h}{2}\,\big(\mathsf{f}_n + \mathsf{f}_{n-1}\big) \end{aligned} \tag{C.52}$$

Accuracy of the ADI method

For simplicity, assume $\mathsf{f} = \mathsf{0}$. Using $(\mathsf{I} - \mathsf{M})^{-1} = \mathsf{I} + \mathsf{M} + \mathsf{M}^2 + \ldots$, Eq. C.52 yields

$$\mathsf{x}_{n+1} = [\mathsf{I} + 2h(\mathsf{A}_1 + \mathsf{A}_2) + \frac{h^2}{2}(\mathsf{A}_1^2 + \mathsf{A}_1\mathsf{A}_2 + \mathsf{A}_2\mathsf{A}_1 + \mathsf{A}_2^2) + \ldots]\mathsf{x}_{n-1} \tag{C.53}$$

Let us compare the results with the exact solution,

$$\mathsf{x}_{k+1} = \mathrm{e}^{2h(\mathsf{A}_1+\mathsf{A}_2)}\mathsf{x}_{k-1} + \int_{t_{k-1}}^{t_{k+1}} \mathrm{e}^{(\mathsf{A}_1+\mathsf{A}_2)(t_{k+1}-\tau)}\mathsf{f}(\tau)\,\mathrm{d}\tau, \quad k = 0, 1, \ldots \tag{C.54}$$

where, recalling that $\mathrm{e}^{\mathsf{M}} = \mathsf{I} + \mathsf{M} + \mathsf{M}^2/2 + \ldots$, we have

$$\mathrm{e}^{2h(\mathsf{A}_1+\mathsf{A}_2)} = \mathsf{I} + 2h(\mathsf{A}_1 + \mathsf{A}_2) + \frac{h^2}{2}(\mathsf{A}_1^2 + \mathsf{A}_1\mathsf{A}_2 + \mathsf{A}_2\mathsf{A}_1 + \mathsf{A}_2^2) + \ldots \tag{C.55}$$

Thus this method is accurate to order h^2.

[4] In diffusion problems, A_1 and A_2 denote, respectively, the finite–difference matrix in the first and in the second direction. In this case, we deal with block diagonal matrices, where each block is tridiagonal, with considerable reductions of the computational time needed for the matrix inversions required.

Stability of the ADI method

It is apparent that the algorithm for the homogeneous problem consists of a sequence of matrix multiplications of the type $\left(\mathsf{I} + h\,\mathsf{A}_1\right)\left(\mathsf{I} - h\,\mathsf{A}_1\right)^{-1}$, alternating with matrix multiplications of the type $\left(\mathsf{I} + h\,\mathsf{A}_2\right)\left(\mathsf{I} - h\,\mathsf{A}_2\right)^{-1}$. These are of the same kind as those in the semi–implicit Euler method, which is unconditionally stable. Thus, the method in also unconditionally stable.

Acknowledgements

The present thesis would not have been possible without the doctoral scholarship awarded to me by the University Roma Tre. I also wish to express my appreciation to Prof. Azer Bestavros, Director of the Boston University Hariri Center, for the hospitality received during the periods November 2011 to January 2012 and November–December 2012. I also wish to acknowledge the support received through the Internalization Program of the University Roma Tre, which made these visits possible. The current work was also supported by the C.A.S.P.U.R. with a standard High Performance Computing grant (std12-065) and by the Scientific Computing Group (IS&T) of the Boston University by granting access to their computing resources.

On a more personal note, I am extremely grateful for all the help and the countless encouragements I have received from my tutor Prof. Luigi Morino. I am also grateful to Dr. Giovanni Bernardini and Dr. Kadin Tseng for their fundamental contributions to my numerical implementations.

I wish to thank all the people that contributed to the development of my thesis like Ing. Michel Onori, Prof. Roberto Camussi, Prof. Sheryl Grace and Dr. Douglas Sondak.

Finally a special thanks goes to my family, and especially my sister, for being there and supporting me. I also wish to thank all the friends that accompanied this journey making it unforgettable: all the friends from the laboratory of the section “Aeronautical Structures” of the Mechanical and Industrial Engineering Department of the University of Roma Tre in particular Simone, Eugenio, Alessandro and Emanuele, but also my friends oversea Paola and Mike. However, the most important acknowledgment goes to Katherine for all her patience and understanding.